Climatic and environmental changes during Marine Isotope Stages 3, 2 and 1 in southern Patagonia - Evidences from Laguna Potrok Aike (Argentina)

Dissertation
zur Erlangung des Doktorgrades (Dr. rer. nat.)
am Fachbereich 8
der Universität Bremen

Pierre Kliem

Göttingen, Januar 2019

Tag des Kolloquiums: 04.11.2019

Gutachter der Dissertation:

Prof. Dr. Bernd Zolitschka
Arbeitsgruppe für Geomorphologie und Polarforschung
Institut für Geographie, Universität Bremen

Prof. Dr. Torsten Haberzettl
Lehrstuhl für Physische Geographie
Institut für Geographie und Geologie, Universität Greifswald

Table of contents

Acknowledgements

Thanks a lot go to:

Agathe Lisé-Pronovost, Annette Hahn, Bernd Zolitschka, Britta Schülzke, Catalina Gebhardt, Christian Ohlendorf, Christoph Mayr, Daniel Veres, Dirk Enters, Frank Schäbitz, Isabelle Matthias, Henrike Baumgarten, Hugo Corbella, Michael Fey, Michael Wille, Sabine Stahl, Sephanie Kastner, Torsten Haberzettl and members of the PASADO science team.

Summary

Since the year 2001 paleolimnological studies at the maar Laguna Potrok Aike (LPA) in southern Patagonia extend our knowledge about the past regional environment conditions and about the climatically important southern hemispheric westerlies (SHW). In the frame of the ICDP (International Continental Scientific Drilling Program) project PASADO (Potrok Aike Maar Lake Sediment Archive Drilling Project) the paleolimnological research at LPA intensified in 2008. After positive experiences of previous projects different research disciplines were brought together in a multi-proxy approach. The data basis was established by extensive drilling on lake sediments and field work in the catchment of the lake. The focus was represented by about 100 m deep core drillings in the lake sediment.

The lithological, chronological and frequency analytical examination of the 106.09 m long composite profile 5022-2CP drilled in the southern profundal of the lake was the focus of this PhD thesis. Furthermore, results of geomorphological and sedimentological field work in the realm of the lake surrounding basin as well as in the proximate catchment were analyzed.

Pelagic deposits, lake internal mass movements and tephra were identified at composite profile 5022-2CP. Striking, the amount of lake internal mass movements represented more than 50 % of the composite profile. The with lower core depths reducing ratio of mass movement deposits was interpreted as decreasing relief energy, slope consolidation and a less inclined slope angle during proceeding sediment filling of the basin. Furthermore, the intensity of lake level changes might have enforced the collapse of slopes which increased the amount of mass movement deposits.

Regarding structure and compounds pelagic sediments deposited during the interglacial times distinctly differentiate from sediments deposited during glacial times. Laminated silt with carbonate crystals dominated in Holocene sediments. Laminated silt with intercalations of fine sand and coarse silt dominated in sediments of the glacial period. Lake internal mass movements and tephra layers were the only hiatus in the continuous sedimentary sequence. After radiocarbon-based age-depths-modeling 5022-2CP represents the time window of the past ca. 51.200 years.

Based on sedimentary, seismic and geomorphological evidences the magnitude, geomorphological response and climate links of LPA lake level oscillation were examined. Five distinct major treads between 136 and 85 m a.s.l were identified and reflect abrasion and lake level oscillations of at least the past 51.200 years. This process expanded the lake basin from originally 2.2 km to 3.8 km.

The highest major tread marks the topographically determined highest possible lake level as an active overflow to the northerly located Rio Gallegos existed under these conditions. The lowest major tread likely marks a former lake level under influence of the local ground water table. The partial (subaquatic) collapse of the lowest major tread resulted in numerous lake internal mass movement deposits.

Temporally, the highest lake levels of the past ~ 50.000 years occurred during the Last Glacial and the Little Ice Age. The lowest lake level existed during the mid Holocene. However, inferring climate changes between the Last Glacial and the Holocene from lake level reconstructions of the LPA is complicated by the evidence of last glacial permafrost in the catchment, because permafrost might have in influenced the lake level by intensified surface runoff.

Frequency analytics were performed on time series of the magnetic susceptibility and the element calcium for the time window ~ 51.200 to 17.000 years in 5022-2CP. For the first time, recurring climate signals with a periodicity of ~ 1.500 years during the coldest period of the last glacial period (Marine Isotope stadium 2 = MIS 2) were detected on a record from the southern hemisphere. Likely, these were connected with minor variations of the SHW and were in majority of minor (local) climatic dimension and thus not reached the magnitude of prominent (regional) last glacial climate signals paced by this periodicity as inferred from antarctic ice cores. The minor magnitude of most MIS 2 climate signals likely resulted from a major northward displacement of the SHW that sufficiently decreased the impact of minor SHW variations with a periodicity of 1.500 years on climatically important antarctic circumpolar deep water that inhibited the amplification of climate signals by green house gas ventilation from the ACC (positive feedback).

Zusammenfassung

Seit dem Jahr 2001 tragen paläolimnologische Untersuchungen am Maarsee Laguna Potrok Aike im südlichen Teil der Steppe Patagoniens dazu bei, den Kenntnisstand über die regionalen Paläoumweltbedingungen und über die klimatisch bedeutsamen südhemisphärischen Westwinde zu erweitern. Im Rahmen des ICDP-Projektes PASADO wurden diese Forschungsarbeiten an der Laguna Potrok Aike im Jahr 2008 deutlich intensiviert. Nach den positiven Erfahrungen aus vorhergehenden Projekten wurden verschiedene Forschungsbereiche in einem Multi-Proxy-Ansatz zusammengeführt. Die Datengrundlage wurde durch umfangreiche Bohrarbeiten an Seesedimenten sowie durch Geländearbeiten im Einzugsgebiet des Sees geschaffen. Den Schwerpunkt bildeten bis etwa 100 m tiefe Kernbohrungen in den Seesedimenten.

Die lithologische, chronologische und frequenzanalytische Auswertung des 106.09 m langen Komposit-Profil 5022-2CP aus dem südlichen Profundalbereich des Sees standen im Vordergrund der vorliegenden Dissertation. Zudem wurden Ergebnisse geomorphologischer und sedimentärer Geländearbeiten im Bereich des seeumrahmenden Beckens sowie im proximalen Einzugsgebiet ausgewertet.

Am Komposit-Profil 5022-2CP wurden pelagische Ablagerungen, seeinterne Massenumlagerungen und Tephren lithologisch identifiziert. Auffällig war der über 50 % vom Gesamtprofil ausmachende Anteil an seeinternen Massenumlagerungen. Der mit abnehmender Sedimenttiefe sich tendenziell verringernde Anteil wurde auf eine verringerte aquatische Reliefenergie, Hangverfestigung und Hangverflachung im Zuge der voranschreitenden Verfüllung des Seebeckens zurückgeführt. Zudem verstärkten Seespiegelschwankungen den Kollaps der subaquatischen Hänge und erhöhten somit den Anteil von seeinternen Massenumlagerungen.

Hinsichtlich Struktur und Zusammensetzung der pelagischen Sedimente waren interglazial- und glazialzeitliche Ablagerungen deutlich zu unterscheiden. In den holozänen Sedimenten dominierten laminierte Silte mit einem Anteil an Calcit-Kristallen. Die glazialzeitlichen Sedimente waren durch laminierte Silte mit eingeschalteten Feinsand- und Grobsiltlagen charakterisiert. Die seeinternen Massenumlagerung und Tephren stellten die einzigen Hiaten in der kontinuierlichen Sedimentationsfolge dar. Auf Grundlage der Alters-Tiefen-Modellierung an Radiokarbondatierungen repräsentiert 5022-2CP das Zeitfenster der letzten ca. 51.200 Jahre.

Auf Grundlage von sedimentären, seismischen und geomorphologischen Ergebnissen wurden die Magnitude, die geomorphologischen Auswirkungen und die klimatischen Zusammenhänge von Seespiegelschwanken der LPA untersucht. Dabei wurden fünf markante Geländestufen

zwischen etwa 136 und 85 m ü. M. im Seebeckenbereich festgestellt, deren Entstehung auf die Abrasion und Seespiegeloszillationen mindestens der vergangenen ~ 50.000 Jahre zurückging. Durch diesen Prozess wurde der Seebeckendurchmesser von ursprünglich etwa 2.2 km auf etwa 3.8 km erweitert.

Die höchste Geländestufe markierte den topographisch bedingt höchstmöglichen Seespiegelstand, da bei dieser Seespiegelhöhe ein aktiver Abfluss von Seewasser zum Rio Gallegos im Norden bestand. Die niedrigste Geländestufe markierte wahrscheinlich einen ehemaligen Seespiegelstand unter Einfluss des lokalen Grundwasserspiegels. Der teilweise (subaquatische) Kollaps der niedrigsten Geländestufe hatte zahlreiche seeinternen Massenumlagerungen zur Folge.

Zeitlich betrachtet waren die höchsten Seespiegelstände der letzten ~ 50.000 Jahre für das letzte Glazial und für die sogenannte Kleine Eiszeit nachweisbar. Der niedrigste Seespiegelstand bestand während des mittleren Holozäns. Jedoch war die Ableitung von klimatischen Veränderungen zwischen Glazial und Holozän aus Seespiegelrekonstruktionen der LPA durch den Nachweis von glazialzeitlichem Permafrost im Einzugsgebiet verkompliziert, weil Permafrost über einen verstärkten Oberflächenabfluss den Seespiegelstand beeinflusst haben könnte.

Die Zeitreihen über Variationen der Magnetischen Suszeptibilität und des Elementes Calcium in 5022-2CP wurden für den Zeitraum ~ 51.200 bis 17.000 Jahre frequenzanalytisch ausgewertet. Erstmalig waren an einem Datensatz aus der Südhemisphäre für den kältesten Zeitraum des letzten Glazials (Marines Isotopenstadium 2 = MIS 2) in periodischen Zeitabständen von ~ 1.500 Jahren wiederkehrende Klimaereignisse nachweisbar. Diese standen wahrscheinlich im Zusammenhang mit geringfügigen Variationen der SHW und waren in der Mehrzahl nur von einer geringen (lokalen) klimatischen Größenordnung, die nicht die Dimension der dem gleichen Rhythmus unterliegenden, prominenten (regionalen) Klimaereignisse des Glazials erreichten, wie sie insbesondere an antarktischen Eisbohrkernen abgeleitet worden waren. Die zumeist nur geringe Magnitude der Klimaereignisse im MIS 2 war wahrscheinlich die Folge der übergeordneten Nordverschiebung der SHW, sodass die SHW auch im Zuge untergeordneter Variationen im Rhythmus von 1.500 Jahren keinen hinreichenden Einfluss auf die Zone des klimatisch bedeutsamen antarktischen zirkumpolaren Tiefenwassers (ACC) erreichten. Eine Verstärkung der Magnitude der Klimaereignisse durch Treibhausgasemissionen aus dem ACC (positive Rückkopplung) war somit unterbunden.

Chapter 1:

Introduction

Lake archives – Basis of paleolimnological work

Lake Archives are foundations paleolimnological research. After Cohen (2003) lake archives can be separated in content archives ("the physical sedimentary inputs to the lake's record"; i.e. fossils, sediments, geochemistry) and container archives ("the place where such records are housed", i.e. the lake water, the geomorphology of the lake basin and the lacustrine sediment) of records.

A record reflects the formation, persistence and characteristic of the history of a lake which can be influenced by variable external factors like the climate, watershed geology, watershed/regional vegetation and human activity. Often, paleolimnological research focuses chronological reconstructions of external factors of the past, aiming estimations about future developments (Dearing et al., 2006).

In this respect records from cores offer high potential and are the most common data basis of paleolimnological work. Advantages are often high temporal resolutions (because of high sedimentation rates), continuous sedimentation rates and relative low depth of bioturbation in comparison with marine or other terrestrial sedimentation areas (Cohen, 2003).

Considering several archives of a lake increases the value of interpretations (= so-called multi-proxy-approach). This approach was realized in the frame of paleolimnological research on Laguna Potrok Aike (LPA). In the frame of the project PASADO (Potrok Aike Sediment Archive Drilling Program) diverse studies on lake sediments, the catchment area and the water body of the lake were performed. Based on these data basis numerous scientific papers were published. Investigations on archives from cores and paleo lake levels of LPA were in focus of this dissertation (Chapter 2 - 4).

Laguna Potrok Aike – A unique terrestrial sediment archive in the Southern Hemispheric westerlies

Laguna Potrok Aike is a circa 100 m deep maar lake located in south-eastern Patagonia (51°S; 70 km north of the Strait of Magellan and 85 km south-west of the city of Rio Gallegos; Fig. 1.1), Argentina. Geologically, the lake is located in the Pali Aike Volcanic Field, which originates from Pliocene to late Quaternary back arc volcanism (Mazzarini and D`Orazio, 2003) in the Magellan Basin. The water body covers a part of the basin that likely results from a maar eruption approximately 770 ka ago (Zolitschka et al., 2006).

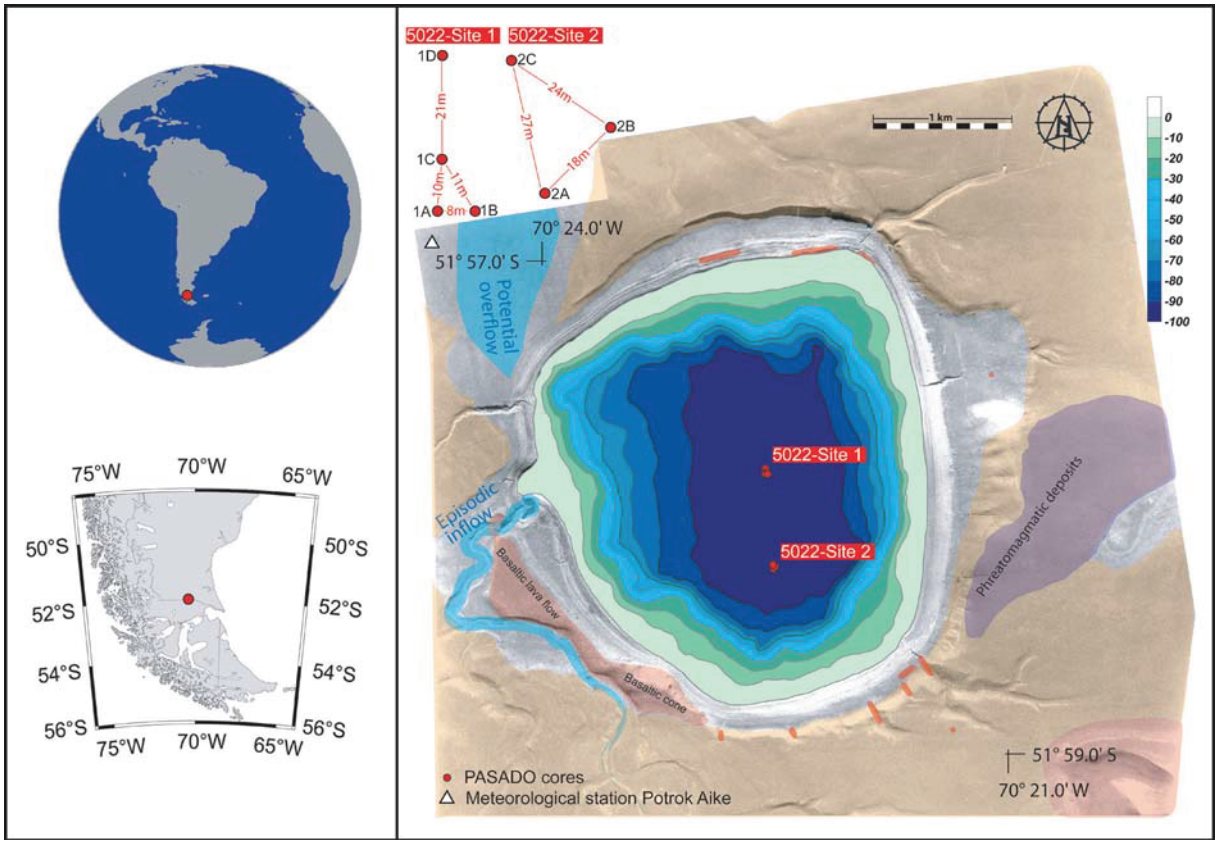

Fig. 1.1: Location of Laguna Potrok Aike in the southern hemisphere, in southern South America and bathymetric map with position of drill sites merged with an aerial photograph and geological data (Corbella, 2002; Zolitschka et al., 2006). Water depth is given in m below lake surface. Young fluvial and lacustrine deposits (grey), a mid-Pleistocene basalt lava flow (red), phreatomagmatic tephra deposits (pink), moraine till (yellow), and the Tertiary Santa Cruz Formation (orange) are color-coded.

Within the atmospheric circulation system LPA is located in the belt of the Southern Hemispheric westerlies (SHW). Due to the location east of the Cordillera the SHW are subject to the rain shadow effect that causes the semiarid climate of the Pali Aike Volcanic Field with a

precipitation of less than 300 mm/a (González and Rial, 2004) and decreases the annual precipitation occasionally to values of 150 mm at a local meteorological station near LPA (Zolitschka et al., 2006). In contrast, air masses arriving LPA from easterly directions advect most precipitation and indicate the influence of the Polar Easterlies (Mayr et al., 2007b). Thus, the climate at LPA indicates shifts of polar and mid-latitude air pressure fields. Moreover, the climate archive provides a high potential to study the nature of the SHW of the past over continental landmass (Chapter 5). To improve the knowledge about past characteristics of the SHW is of scientific interest, as it might play a key role for our understanding of the global-climate-system (White and Peterson, 1996; Knorr and Lohmann, 2003; Kaiser et al., 2007; Toggweiler, 2009).

Several investigations on records from lake archives could improve the knowledge about the Holocene and Late Glacial characteristic of the SHW over the southernmost part of the continental landmass. However, records far beyond the Late Glacial are rare. Only the sediments recovered from the Laguna Parillar (44.000 cal a BP) range distinctly beyond the Late Glacial time span, but the lake sedimentation of the glacial time span was affected by an perennial lake ice cover and glacier ice dam blocking the outlet of the lake (Heirman, 2011). The sediments of Lago Cardiel spanning the past ~20 ka BP and the lake almost dried out around 13 cal. ka BP (Gilli et al., 2001; Markgraf et al., 2003; Gilli et al., 2005b). Records back to the Late Glacial and Postglacial are known from the Nevado area (53°S) in Chile (Kilian et al., 2000).

Records covering the time range back to the MIS 3 were obtained during several drill campaigns at LPA. The precipitation history of the past ~ 16.000 years was reconstructed from cores drilled in the frame of the project SALSA (Haberzettl et al., 2007). Based on cores drilled in the frame of the following project PASADO a high resolute composite profile covering the time span of the past ~ 51.200 years was compiled (Chapter 3). The composite profile is in focus of this thesis and of outstanding quality for paleoclimatic and paleoenvironmental studies because of the following properties and general framework:

1. The relative small catchment: Hydrological interpretations refer to a small area. Also during the last glacial period the glaciers of the westerly located Andes did not reach the catchment area of LPA, i.e. no disturbances by glacial erosion or hydrological influences by glacial melt water of the lake (Caldenius, 1932; Mercer, 1976; Rabassa and Clapperton, 1990; Meglioli, 1992; Coronato et al., 2013). Moreover, because of a

small catchment only a relatively small variety of lithology have to be considered regarding the interpretation of the data.

2. The lake was permanently filled with water during the time window recovered with 5022-2CP, i.e. unconformities because of desiccations have not to be considered (Chapter 3).
3. Radiocarbon-dating of lake sediment is not effected by a reservoir effect (Haberzettl et al., 2005).
4. Lake level indicators of the record from the profundal area can by verified by absolute lake level indicators from past littoral zones (Chapter 4).

Framework

First paleolimnological studies on LPA were realized together with studies on further Patagonian lakes in the frame of the project SALSA (South Argentinean Lake Sediment Archives and modeling – 01.09.2001-31.08.2006). Using multi-proxy analyses the paleo climate and paleo environment of the southern latitudes was studied. The site LPA exhibits the highest potential for further research projects. Several lacustrine cores were retrieved from lake sediments and analyzed. A sediment profile with high time resolution covered the time range of the past ~ 16.000 years. A discontinuous profile extended the time limit back to ~ 53.000 years.

The scientific efforts in the realm of the lake were intensified during the subsequent project PASADO. The data basis was established in the frame of the International Continental Scientific Drilling Program (ICDP) expedition 5022 between September and November 2008 and mainly consists of lacustrine sediment cores (total sum: 533 m; maximum depth: 101.5 m below lake floor) from two sites of the profundal zone of the lake (Fig. 1.1). Cores from three holes of site 2 were compiled to the almost continuous composite profile (CP) 5022-2CP. Further studies in the catchment and the lake water body completed the data basis.

This thesis was realized in the frame of the project PASADO, which is a multinational scientific initiative within the framework of the ICDP and the southernmost located project of the ICDP.

Objectives and outline

The publications presented in Chapters 2-4 were compiled in the frame of the project PASADO. Diverse geological data from the lake sediment and the catchment of the lake were analyzed. The objectives and outline of the studies were summarized as follows:

1. The first publication focuses the macroscopic core description (including interpretation of sediment structures and determination of lithostratigraphic units) and radiocarbon dating of the ca. 106 m long 5022-2CP. Considering the sedimentological results of 5022-2CP an event-corrected composite profile was elaborated and radiocarbon based age-depth-modeled. The age-depth-model was validated by geomagnetic intensity and tephrochronology. Results were published in the journal *Quaternary Science Reviews* (Chapter 2).
2. The second publication focuses geomorphological studies in the lake basin and the proximity of the lake aiming knowledge about the geomorphological evolution of the lake basin and lake level history in the context of climatic and environmental changes. Ages of littoral and eolian sediments as well as fossil sand wedges were dated for the first time by using the OSL method. Supra-aquatic tephra layers were correlated with dated subaquatic tephra layers. A digital elevation grid of bathymetric und catchment GPS data was analyzed to identify lake level terraces. Results were published in the journal *Quaternary Science Reviews* (Chapter 3).
3. Performance of frequency analyses on high-resolution records of the magnetic susceptibility and the element calcium in 5022-2CP. Both parameters were identified as dust proxy during cold climates in various studies on LPA sediments (Haberzettl et al., 2009; Hahn et al., 2014; Lisé-Pronovost et al., 2015). Results were published in the journal *Quaternary Research* (Chapter 4).

Own contribution

The own contribution of the author contains portions of field works, samplings, laboratory analyses, data processings and publications in scientific journals.

The field works were carried out from August to October 2008 on an offshore drilling rig and in the proximate catchment of the lake. The sampling of core catcher sediment as well as the handling of liners of the hydraulic piston corer on the drilling rig occurred in rotation with members of the PASADO science team. Photographical documentations and mappings in the proximate lake catchment are contributions of the author. Outcrop sampling of volcaniclastic, lacustrine, eolian and relict periglacial sediments were performed in rotation with members of the PASADO science team. The author performed a digital elevation survey in the proximate catchment of the lake to extent an existing data set.

Expansive laboratory studies on the lacustrine sediment cores from site 2 occurred together with student assistants and members of the PASADO science team in the laboratory of the working group GEOPOLAR, University of Bremen. The laboratory studies included sediment description and sampling, determination of the dry density (DD), element detection by X-ray diffraction (XRF) and determination of the magnetic susceptibility. The sampling and sample preparation of plant macro remains for radiocarbon dating was carried out by the author.

The author conducted the following data analyses and data evaluations:

- event-correction of 5022-2CP
- correlation of radiocarbon dates from PTA03/ 12+13 to 5022-2CP
- calibration and re-calibration of radiocarbon dates
- radiocarbon based age-depth-modeling
- modeling of the digital elevation grid using bathymetric and differential GPS data
- counting of tree rings
- reconstruction of the lake level history based on field survey, digital elevation modeling as well as seismic and sediment core data
- calculation of 200 yr running means and correlation coefficients for the records: dry density, elemental calcium and magnetic susceptibility.

The author drafted the majority of tables, figures and manuscripts in the three scientific publications (chapters 2-4). The co-authors improved the aforementioned drafts and contributed drafts of tables, figures and text about methods and results of tephra analyses, stimulated luminescence dating and spectral analyses.

References

Caldenius, C., 1932. Las glaciaciones cuarternarias en la Patagonia y Tierra del Fuego. Geografisker Annaler 22, 1-164.

Cohen, A.S., 2003. Paleolimnology. The History and Evolution of Lake Systems. Oxford University Press, Oxford.

Coronato, A., Ercolano, B., Corbella, H. and Tiberi, P., 2013. Glacial, fluvial and volcanic landscape evolution in the Laguna Potrok Aike maar area, southernmost Patagonia, Argentina. Quaternary Science Reviews 71, 13-26.

Dearing, J.A., Battarbee, R.W., Dikau, R., Larocque, I. and Oldfield, F., 2006. Human-environment interactions: lerning from the past. Regional Environmental Change 6, 1-16.

Gilli, A., Anselmetti, F., Ariztegui, D., Bradbury, J., Kelts, K., Markgraf, V. and McKenzie, J., 2001. Tracking abrupt climate change in the Southern Hemisphere: a seismic stratigraphic study of Lago Cardiel, Argentina (49°S). Terra Nova 13, 443-448.

Gilli, A., Ariztegui, D., Anselmetti, F.S., McKenzie, J.A., Markgraf, V., Hajdas, I. and McCulloch, R.D., 2005. Mid-Holocene strengthening of the Southern Westerlies in South America - sedimentological evidences from Lago Cardiel, Argentina (49°S). Global and Planetary Change 49, 75-93.

González, L. and Rial, P., 2004. Guía geográfica interactiva de Santa Cruz., 59pp.

Haberzettl, T., Fey, M., Lücke, A., Maidana, N., Mayr, C., Ohlendorf, C., Schäbitz, F., Schleser, G.H., Wille, M. and Zolitschka, B., 2005. Climatically induced lake level changes during the last two millennia as reflected in sediments of Laguna Potrok Aike, southern Patagonia (Santa Cruz, Argentina). Journal of Paleolimnology 33, 283-302.

Haberzettl, T., Corbella, H., Fey, M., Janssen, S., Lücke, A., Mayr, C., Ohlendorf, C., Schäbitz, F., Schleser, G.H., Wille, M., Wulf, S. and Zolitschka, B., 2007. Lateglacial and Holocene wet-dry cycles in southern Patagonia: chronology, sedimentology and geochemistry of a lacustrine record from Laguna Potrok Aike, Argentina. The Holocene 17, 297-310.

Haberzettl, T., Anselmetti, F.S., Bowen, S.W., Fey, M., Mayr, C., Zolitschka, B., Ariztegui, D., Mauz, B., Ohlendorf, C., Kastner, S., Lücke, A., Schäbitz, F. and Wille, M., 2009. Late Pleistocene dust deposition in the Patagonian steppe - extending and refining the paleoenvironmental and tephrochronological record from Laguna Potrok Aike back to 55 ka. Quaternary Science Reviews 28, 2927-2939.

Hahn, A., Kliem, P., Ohlendorf, C., Zolitschka, B., Rosén, P. and the PASADO science team, 2014. Elemental composition of the Laguna Potrok Aike sediment sequence reveals paleoclimatic changes over the past 51 ka in southern Patagonia, Argentina. Journal of Paleolimnology 52.

Heirman, K., 2011. 'A Wind of Change': Changes in Position and Intensity of the Southern Hemisphere Westerlies during Oxygen Isotope Stages 3,2 and 1. PhD thesis, Ghent University, Belgium.

Kaiser, J., Lamy, F., Arz, H. and Hebbeln, D., 2007. Variability of sea-surface temperatures off Chile and the dynamics of the Patagonian Ice Sheet during the last glacial period based on ODP Site 1233. Quaternary International 161, 77-89.

Kilian, M., van Geel, B. and van der Plicht, J., 2000. ^{14}C AMS wiggle matching of raised bog deposits and models of peat accumulation. Quaternary Science Reviews 19, 1011-1033.

Knorr, G. and Lohmann, G., 2003. Southern Ocean origin for the resumption of Atlantic thermohaline circulation during deglaciation. Nature 424, 532-536.

Lisé-Pronovost, A., St-Onge, G., Gogorza, C., Haberzettl, T., Jouve, G., Francus, P., Ohlendorff, C., Gebhardt, C., Zolitschka, B. and the PASADO Science Team, 2015. Rock-magnetic proxies of wind intensity and dust since 51,200 cal BP from lacustrine sediments of Laguna Potrok Aike, southeastern Patagonia. Earth and Planetary Science Letters 411, 72-86.

Markgraf, V., Bradbury, J.P., Schwalb, A., Burns, S.J., Stern, C., Ariztegui, D., Gilli, A., Anselmetti, F.S., Stine, S. and Maidana, N., 2003. Holocene palaeoclimates of southern Patagonia: limnological and environmental history of Lago Cardiel, Argentina. The Holocene 13, 581-591.

Mayr, C., Wille, M., Haberzettl, T., Fey, M., Janssen, S., Lücke, A., Ohlendorf, C., Oliva, G., Schäbitz, F., Schleser, G.H. and Zolitschka, B., 2007b. Holocene variability of the Southern

Hemisphere westerlies in Argentinean Patagonia (52°S). Quaternary Science Reviews 26, 579-584.

Mazzarini, F. and D`Orazio, M., 2003. Spatial distribution of cones and satellite-detected lineaments in the Pali Aike Volcanic Field (southernmost Patagonia): insights into the tectonic setting of a Neogene rift system. Journal of Volcanology & Geothermal Research 125, 291-305.

Meglioli, A., 1992. Glacial geology and geochronology of southernmost Patagonia and Tierra del Fuego, Argentina and Chile. Ph.D. Dissertation, Leigh University, Bethlehem PA U.S.A., 216.

Mercer, J.H., 1976. Glacial history of southernmost South America. Quaternary Research 6, 125-166.

Rabassa, J. and Clapperton, C.M., 1990. Quaternary glaciations of the southern Andes. Quaternary Science Reviews 9, 153-174.

Toggweiler, J.R., 2009. Shifting Westerlies. Science 323, 1434-1435.

White, W.B. and Peterson, R., 1996. An Antarctic Circumpolar Wave in surface pressure, wind, temperature, and sea ice extent. Nature 380, 699-702.

Zolitschka, B., Schäbitz, F., Lücke, A., Corbella, H., Ercolano, B., Fey, M., Haberzettl, T., Janssen, S., Maidana, N., Mayr, C., Ohlendorf, C., Oliva, G., Paez, M.M., Schleser, G.H., Soto, J., Tiberi, P. and Wille, M., 2006. Crater lakes of the Pali Aike Volcanic Field as key sites for paleoclimatic and paleoecological reconstructions in southern Patagonia, Argentina. Journal of South American Earth Sciences 21, 294-309.

Chapter 2:

Lithology, radiocarbon chronology and sedimentological interpretation of the lacustrine record from Laguna Potrok Aike, southern Patagonia

Published in: Quaternary Science Reviews (2013) 71: 54-69

Pierre Kliem (1), Dirk Enters (1), Annette Hahn (1), Christian Ohlendorf (1), Agathe Lisé-Pronovost (2,3), Guillaume St-Onge (2,3), Stefan Wastegård (4), Bernd Zolitschka (1) and the PASADO science team (5)

(1) Geomorphology and Polar Research (GEOPOLAR), Institute of Geography, University of Bremen, Celsiusstr. FVG-M, D-28359 Bremen, Germany. (kliem@uni-bremen.de)

(2) Canada Research Chair in Marine Geology, Institut des sciences de la mer de Rimouski (ISMER), Université du Québec à Rimouski (UQAR), Québec, Canada

(3) GEOTOP research center, Québec, Canada

(4) Dept. of Physical Geography and Quaternary Geology, Stockholm University, SE-106 91 Stockholm, Sweden

(5) PASADO science team as listed at http://www.icdp-online.org/front_content.php?idcatart=2794

Abstract

The 106 m long composite profile from site 2 of ICDP expedition 5022 (PASADO) at Laguna Potrok Aike documents a distinct change in sedimentation patterns from pelagic sediments at the top to dominating mass movement deposits at its base. The main lithological units correspond to the Holocene, to the Late Glacial and to the last glacial period and can be interpreted as the result of distinct environmental variations. Overflow conditions might have been achieved during the last glacial period, while signs of desiccation are absent in the studied sediment record. Altogether, 58 radiocarbon dates were used to establish a consistent age-depth model by applying the mixed-effect regression procedure which results in a basal age of 51.2 cal. ka BP. Radiocarbon dates show a considerable increase in scatter with depth which is related to the high amount of reworking. Validation of the obtained chronology was achieved with geomagnetic relative paleointensity data and tephra correlation.

Keywords: mixed-effect regression, mass movement deposits, lake level fluctuations, Late Pleistocene, Holocene, Patagonia, Argentina, ICDP-project PASADO

Introduction

Lacustrine sediments are often outstanding natural archives and complement marine and ice core records to reveal a consistent global picture of past environmental and climatic changes. However, terrestrial paleoclimatic data reaching far back into the Pleistocene are rare, especially from the Southern Hemisphere where southernmost South America is the only continental land mass between 40°S and 60°S. But here climate archives, mostly fen and lake sediments at the foot of the Andes, comprise only the past 18 cal. ka BP (Gilli et al., 2005b; Markgraf et al., 2007; Wille and Schäbitz, 2009; Markgraf and Huber, 2010; Moy et al., 2011). Older records can only be found in extra-Andean Patagonia like at Laguna Potrok Aike, Patagonia (51°58' S, 70°23' W). This site emerged as a valuable terrestrial paleoclimate archive for the last 16 cal. ka BP (Zolitschka et al., 2006; Haberzettl et al., 2007; Anselmetti et al., 2009; Mayr et al., 2009), and the Potrok Aike Maar Lake Sediment Archive Drilling Project (PASADO) was established to extend the climate record back in time. Such a sediment archive would allow to investigate shifts in polar to mid-latitude pressure fields and precipitation changes related to the Southern Hemispheric Westerlies as well as the Antarctic Oscillation and allows inter-comparisons between paleodata and climate models (Wagner et al., 2007; Meyer and Wagner, 2008). Due to the location of Laguna Potrok Aike in the Patagonian steppe leeward of the Andean mountain range, it should also be suited to establish a tephra and dust record which may be linked to marine records and ice cores from Antarctica. Furthermore, the possible extension of the Patagonian tephrochronology beyond the Late Glacial will provide the needed chronological control for other investigations using terrestrial as well as marine records.

Especially for multidisciplinary projects like PASADO, the initial lithological core description is essential and gives an overview about the compositional variability of the sediment record (lithological units) and the occurrence of unconformities and bedding structures (Schnurrenberger et al., 2003). This information is important to adjust the sampling scheme and to omit reworked sediment units from further time-consuming and expensive analyses. Moreover and most important, the significance of the obtained paleoenvironmental information depends on a reliable age-depth model. Only if time control is available, a comparison with other records becomes possible and lithological changes can be quantified with variations in sedimentation rates. Thus, the objectives of this study are to (1) describe the lithological changes encountered along the sediment record, (2) establish a robust radiocarbon-based age-depth model and (3) interpret the observed sedimentological variability.

Site description

Laguna Potrok Aike is a polymictic and subsaline maar lake located in the Pali Aike Volcanic Field (PAVF) at 113 m a.s.l. (Fig. 2.1). It has a maximum diameter of 3.5 km and a water depth of 100 m with a volume of 0.41 km³ (Zolitschka et al., 2006). According to the isotopic composition of the water body Laguna Potrok Aike is a groundwater lake (Mayr et al., 2007a). Rapid hydrological variations are documented by subaerial and subaqueous lake level terraces (Haberzettl et al., 2005; Anselmetti et al., 2009). At present the lake neither has a permanent tributary nor an outflow. A paleo-outflow related to a higher lake level is discussed for the Late Glacial (Haberzettl et al., 2007). Currently, only episodic or ephemeral surface runoff incised deep gullies in the surrounding subaerial terraces (Mayr et al., 2007a).

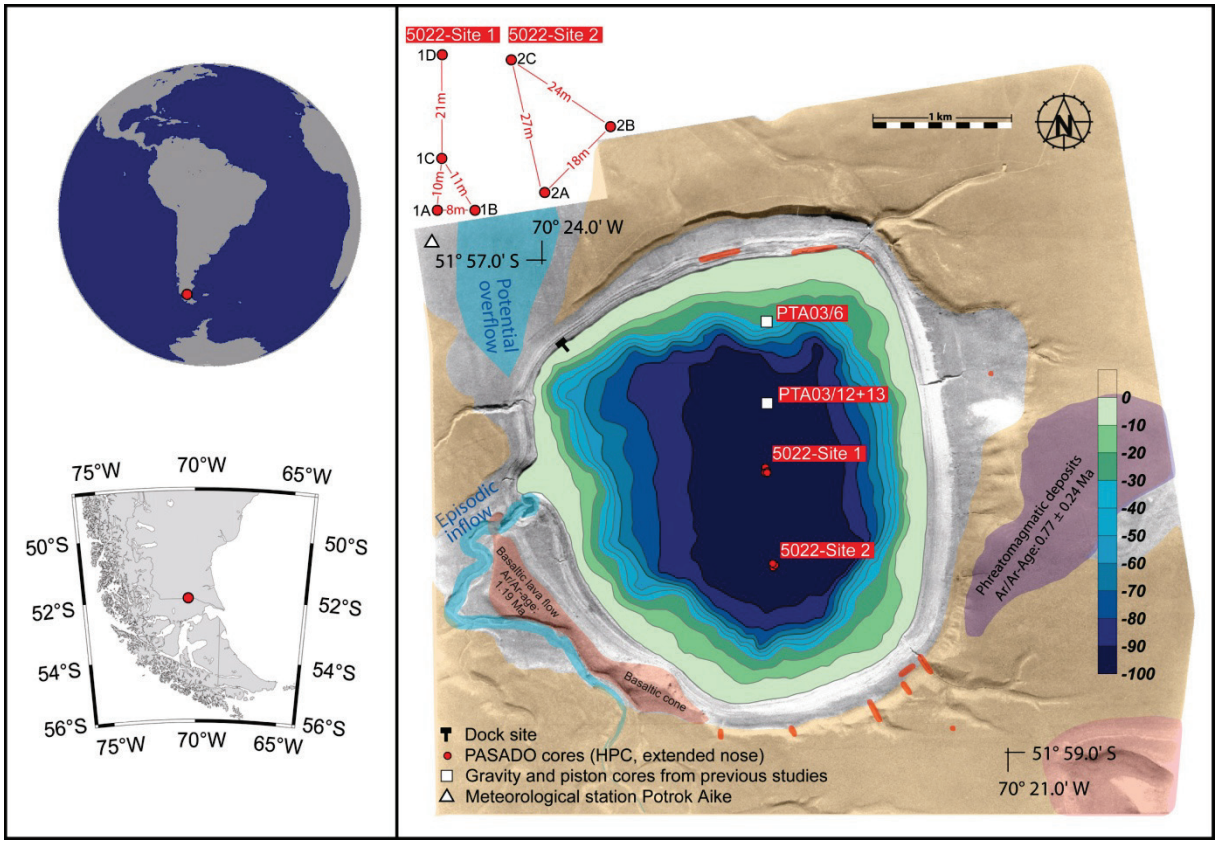

Fig. 2.1: Location of Laguna Potrok Aike in the southern hemisphere, in southern South America and bathymetric map with position of drill sites merged with an aerial photograph and geological data (Corbella, 2002; Zolitschka et al., 2006). Depth is given in m below lake surface. Young fluvial and lacustrine deposits (grey), a mid-Pleistocene basalt lava flow (red), phreatomagmatic tephra deposits (pink), moraine till (yellow), and the Tertiary Santa Cruz Formation (orange) are color-coded.

The PAVF is a region in the Province of Santa Cruz (Argentina) characterized by backarc volcanism (Mazzarini and D`Orazio, 2003). This intra-plate volcanism consists of Pliocene (3.8 Ma) to Holocene (0.01 Ma) alkali-olivine basalts (Corbella, 2002). The investigated maar itself is located in the older western part of the PAVF with scoria cones, plateau lavas and maar volcanoes occurring in the catchment area. A basaltic clast from the phreatomagmatic tephra of the maar eruption was dated by Ar/Ar and provides an age of 0.77 ± 0.24 Ma (Zolitschka et al., 2006). Outcrops of weakly compacted sandstone exist along the perimeter of the lake on subaerial terraces. These belong to Lower Miocene fine-grained molasse-type fluvial sandstones of the Santa Cruz Formation which is the youngest formation in the Magellanes Basin (Uliana and Biddle, 1988). Plio- and Pleistocene glaciations left behind fluvioglacial deposits and till in the catchment area, but glaciers did not reach the catchment area during the last few glaciations (Caldenius, 1932; Mercer, 1976; Rabassa and Clapperton, 1990; Meglioli, 1992).

Due to the proximity of the Antarctic continent, during austral summers the small land mass of southern Patagonia does not warm up as much as continents in the same latitude of the Northern Hemisphere (Weischet, 1996). The mean annual temperature at Rio Gallegos (6 m a.s.l., 85 km north-east of the study site) is only 7.4 ± 0.7 °C (Zolitschka et al., 2006). The regional climate is affected by the Southern Hemispheric Westerlies. The rain shadow effect of the north-south striking Andean mountain chain decreases precipitation to less than 300 mm (Mayr et al., 2007b). At the meteorological station next to Laguna Potrok Aike an annual precipitation sum of 150 mm has been observed (Zolitschka et al., 2006). Mean annual wind speeds of 7.4 m/s occur at Rio Gallegos; primarily from westerly directions (Weischet, 1996; Baruth et al., 1998). Recent series of precipitation measurements (1999-2005) at Laguna Potrok Aike reveal that easterly wind directions are often combined with precipitation whereas west winds do not carry considerable amounts of moisture into the area (Mayr et al., 2007b).

Field work and laboratory methods

From August to November 2008 the ICDP lake deep drilling expedition 5022 (PASADO) was carried out with the GLAD800, a containerized barge system equipped with a CS-1500 drill rig and operated by the non-profit organization DOSECC (Drilling, Observation and Sampling of the Earths Continental Crust). Hydraulic piston corer and extended nose devices were used as drill tools. Full core runs consisted of 2.92 m sediment sections in Butyrate liners (inner diameter: 66.34 mm) plus 8 cm sediment of the core catcher. At two drill sites a total of

four (Site 1) and three (Site 2) overlapping core series have been recovered (Fig. 2.1). Liners were cut into 1.5 m sections on the drilling barge, then shuttled to the shore using a custom-built catamaran and finally stored in a cooling container in which they were shipped to the University of Bremen, Germany, for storage in the GEOPOLAR core repository at 4°C.

Smear slides of core catcher sediment were prepared in the shore-based field laboratory according to Myrbo (2007) for the microscopic identification of sedimentary components such as carbonates or volcanogenic minerals.

A new protocol for sediment core treatment and subsampling for multiproxy analyses was developed for PASADO (Ohlendorf et al., 2011) and applied after plastic liners were cut lengthwise with a manual splitter at the laboratory of the University of Bremen. Depending on sediment consistency, core sections were split with sharpened plates made of phosphorous bronze, nylon wire or steel guitar strings. In a next step the sediment surface was cleaned and smoothed with a sharpened blade. Photographic images were taken from fresh surfaces using a digital camera image scanner (SmartCIS, Smartcube) with a resolution of 500 dpi. With this system individual 10 cm long images (jpg format) of the sediment are automatically stitched together into a composite of the complete core section. Core sections were described lithologically, using the categories rock class (sedimentary), rock type (siliciclastic, volcaniclastic, organic), grain size, structure, texture, components (gastropods, plant macro remains, animal bones) and color. Core descriptions were entered into the ICDP Drilling Information System (DIS) database (Conze et al., 2007) to make them available to the entire PASADO scientific community. Based on lithologic characterization and after macroscopic correlation of parallel cores from both sites, two composite profiles were assembled. Site 2 was established as the key site with the composite record 5022-2CP based on three parallel holes (Fig. 2.2) with a total recovery rate of 95.2%. Sections of undisturbed sediment and without gaps were selected to establish the chronostratigraphy for this composite profile.

Plant macro remains of aquatic mosses were sampled from 5022-2CP for radiocarbon dating. Samples were sieved through a 200 µm sieve, cleaned with demineralized water and dried at 60°C before they were sent to the Poznan Radiocarbon Laboratory for AMS-^{14}C determination. The top 18 m of 5022-2CP were not sampled for radiocarbon dating. Instead, ^{14}C dates were transferred for this section from the profile PTA03/12+13 (Haberzettl et al., 2007) using lithological features and magnetic susceptibility data as means for correlation. The latter have been obtained from cling-film covered cores in 5 mm increments with a Bartington MS2F-sensor mounted on an automated scanner.

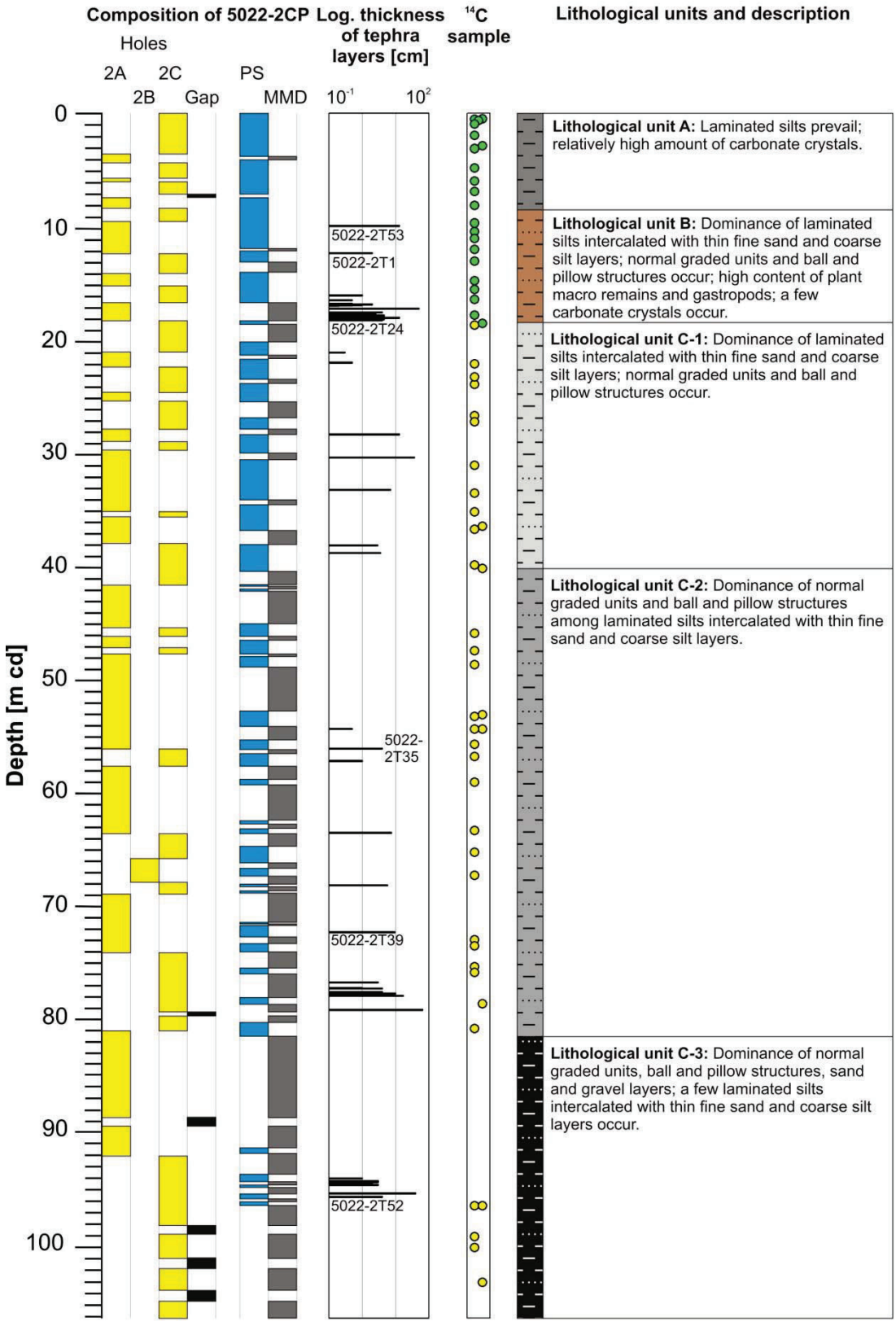

Fig. 2.2: Composition and lithology of the composite profile from site 2 (5022-2CP) of Laguna Potrok Aike. 2A, 2B and 2C: holes of site 2; PS: pelagic sediment; MMD: mass movement deposits and gaps illustrated if their thicknesses increase 10 cm. Tephra layers are indicated according to their average depths. Radiocarbon samples in green circles are correlated ages from PTA03/12+13 (Haberzettl et al., 2007); those in yellow are samples from 5022-2CP.

Calibration of all radiocarbon dates from 5022-2CP as well as re-calibration of the correlated dates from PTA03/12+13 was carried out with the CalPal_2007_HULU calibration dataset (Weninger and Jöris, 2008) and the download-version of the CalPal calibration software (Weninger et al., 2010). CalPal was preferred, because other calibration software like Calib or OxCal do not allow to calibrate radiocarbon ages back 50 ka BP. There was no need to apply any age correction, as a hard-water effect was neither detected for modern aquatic plants growing in the littoral zone of the lake nor for autochthonously precipitated carbonates (Haberzettl et al., 2005). For age-depth modeling the depth scale was event-corrected, i.e. the thicknesses of instantaneous events like volcanic ash layers and mass movement deposits were subtracted from the overall sediment thickness. This event-correction encompasses 60.29 m. The maximum chronostratigraphic sediment depth for age-depth modeling was thus reduced to 45.80 m cd-ec (m of event-corrected composite depth). For this corrected depth scale two age-depth models were developed using the mixed-effect regression after Heegaard et al. (2005): the first age-depth model by running two iterations with the mixed-effect regression and the second by running the mixed-effect regression only with ages that strictly follow the law of superposition. The mixed-effect regression is regarded as a method relatively robust with regard to outliers. In addition to the uncertainty of the individual radiocarbon date it considers how representative the dates are in relation to the population of other close by dates. This method also produces error margins for the established age-depth model. The statistical software Tinn-R (Version: 2.3.5.2) and the libraries mgcv and agedepth (downloaded from http://www.eecrg.uib.no/ on 3.11.2010) were used for calculations. To support the radiocarbon-based chronology, two additional stratigraphic methods were considered: tephrochronology and geomagnetic relative paleointensities.

To characterise volcanic ash layers, glass components of tephra samples were analyzed for their element geochemistry with an electron microprobe at the Tephrochronology Analytical Unit of the University of Edinburgh, UK. Analyses were performed on polished thin-sections on a five-spectrometer Cameca SX-100 electron microprobe with a beam diameter of 5 µm and an accelerating voltage (beam current) of 15 keV (2 nA) for major elements and 15 keV (80 nA) for minor elements. Standard calibration blocks and glass standards were used for calibration and control of accuracy during analyses.

The comparison of geomagnetic relative paleointensity focuses on the period from 55 to 25 cal. ka BP because this is the period most critical for chronology. The average initial temporal resolution in years (a) per individual data point of the records used are 11.34 a (age-model 1), 9.44 a (age-model 2), 10 a after cutoff frequency 1/3000 a (^{10}Be-flux to Summit in Greenland:

Muscheler et al. (2005)), 48 a (SAPIS: Stoner et al. (2002)), 200 a (stack from the Mediterranean Sea and Somali Basin: Meynadier et al. (1992)) and 220 a (Lake Baikal: Peck et al. (1996)). The stack from the Mediterranean Sea and Somali Basin comprises the highest resolution records (> 10 cm/ka) from the marine stack SINT-200 (Guyodo and Valet, 1996) and the stack from the South Atlantic Ocean (SAPIS: Stoner et al. (2002)) comprises five high-resolution records (14.9 to 25 cm/ka) located in the sub-Antarctic region. Each of the Laguna Potrok Aike datasets was interpolated at 10 a intervals, then smoothed in order to illustrate the millennial variability and, finally, the correlation coefficients were calculated. For more details on the paleomagnetic record of Laguna Potrok Aike, the reader is referred to Lisé-Pronovost et al. (Lisé-Pronovost et al., 2013).

Results

Lithology

The total length of the composite profile from Site 2 (5022-2CP) is 106.09 m and comprises 101.02 m of sediment (Fig. 2.2). Broken liners, ineffective core catchers and the lack of sedimentary features for core correlation caused 24 gaps summing up to the missing 5.06 m. Six gaps of 52 cm thickness are assumed to theoretically have contained pelagic sediment as they are over- and underlain by this type of sediment. The remaining eighteen gaps of 454 cm in combined thickness are related to event deposits as they are either over- or underlain by very coarse-grained mass movement deposits. Often the very coarse-grained sediment from the basal units of mass movements caused broken liners or flushed-out sections and consequently created gaps in the record in 5022-2CP.

The composite profile consists of six different but recurring sediment structures: laminated silts (Fig. 2.3A), laminated silts intercalated with thin fine sand and coarse silt layers (Fig. 2.3B), ball and pillow structures (Fig. 2.3C), normally graded beds (Fig. 2.3D), structureless sand with fine gravel layers (Fig. 2.3E) and light-colored silt layers (Fig. 2.3H).

Laminated silts (Fig. 2.3A) have contributions of clay and small amounts of sand. The lamination is characterized by changing colors ranging from light to dark grey, greenish to bluish grey and brownish grey and is most distinct for the topmost 18 m. Laminae thickness varies in the cm- and dm-scale without any sharp boundaries. Laminated silts are interpreted as pelagic sediments as their accumulation results from continuous settling of particles through the water column to the lake floor.

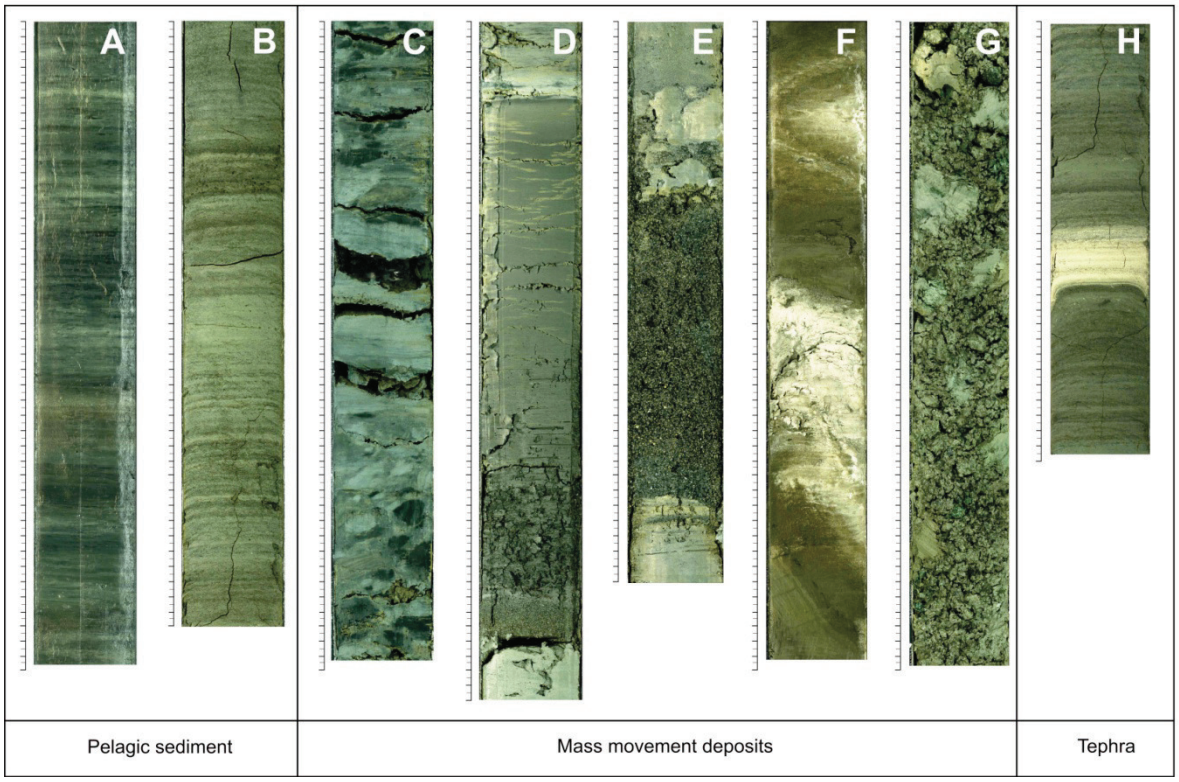

Fig. 2.3: Different classes of sediment structures from 5022-2CP. The scale to the left of each photography is in cm. A) Laminated silts (1.87-2.28 m cd), B) laminated silts intercalated with thin fine sand and coarse silt layers (55.49-55.90 m cd), C) ball and pillow structure (19.45-19.88 m cd), D) normally graded beds (21.38-21.93 m cd), E) structureless sand and fine gravel layer (34.18-34.56 m cd), F) unique folded layer (77.45-77.99 m cd), G) unique matrix supported structure (87.92-88.36 m cd), H) Light-colored layer of sorted silt (55.80-56.08 m cd).

Laminated silts intercalated with thin fine sand and coarse silt layers (Fig. 2.3B) differ from laminated silts as they contain a few coarser layers which are millimeter-thick and dark grey to black in color. As these layers are homogenous or normally graded, the contact to the overlying sediment is either sharp or gradual while the contact to underlying laminated silts is always sharp. Laminated parts are interpreted as pelagic sediments, whereas the coarse-grained intercalations reflect event-deposits. The frequency of these event-deposits varies between one per centimeter to one per decimeter. Although their frequency can be high, their contribution to this sediment type remains low. Thus, they are not subtracted for event correction.

Normally graded beds interrupt pelagic sediments. In 5022-2CP they reach up to 3.5 m in thickness and mostly consist of three units: 1) a fining-upward base of dark grey to black coarse silt, sand or gravel often containing abundant plant fragments, 2) a homogeneous silt to clay layer and 3) a thin layer of light-colored clay and silt on top (Fig. 2.3D). Such structures

in lacustrine sediments have been interpreted as turbidites or homogenites resulting from mass movements (Sturm et al., 1995; Girardclos et al., 2007; Bertrand et al., 2008).

Sometimes ball and pillow structures (Fig. 2.3C) underlie these graded beds and originate from the same mass movement. They consist of brownish, bluish or greenish-grey rounded silt and clay nodules up to several decimeters in size embedded in a dominantly coarse (up to gravel) and unsorted mostly dark grey matrix. Structureless sand and fine gravel layers (Fig. 2.3E) consist of homogenous, not graded blackish sands and/or fine gravel showing sharp upper and lower contacts. They reach a thickness of a few decimeters and sometimes contain organic macro remains (Fig. 2.6B). They are also interpreted as the result of mass movement deposits but very likely of a different type compared to normally graded beds.

Light-colored and sorted silt layers comprise bent, laminated or homogeneous sediment structures (Fig. 2.3H). Contacts to over- and underlying sediments are relatively sharp and sometimes irregular. Some layers show a coarser base of not more than 1 cm in thickness containing light-colored as well as black grains. Smear slides reveal a dominance of volcanic glass shards, pumice and amorphous clasts and sometimes also phenocrysts of volcanogenic minerals. Consequently, these deposits have been interpreted as tephra layers, which are distributed throughout 5022-2CP and reach individual thicknesses of up to 50 cm (Fig. 2.2). As all described tephra layers result from Andean volcanic eruptions in a distance of at least 150 km (Haberzettl et al., 2007; Haberzettl et al., 2008), thick tephra layers probably not completely result from fallout, but also from lake internal reworking and fluvial or eolian reworking of volcanic ash material that was deposited in the sparsely vegetated steppe environment surrounding the lake. Some tephra layers actually show structures of reworking (bent layers, mixing with lacustrine sediment components). The coarser base of some tephras might be the effect of sorting after settling through the water column or the result of a gradual decrease in explosivity of the related volcanic eruption.

Based on the dominating sedimentary characteristics and on the degree of dominance of mass movement deposits, 5022-2CP is divided into five lithological units (Fig. 2.2):

Lithological unit A (0-8.82 m cd) is almost completely dominated by pelagic laminated silts. The color spectrum changes downwards from light and brownish grey to dark grey while lamination gets more diffuse. Smear slides show a relatively high content of carbonate crystals. Furthermore, low amounts of aquatic mosses and gastropods are characteristic for this unit.

Lithological unit B (8.82-18.72 m cd) mainly consists of pelagic laminated silts intercalated with thin fine sand and coarse silt layers. The color spectra of laminations vary between dark

grey (in the upper part) and brownish and light gray (in the lower part). Furthermore, a few normally graded beds, ball and pillow structures as well as homogenous sand layers occur. The thickness of normally graded beds does not exceed 20 cm while clay caps are absent. Their color spectrum varies from brownish grey at the top to dark grey at the base. These sediment structures deviate from the thicker and clay-capped graded units which dominate the underlying lithological unit C. A high amount of aquatic mosses occurs between 15 and 18.6 m cd. Gastropods are relatively frequent as well as a few fish bones and carbonate crystals above 14.2 m cd.

Lithological unit C (18.72-106.09 m cd) is subdivided into three subunits (C-1, C-2, C-3) according to percentage, frequency and thickness of mass movement deposits. No gastropods, bones or carbonate crystals occur in this unit.

Lithological unit C-1 (18.72-40.23 m cd) is dominated by pelagic laminated silts intercalated with thin fine sand and coarse silt layers. The lamination is poor in contrast to lithological units A and B. The color spectrum turns to greenish and bluish grey. All three identified types of mass movement deposits (normally graded beds; ball and pillow structures; structureless sand and fine gravel layers) occur.

Lithological unit C-2 (40.23-81.53 m cd) is mainly composed of the same sedimentary structures as lithological unit C-1. However, the percentage of mass movement deposits increases (Fig. 2.2) and some events exceed 1 m in thickness. The majority of mass movement deposits consists of normally graded beds, some of them containing fine gravel at the base. A prominent feature is one folded structure of pelagic sediment and tephra (Fig. 2.3F) followed by a 90 cm thick normally graded bed.

Lithological unit C-3 (81.53-106.09 m cd) is dominated by normally graded sediment structures which typically increase 1 m in thickness. Pelagic sediments are almost absent and the amount of gravel in mass movement deposits is generally higher compared to units C-1 or C-2. Fine gravels occur in some ball and pillow structures as well as at the base of normally graded beds. One outstanding and 1.5 m thick matrix supported layer occurs at 88 m cd. It consists of angular silt and clay clasts in a matrix of basaltic sand and gravel (Fig. 2.3G). The clasts appear to be remobilized pelagic sediments as lamination is preserved in some of these clasts and the angular morphology suggests a short-distance transport. The angular basaltic gravel probably originates from erosion of basaltic lava at the southwestern lake shore.

Tephra analyses and correlation

Prior to this study, six tephra layers have been documented in different sediment cores from Laguna Potrok Aike (Haberzettl et al., 2009). The upper three ash layers from PTA03/12+13 were correlated stratigraphically to 5022-2CP (Fig. 2.4), while the older three tephra layers were geochemically compared with microprobe data obtained from a total of 19 volcanic ashes from 5022-2CP (Wastegård et al., 2013).

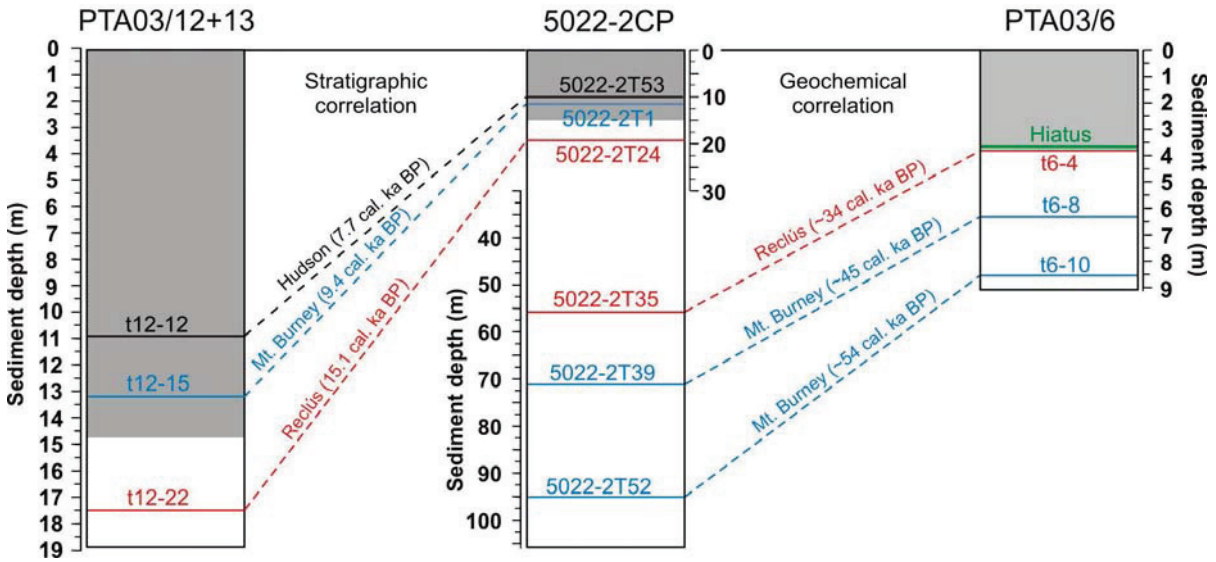

Fig. 2.4: Stratigraphic tephra correlation of 5022-2CP (100 m water depth) with PTA03/12+13 (95 m water depth) and geochemical tephra correlation of 5022-2CP with PTA03/6 (30 m water depth). Ages of tephra layers t12-12, t12-15 and t12-22 are recalibrated after Stern et al. (2008) and t6-4, t6-8 and t6-10 are from Haberzettl et al. (2009). The hiatus of PTA03/6 was caused by erosion due to a low lake level (Anselmetti et al., 2009; Haberzettl et al. 2008). Note different depth scales. Gray shading marks Holocene deposits.

The latest compilation of available dates for the upper three tephra layers from the Andean volcanoes Hudson, Mt. Burney and Reclús was published by Stern (2008) and recalibrated with the CalPal_2007_HULU calibration curve (Tab. 2.3). In the case of the Mt. Burney ash layer, three geochemically indifferent Mt. Burney eruptions have been documented between the Hudson and Reclús tephras spanning the time window from 7,64 to 10,320 cal. BP (Kilian et al., 2003). For the sediments of Laguna Potrok Aike, only one Mt. Burney tephra occurs between Hudson and Reclús ash layers. This volcanic ash has been correlated to the youngest Mt. Burney tephra layer (Haberzettl et al., 2007), which is interpreted as the major eruption with a large ash fan whereas the other two eruptions produced only local ash deposits (Kilian et al., 2003).

The lower three ash layers from Mt. Burney and Reclús volcanoes described by Haberzettl et al. (2007, 2008, 2009) are geochemically identical with 5022-2T35, 5022-2T39 and 5022-2T52 (Tab. 2.1) and have been used for correlation. Analyses show that 5022-2T39 and 5022-2T52 are rhyolitic with SiO_2 values ranging from 74 to 77% and K_2O values from 1.5 to 1.7% (Fig. 2.5A) suggesting Mt. Burney as the volcanic source (Stern, 2008; Haberzettl et al., 2009). Although the geochemical composition is similar, 5022-2T39 has a higher contents in MgO, FeO_{tot} and CaO compared to 5022-2T52 (Fig. 2.5B) and can be clearly distinguished. The main component of 5022-2T35 (type a) has a dacitic composition making it difficult to determine the source of the volcanic eruption. The SiO_2 vs. K_2O scatterplot (Fig. 2.5) indicates volcanoes of the Northern Andean Volcanic Zone (NAVZ) as a potential source, i.e. volcanoes Viedma, Lautaro or Aguilera (Kilian et al., 2003; Stern, 2008). In contrast, a tephra layer with a similar geochemistry was inferred to be an older Reclús tephra by Haberzettl et al. (2008). A minor rhyolitic component (type b) was also analyzed for this tephra.

Tab. 2.1: Geochemical data of tephra layers 5022-2T35, 5022-2T39 and 5022-2T52, shown as mean oxide concentrations (wt %) and 1 standard deviation in parentheses. Only analyses above 94% are included in the means (n: number of analyses).

	5022-2T35 (type a)	**5022-2T35 (type b)**	**5022-2T39**	**5022-2T52**
n	9	2	24	14
SiO_2	68.70 (1.34)	73.76 (0.26)	71.64 (0.75)	73.57 (0.93)
TiO_2	0.52 (0.05)	0.12 (0.02)	0.35 (0.02)	0.25 (0.02)
Al_2O_3	14.74 (0.29)	12.38 (0.86)	12.93 (0.27)	12.63 (0.23)
FeO_{tot}	2.73 (0.13)	1.23 (0.30)	1.92 (0.10)	1.42 (0.10)
MnO	0.05 (0.01)	0.04 (0.03)	0.05 (0.01)	0.04 (0.01)
MgO	0.84 (0.15)	0.29 (0.13)	0.52 (0.03)	0.38 (0.03)
CaO	3.07 (0.12)	1.38 (0.06)	2.31 (0.10)	1.84 (0.14)
Na_2O	4.23 (0.13)	3.58 (0.37)	4.51 (0.13)	4.55 (0.17)
K_2O	2.38 (0.06)	3.22 (0.14)	1.60 (0.07)	1.60 (0.07)
P_2O_5	0.10 (0.01)	0.03 (0.01)	0.05 (0.01)	0.04 (0.01)
Total	**97.36 (1.83)**	**96.03 (1.37)**	**95.88 (0.94)**	**96.33 (1.15)**

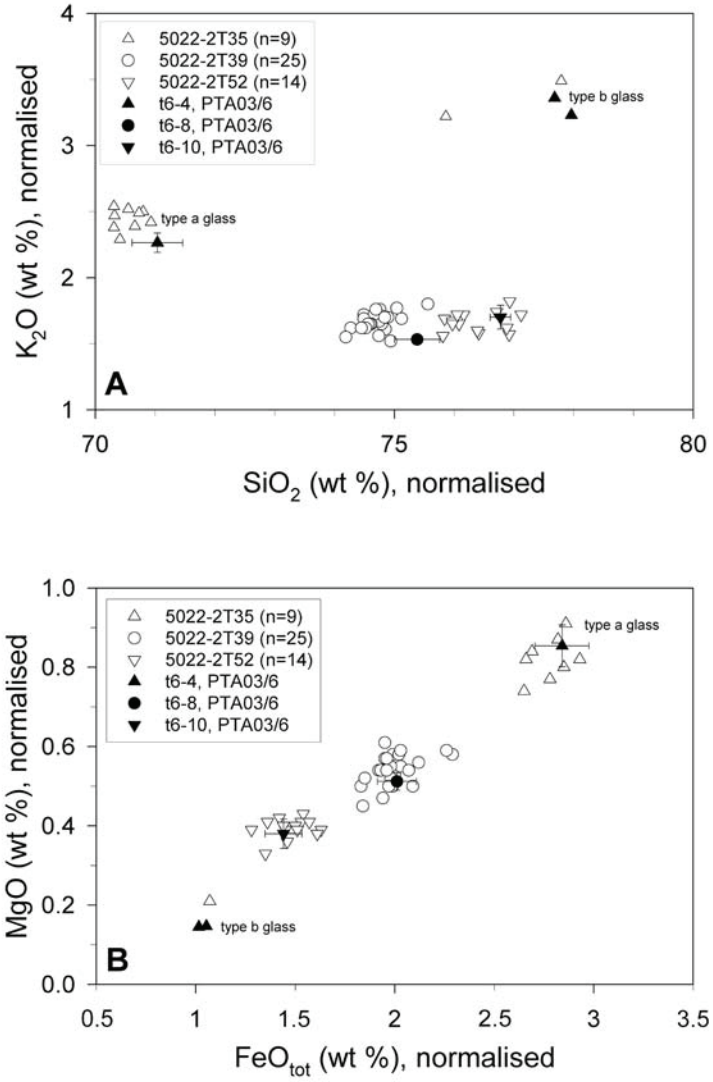

Fig. 2.5: Microprobe analyses of selected tephra layers from Laguna Potrok Aike (for all analyzed data: see Wastegard et al., 2013). All data from PTA03/6 show mean values and 1 sd (standard error) (Haberzettl et al., 2008 and Wulf, personal communication, 2010). A) Bi-plot of SiO_2 vs. K_2O, B) bi-plot of FeO_{tot} vs. MgO. All data are normalised to 100%.

All three geochemically analyzed tephras can be correlated with tephras from core PTA03/6 (Haberzettl et al., 2008) (Fig. 2.5). The rhyolitic ashes are correlated with tephra layers at 643 cm (t6-8) and 859 cm (t6-10) of PTA03/6 while both glass components of 5022-2T35 correspond to tephra layer t6-4 at 359 cm of PTA03/6. The agreement between the different analyses is high and the small deviations in glass chemistry (e.g. slightly higher SiO_2 values in Haberzettl et al. (2008)) are probably due to different instruments and analytical procedures applied.

Radiocarbon dates, chronology and sedimentation rate

For the Holocene and the Late Glacial part of the lacustrine record from Laguna Potrok Aike radiocarbon dating was carried out on carbonates precipitated from the water column, bulk sediment and different organic macro remains (Haberzettl et al., 2007). As carbonates are

generally absent below 18 m cd for 5022-2CP, plant remains, in most cases stems of aquatic mosses, were the only biogenic sediment component available for AMS ^{14}C dating. These aquatic mosses are concentrated in layers intercalated within pelagic sediment sections (Fig. 2.6A) as well as in basal layers of mass movement deposits (Fig. 2.6B). The former were preferably sampled because the likelihood of obtaining ages that do not represent the time of deposition is much higher for mass movement deposits. Nevertheless, dating was also carried out for some samples from such deposits in order to obtain ^{14}C ages over the entire length of the composite sediment sequence. In general, dating of aquatic mosses might involve some degree of reworking at Laguna Potrok Aike. An alternative option would be to obtain other material for dating (e.g. pollen, aquatic algae) which is not concentrated in layers. This would not necessarily eliminate reservoir effects and was not performed at 5022-2CP as it implies to sieve large amounts of pelagic sediment.

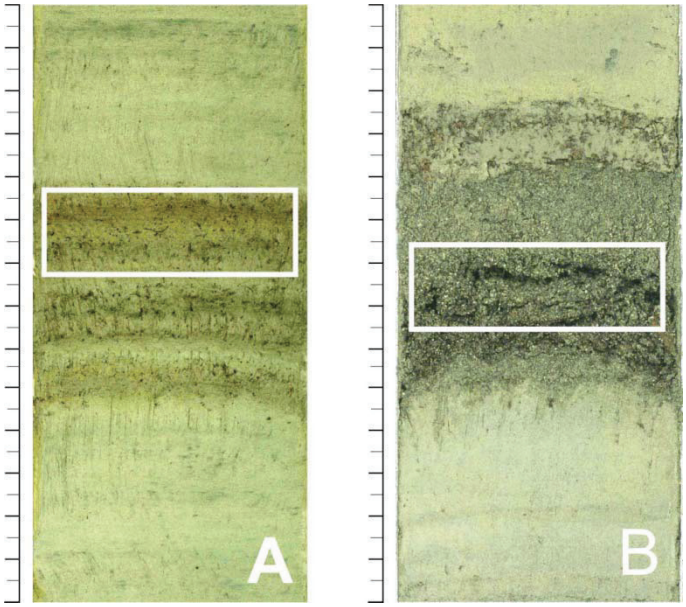

Fig. 2.6: Layers with high concentration of plant macro remains from aquatic mosses in A) laminated silts (related radiocarbon date: POZ-32495) and B) in a structure less sand layer (POZ-32492). Both positions were used for radiocarbon dating; white boxes show sampling location.

In total, 58 radiocarbon dates are available (Tab. 2.2; Fig. 2.7). 21 ages were correlated from PTA03/12+13 for the upper 18 m of 5022-2CP. These comprise the last 16 cal. ka BP. Three dates were interpreted as reworked (Haberzettl et al., 2007) and thus omitted. In order to achieve a consistent interpretation, Poz-8391 and Poz-5071 were reinterpreted as event deposit as the former was obtained from a sand-layer and the latter from reworked Reclús tephra of PTA03/12+13. Below 18 m cd, 37 dates cover a time range between 18 and 51 cal. ka BP.

Extremely low ^{14}C values were measured for three samples yielding infinite ages (Tab. 2.2). These ages were excluded from age-depth modeling.

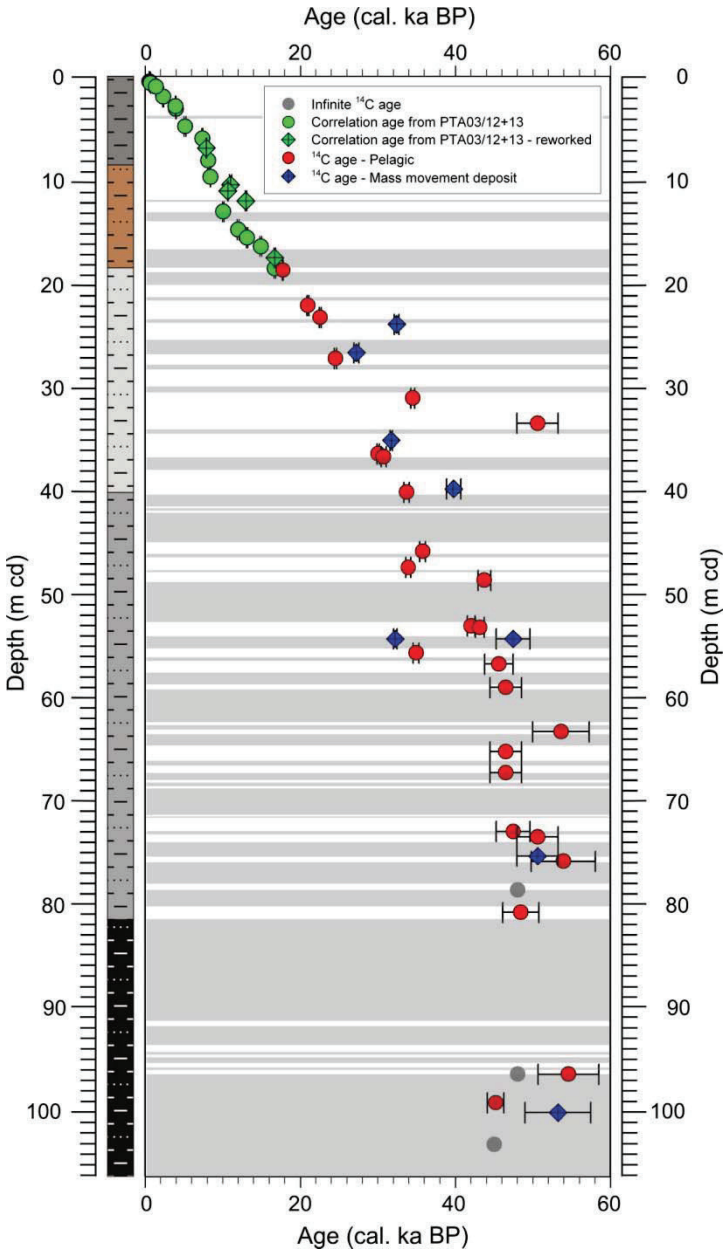

Fig. 2.7: Depth distribution of ^{14}C ages in 5022-2CP (1σ error). Lithology and event deposits (grey shading) are indicated.

Intervals with mass movement deposits as well as tephra layers were removed to compile an event-corrected composite profile (cd-ec) for age-depth modeling which was carried out by mixed-effect regression for 45.80 m cd-ec. This method is regarded to be relatively robust to outliers (Heegaard et al., 2005). However, it ignores the law of superposition. Two age-models (1 and 2) have been developed, one following the mixed-effect regression and the other by additionally acknowledging the law of superposition.

Tab. 2.2: AMS radiocarbon ages from 5022-2CP of Laguna Potrok Aike calibrated with CalPal applying the CalPal_2007_HULU calibration curve. Ages from reworked sediment sections are printed in bold. $\delta^{13}C$ and C-mass as measured during AMS ^{14}C determination.

Laboratory no.	Sediment depth (m cd)	Event corrected sediment depth (m cd-ec)	^{14}C Age (BP)	Error (1σ)	$\delta^{13}C$ (‰)	C-mass (mg)	Sample description	Calibrated age (cal. BP)	Error (1σ)
Poz-834[1]	0.51	0.51	440	30	-22.7	0.85	Stems of aquatic moss	510	30
Poz-897[1]	0.56	0.55	655	25	-15.7	1.49	Bulk sediment	630	50
Poz-3570[1]	0.67	0.67	735	25	-8	1.30	Calcite fraction of bulk sample	690	20
Poz-896[1]	0.92-1.04	0.92-1.04	1470	40	-20.8	2.0	Stems of aquatic moss	1370	40
Poz-5182[2]	1.96	1.95	2300	35	-22.7	1.57	Twig of Berberis	2290	70
Poz-8549[2]	2.88	2.87	3600	35	2.2	6.28	Calcite fraction of bulk sample	3910	50
Poz-8390[2]	3.10-3.15	3.10-3.15	3625	35	-33.9	0.5	Stems of aquatic moss	3940	50
Poz-8398[2]	4.83	4.53	4465	50	-28.3	1.09	Stems of aquatic moss	5130	120
Poz-8550[2]	6.00	5.71	6440	70	-5.1	6.28	Calcite fraction of bulk sample	7360	60
Poz-8391[2]	6.91	6.63	7025	50	-21.5	0.51	**Stems of aquatic moss**	7870	60
Poz-8546[2]	8.12	7.83	7260	50	3.8	2.01	Calcite fraction of bulk sample	8090	60
Poz-8392[2]	9.69	9.37	7580	50	-28.3	2.56	Stems of aquatic moss	8390	40
Poz-8393[2]	10.44	9.97	9640	50	-28.4	2.43	**Stems of aquatic moss**	11000	140
Poz-8547[2]	11.00-11.08	10.53-10.61	9410	50	6.6		**Calcite fraction of bulk sample**	10640	60
Poz-8394[2]	12.00	11.37	11090	60	-26.8	1.94	**Stems of aquatic moss**	12980	80
Poz-5985[2]	13.04	12.22	8930	50	-18.9	2.28	Bone of Tuco Tuco	10060	110
Poz-8548[2]	14.78	13.00	10240	60	8.4	3.61	Calcite fraction of bulk sample	11970	130
Poz-8396[2]	15.55	13.78	11200	60	-30	1.69	Stems of aquatic moss	13130	80
Poz-8397[2]	16.40	14.61	12490	70	-31.2	1.60	Stems of aquatic moss	14900	140
Poz-5072[2]	16.78-18.20	14.70	12850	70	-25.8	2.64	**Stems of aquatic moss**	15420	90
Poz-5073[2]	18.48-18.54	14.93-14.99	13450	70	-28.7	2.69	Stems of aquatic moss	16710	100
Poz-37017	18.69	15.13	14540	70	-27.6	1.56	Stems of aquatic moss	17760	50
Poz-37022	22.09	16.74	17460	80	-29.2	1.63	Stems of aquatic moss	20970	120
Poz-37007	23.25	17.90	18700	120	-39.9	0.91	Stems of aquatic moss	22570	110
Poz-32491	23.90	18.23	27910	240	-25.9	2.12	**Stems of aquatic moss**	32420	280
Poz-34233	26.65	19.42	22450	140	-30.7	2.24	**Stems of aquatic moss**	27230	320
Poz-37020	27.20	19.69	20490	120	-28	1.11	Stems of aquatic moss	24510	150
Poz-37008	31.01	22.14	30300	300	-32.9	1.51	Stems of aquatic moss	34500	240
Poz-37010	33.45	24.46	47000	2000	-23.5	1.40	Organic macro remains	50590	2670

Tab. 2.2f: AMS radiocarbon ages from 5022-2CP of Laguna Potrok Aike calibrated with CalPal applying the CalPal_2007_HULU calibration curve. Ages from reworked sediment sections are printed in bold. $\delta^{13}C$ and C-mass as measured during AMS ^{14}C determination.

Laboratory no.	Sediment depth (m cd)	Event corrected sediment depth (m cd-ec)	^{14}C Age (BP)	Error (1σ)	$\delta^{13}C$ (‰)	C-mass (mg)	Sample description	Calibrated age (cal. BP)	Error (1σ)
Poz-34235	35.10	25.49	26930	210	-28.5	3.03	**Stems of aquatic moss**	31720	140
Poz-34236	36.38	26.67	25110	180	-25	1.45	Stems of aquatic moss	30030	170
Poz-34237	36.66	26.95	25820	190	-27.3	2.64	Stems of aquatic moss	30750	320
Poz-32492	39.77	28.69	34500	500	-27.7	2.54	**Stems of aquatic moss**, Fig 6B	39770	910
Poz-37011	40.09	28.98	29300	300	-28.9	1.86	Stems of aquatic moss	33700	350
Poz-37012	45.81	30.30	31900	300	-28.3	2.33	Organic macro remains	35780	380
Poz-37002	47.34	31.34	29600	300	-30.7	1.24	Stems of aquatic moss	33930	310
Poz-37013	48.58	32.32	40000	1000	-28	2.27	Stems of aquatic moss	43730	810
Poz-34238	52.98	32.82	37300	800	-28.5	2.37	Stems of aquatic moss	42040	500
Poz-37003	53.12	32.96	39200	700	-28.6	1.64	Stems of aquatic moss	43140	570
Poz-32493	54.23	33.88	27680	230	-24.3	1.30	**Stems of aquatic moss**	32230	230
Poz-37014	54.23	33.88	44000	2000	-24	1.18	**Stems of aquatic moss**	47450	2200
Poz-37075	55.59	34.15	30800	400	-18.1	0.63	Stems of aquatic moss	34920	380
Poz-34239	56.66	34.71	42000	2000	-28.7	2.25	Stems of aquatic moss	45610	1850
Poz-34240	58.91	36.00	43000	2000	-30	1.29	Stems of aquatic moss	46510	2040
Poz-34241	63.18	36.70	50000	3000	-30.4	2.36	Stems of aquatic moss	53610	3630
Poz-37018	65.11	37.33	43000	2000	-26.8	2.13	Organic macro remains	46510	2040
Poz-32494	67.13	38.87	43000	2000	-28.3	1.08	Stems of aquatic moss	46510	2040
Poz-34242	72.80	40.56	44000	2000	-30.3	2.43	Stems of aquatic moss	47450	2200
Poz-37004	73.32	40.66	47000	2000	-39.7	1.71	Stems of aquatic moss	50590	2670
Poz-34243	75.18	41.40	47000	2000	-34.8	2.27	**Stems of aquatic moss**	50590	2670
Poz-37006	75.68	41.67	51000	4000	-32.3	1.50	Stems of aquatic moss	53910	4130
Poz-37021	78.43	42.39	>48000		-18.9	1.18	Organic macro remains		
Poz-32495	80.60	42.97	45000	2000	-27.2	1.64	Stems of aquatic moss, Fig. 6A	48430	2320
Poz-34245	96.21	45.71	>48000		-30.4	2.46	Stems of aquatic moss		
Poz-37015	96.21	45.71	52000	4000	-27.2	1.26	Organic macro remains	54580	3940
Poz-37016	98.95	45.79	42000	1000	-26.2	1.06	Organic macro remains	45200	1060
Poz-34246	99.89	45.80	50000	4000	-30.6	2.05	**Stems of aquatic moss**	53220	4250
Poz-32496	102.96	45.80	>45000		-32	0.82	**Stems of aquatic moss**		

[1]Haberzettl et al. 2005; [2]Haberzettl et al. 2007.

For age-model 1 (Fig. 2.8A and B) thirteen dates on remobilized material were excluded prior to the mixed-effect regression. The first iteration (Fig. 2.8A) reveals that (1) some radiocarbon dates considerably exceed the 95% confidence interval of the calculated age-depth model and (2) the age-depth modeling below 43 m cd-ec produces an age reversal caused either by a lack of reliable material for dating or because the radiocarbon method is close to its age-limit (>45 cal. ka BP). Therefore, a second iteration with the mixed-effect regression was restricted to dates above 43 m cd-ec (two more dates were not considered) and excludes four dates considerably exceeding the confidence interval of the first iteration (Fig. 2.8B). As this chronology does not extent to the base of the composite record, the age-depth model was extrapolated below 43 m cd-ec down to a basal depth of 45.80 m cd-ec resulting in an age of 51.2 cal. ka BP. This is the maximum age for 5022-2CP with age-model 1 as only event deposits occur below.

Age-model 2 was developed on the youngest possible radiocarbon ages and strictly according to the law of superposition (Fig. 2.9). Thus not only radiocarbon ages on some of the reworked material (iteration 1) and dates excluded during iteration 2 were discarded but a total number of 29 calibrated dates (19 for age-model 1). Hence, age-model 2 is based only on four dates below 20 m cd-ec. Most of the discarded radiocarbon ages exceed the 95 % confidence interval of age- model 2. The extrapolation below 44.79 m cd-ec yields a bottom age of 45.2 cal. ka BP for the basal depth of 45.80 m cd-ec.

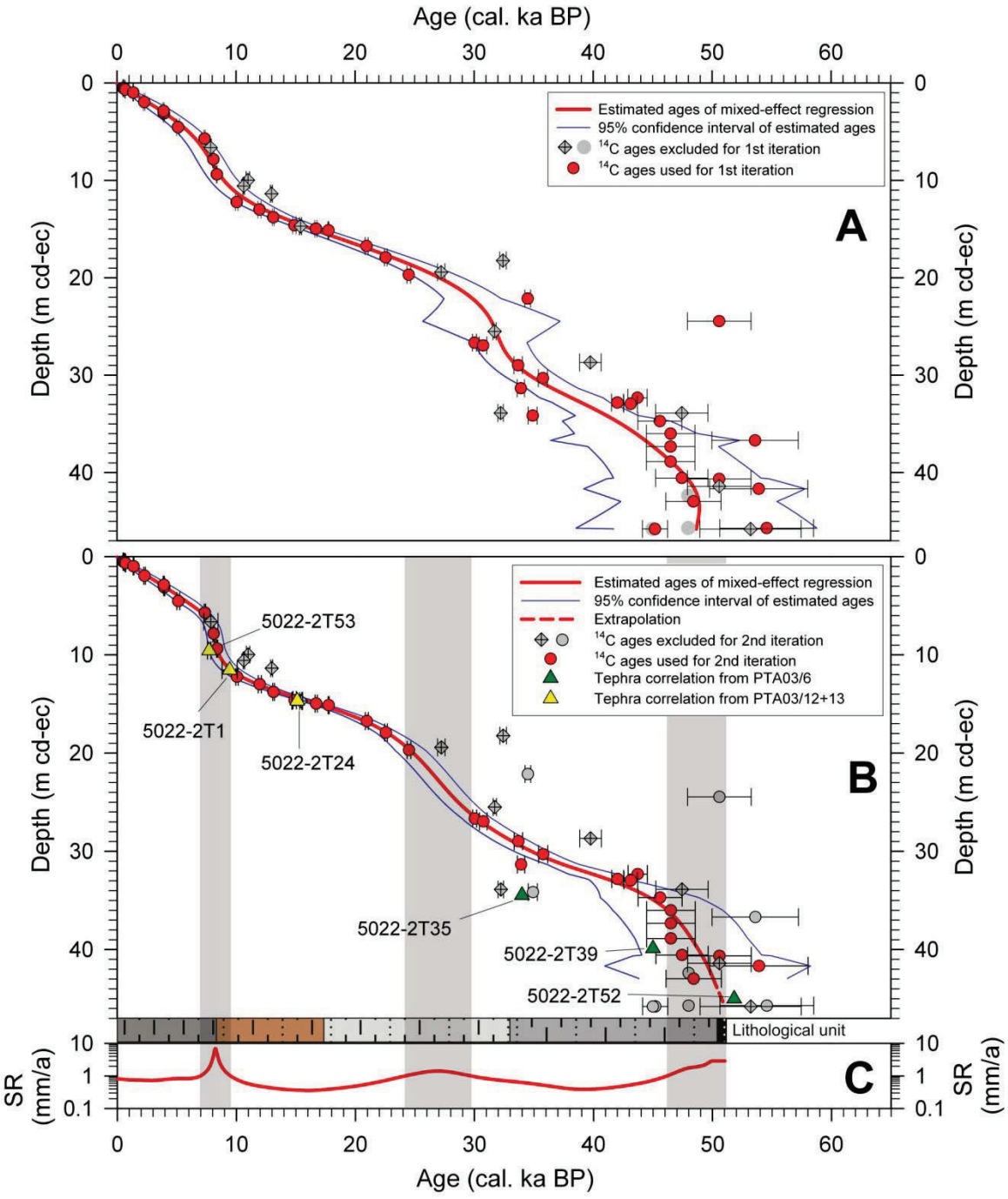

Fig. 2.8: First (A) and second (B) iteration (age-model 1) of the mixed-effect regression for 5022-2CP-ec using the constant-variance function. (C) Sedimentation rate based on this age-depth model processed for each millimetre. Gray shading marks periods with increased sedimentation rates. Tephra correlation according to Haberzettl et al. (2008, 2009).

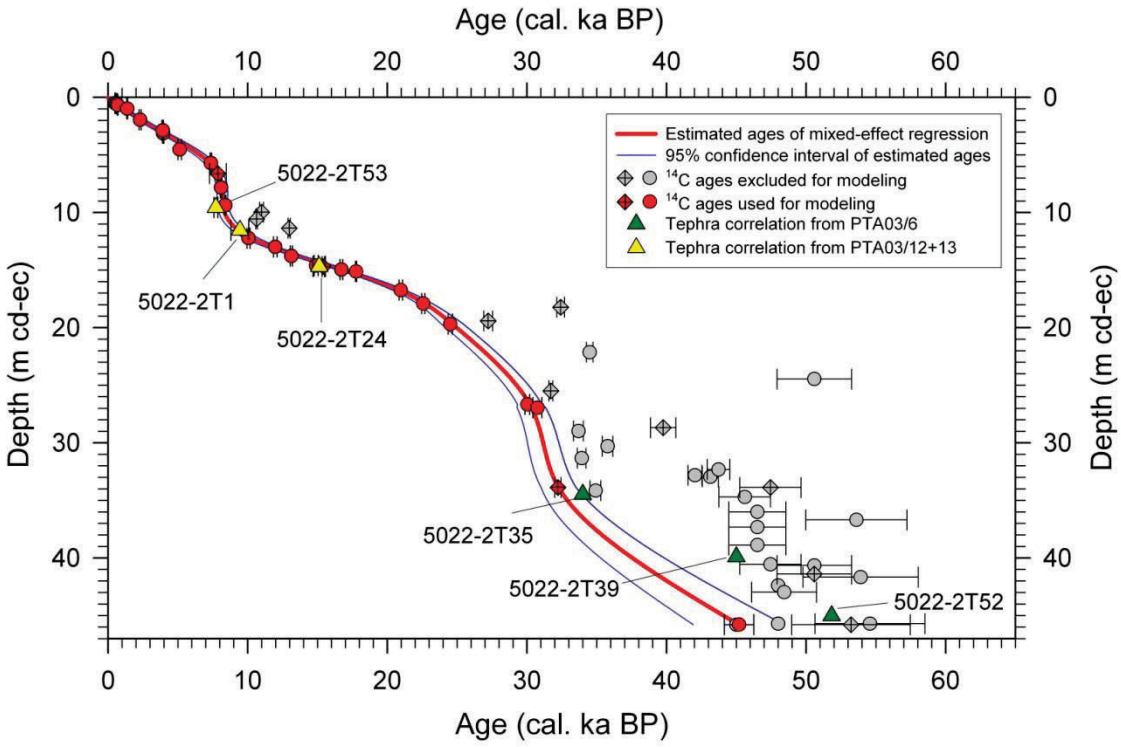

Fig. 2.9: Mixed-effect regression for 5022-2CP-ec using the constant-variance function. Ages for modeling were selected strictly according to the law of superposition (age-model 2).

In order to validate these age-depth models, we compared the PTA03/12+13 age-depth relation with age-models 1 and 2 for the last 16 cal. ka BP based on their magnetic susceptibility records (Fig. 2.10). Generally, they show a fairly good correlation with PTA03/12+13 suggesting a consistent age transfer to 5022-2CP. Slight shifts of magnetic susceptibility peaks between 8 and 10 cal. ka BP and prior to 12 cal. ka BP result from differences of our age model compared to the model performed by Haberzettl et al. (2007). They used a linear interpolation and included the Mt. Burney tephra (t12-15) dated by Kilian et al. (2003) for their age model. The upper three tephras from PTA03/12+13 have been dated independently by peat bogs and lake sediments (Kilian et al., 2003; McCulloch et al., 2005; Stern, 2008) and tend to be younger than the estimated ages from both of our age models; but their 95 % confidence intervals overlap (Tab. 2.3).

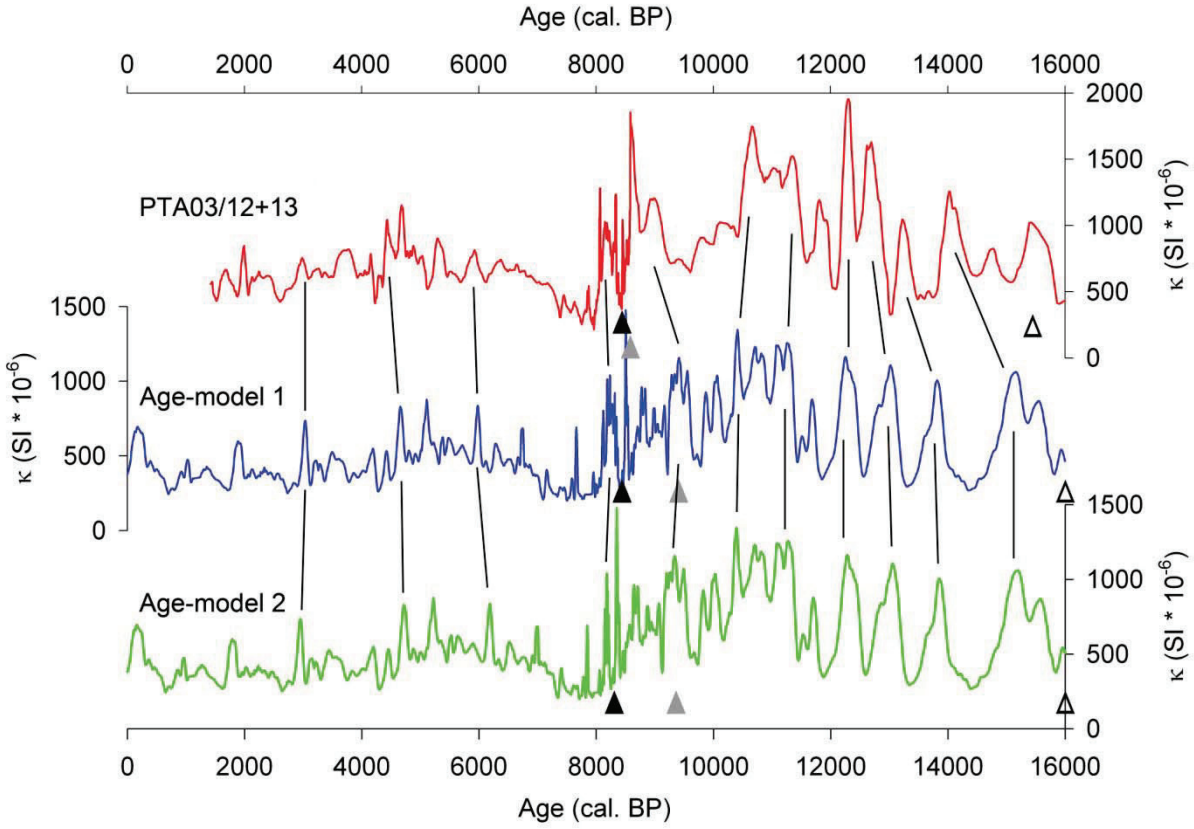

Fig. 2.10: Correlation of magnetic susceptibility from PTA03/12+13 and 5022-2CP with age-model 1 and age-model 2 using 11-point running means. Ages of PTA03/12+13 have been recalibrated with the CalPal_2007_HULU calibration curve prior to linear interpolation according to Haberzettl et al. (2007). Triangles show tephra layers with their ages in the respective age model.

Tab. 2.3: Correlated tephra layers with ages according to age-model 1 compared to ages from Stern et al. (2008). Uncalibrated literature dates of 5022-2T1, 5022-2T24 and 5022-2T53 were recalibrated with CalPal and the CalPal_2007_HULU calibration curve. Dates of 5022-2T35, 5022-2T39 and 5022-2T52 are according to the age model of Haberzettl et al. (2009).

Tephra layer	Source volcano	Age model 1 (cal. ka BP)	Age (cal. ka BP)
5022-2T53	Hudson	8.40 ± 0.63	7.72 ± 0.14 (Stern et al. (2008))
5022-2T1	Mt. Burney	9.43 ± 0.72	9.44 ± 0.64 (Stern et al. (2008))
5022-2T24	Reclús	16.03 ± 0.56	15.12 ± 0.45 (Stern et al. (2008))
5022-2T35	(NAVZ)	44.53 ± 3.81	~34 (Haberzettl et al (2009)
5022-2T39	Mt. Burney	48.70 ± 4.95	~45 (Haberzettl et al (2009)
5022-2T52	Mt. Burney	50.87 ± 6.35	~54 (Haberzettl et al (2009)

The tephra correlation beyond 30 cal. ka BP from PTA03/6 to 5022-2T35 seems to confirm age-model 2, whereas the correlation to 5022-2T39 and to 5022-2T52 seems to verify age-

model 1 (Fig. 2.8, 2.9). However, the age of 5022-2T35 as obtained from PTA03/6 is not very reliable because it results from a linear interpolation between a ^{14}C dated tephra layers ca. 5 m above (14.9 ± 0.3 cal. ka BP) and at 3.5 m below (48.5 ± 2.5 cal. ka BP) this tephra. Moreover, it is a combination of two different coring locations from the slope of the lake basin (Haberzettl et al., 2009). Here we improve the dating of these tephra layers by applying age-model 1 (Tab. 2.3).

Finally, relative paleointensity results (cf. Lisé-Pronovost et al., 2013) were compared with independently dated records worldwide to further validate our age models (Fig. 2.11). The millennial-scale variability using age-model 1 correlates much better to the global dipole field derived from independent archives, including cosmogenic isotopes, marine and lacustrine sediments (Meynadier et al., 1992; Guyodo and Valet, 1996; Peck et al., 1996; Stoner et al., 2002; Muscheler et al., 2005). In all cases, the correlation coefficients are significantly higher using age-model 1 compared to age-model 2 (Fig. 2.11). The minimum in relative paleointensity at ca. 38-39 cal. ka BP (using age-model 1), coeval with the intensity low derived from the ^{10}Be flux of the Summit ice core from Greenland, might correspond to the Laschamp geomagnetic excursion (Lisé-Pronovost et al., 2013), which was dated to 40.4 ± 2 ka (2σ) on lava flows at the type locality in the Massif Central, France (Guillou et al., 2004). Some of the differences in the paleointensity records most likely result from temporal offsets associated with the individual chronologies, which are to the limits of the radiocarbon method at 35 to 50 cal. ka BP (Hughen, 2007). This is illustrated, for example, by comparing SAPIS and PASADO records, where the correlation coefficient would be higher if the chronologies were slightly adjusted within dating uncertainties. Nonetheless and even on their own chronologies, the good correspondence between the SAPIS and PASADO records between 40 and 50 cal. ka BP supports age-model 1.

In conclusion, age-model 1 is favoured and was used to calculate sedimentation rates for event-corrected 5022-2CP (Fig. 2.8C). Three periods are noticeable during which sedimentation rates exceed 1 mm/a: 6.6-9.4 ka BP, 23.7-31.1 ka BP and 46.3-51.2 ka BP. Minima occur at ~3 cal. ka BP (0.75 mm/a), ~15 cal. ka BP (0.37 mm/a) and ~38 cal. ka BP (0.40 mm/a). The event-corrected sedimentation rate averages 0.9 mm/a. Including the mass movement deposits it increases to 2.07 mm/a.

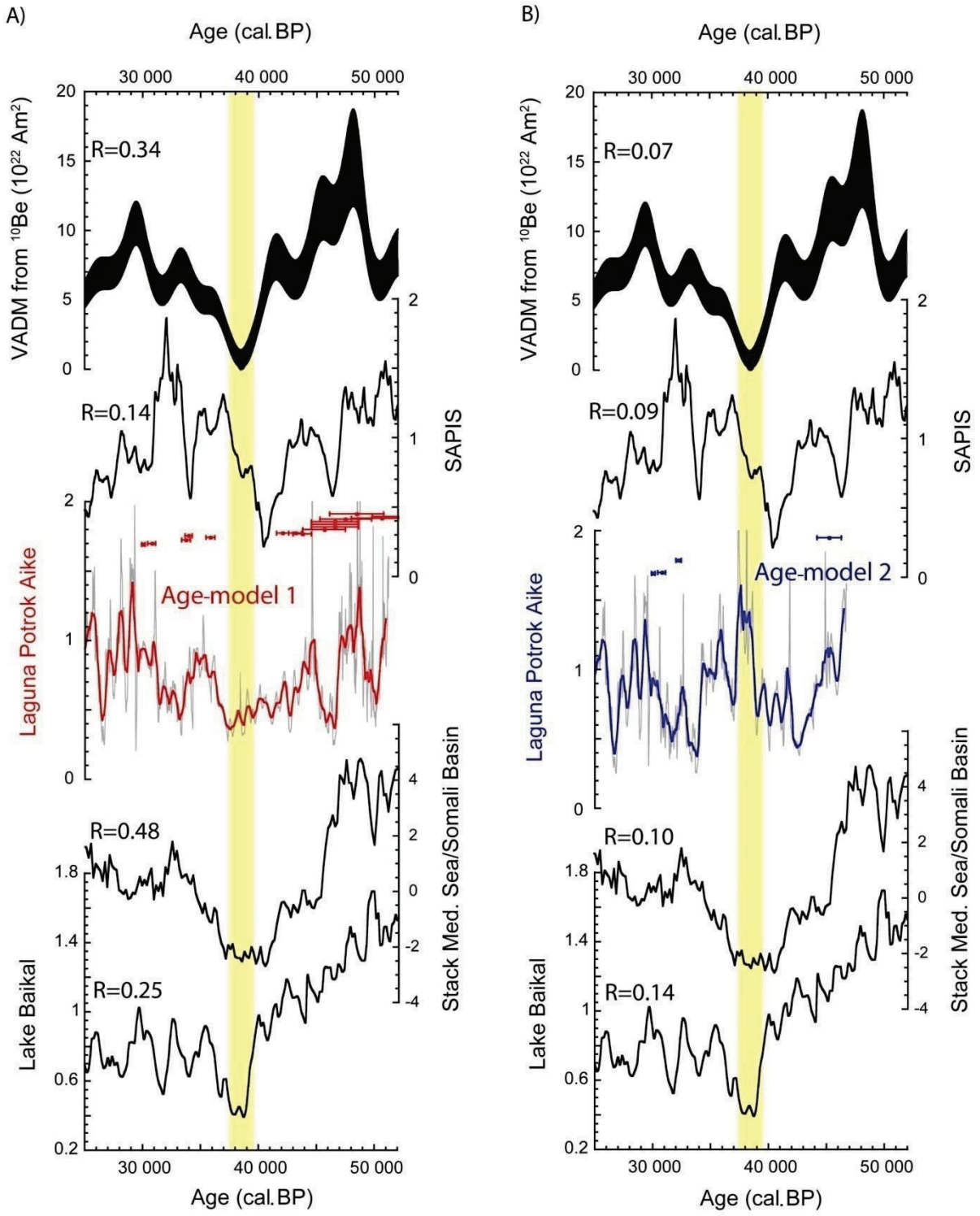

Fig. 2.11: Relative paleointensity proxy from Laguna Potrok Aike using A) age-model 1 and B) age-model 2 compared with independent geomagnetic field reconstructions from 55 to 25 cal. ka BP. From top to bottom: geomagnetic field intensity derived from the ^{10}Be-flux of the Summit ice core, Greenland (Muscheler et al., 2005), stack for the South Atlantic Ocean (SAPIS; Stoner et al., 2002), marine stack of the Mediterranean Sea and Somali Basin (Meynadier et al., 1992; Guyodo and Valet, 1996) and stack from Lake Baikal (Peck et al., 1996). Correlation coefficients are indicated. The shaded area indicates the geomagnetic Laschamp excursion at ca. 38-39 ka cal. BP in the PASADO and ^{10}Be-derived records.

Discussion

Lithology

The lithological units coincide with the mid to late Holocene (lithological unit A: present to 8.3 cal. ka BP) and the Glacial period (lithological unit C: 17.2 to 51.2 cal. ka BP) separated by a transitional zone that started prior to the Late Glacial and ended in the early Holocene (lithological unit B: 8.3 to 17.2 cal. ka BP) (Fig. 2.8B). This transition is well defined in the lower part of lithological unit B by the highest concentration of plant macro remains within the entire record. The abrupt onset of plant macro remains at 17.2 ± 0.5 cal. ka BP suggests a climatic and a related environmental change that persists until 12.2 ± 0.7 cal. ka BP. This corresponds with the time range between the first (~19-17 cal. ka BP) and the second (~13-12 cal. ka BP) major deglacial warming steps documented from marine sediments off Chile and Antarctic ice records (Lamy et al., 2007). This is also confirmed by the continental record from Lago Pollux (Chile, 46°S) suggesting deglacial warming after 18.6 cal. ka BP (Markgraf et al., 2007). Moreover, based on exposure ages deglaciation started in Patagonia after a final glacier advance at around 18 ka (Hein et al., 2010).

The high amount of plant macro remains (aquatic mosses) might result from an increased productivity due to deglacial warming and increased nutrient availability. As sand-wedges document former permafrost in southern Patagonia (Bockheim et al., 2009), its decay might have released organic carbon and nutrients in the drainage basin (Frey and Smith, 2005) which increased lacustrine productivity, predominantly in the littoral zone which is where aquatic mosses grow. However, it has been shown that recent permafrost degradation in the subarctic did not directly affect the trophic state of a lake and thus its sediments (Kokfelt et al., 2009).

Increased productivity of the lake is one possibility to explain the abundance of plant macrofossils at the transition from the Last Glacial Maximum (LGM) to the Late Glacial. Another explanation could be related to lake level fluctuations. Based on luminescence dates from overflow terraces, the lake level was highest around 17 cal. ka BP (Kliem et al., 2013a). Thus the transition from lithological unit C-1 to B might be a sedimentary response to the start of a post-LGM lake level lowering. This might have continued until 13.6 cal. ka BP, when the threshold of the lacustrine system with regard to carbonate precipitation was passed (Hahn et al., 2013; Jouve et al., 2013). Thus it might be argued, that the lake level during the early Late Glacial was comparable to modern conditions. A lake level decrease could also explain why aquatic mosses are so common immediately after 17 cal. ka BP: they were eroded from the

freshly exposed former littoral zone of the lake. However, this would have caused additional profundal accumulation. In contrast, the period is characterized by very low sedimentation rates (Fig. 2.8).

Laminations of lithological units A and B range in thickness from cm- to dm-scales with sedimentation rates from 0.37 to 1 mm/a. They seem to reflect changes in depositional conditions of decadal to centennial timescales. The processes generating these laminations are not clear but must have been more pronounced during the Holocene and the Late Glacial with rather distinct laminations. This is also supported by smear slide analyses. Assuming that the occurrence of autochthonous carbonate crystals indicates warmer and drier climatic conditions with responding lower lake levels for the Holocene and the Late Glacial (Haberzettl et al., 2007), no such period with carbonate precipitation occurred during the recovered glacial record at Laguna Potrok Aike.

Intercalations of thin fine sand and coarse silt layers in laminated silts as well as mass movement deposits increase below lithological unit A. Thus, the lacustrine sedimentation pattern was completely different between the Holocene and the glacial period with the Late Glacial as a transition. Nevertheless, also Holocene mass movement deposits have been identified by seismic and sediment core data (Haberzettl et al., 2007; Haberzettl et al., 2008; Anselmetti et al., 2009). Earthquakes as well as very low lake levels during the early Holocene might have triggered these events. In the case of multiple and simultaneous mass movements in the entire lake basin, as identified by seismic analysis, earthquakes were likely the trigger (Anselmetti et al., 2009). In addition, very low lake levels can decrease slope stability because of increased sedimentation on tilted subaquatic strata (Hampton et al., 1996; Locat and Lee, 2002; Strasser et al., 2007) and in combination with pore-fluid overpressure (Sultan et al., 2004). The latter might be the effect of a reduced water column in combination with increased deposition of fine-grained sediments on subaqueous slopes potentially closing off pore water under undrained conditions (Anselmetti et al., 2009). The relative position between mass movement deposits and erosional gaps suggests a successive collapse of subaquatic terraces (Kliem et al., 2013a).

As high-resolution data of the 3.5 kHz seismic survey allows sediment penetration only down to ~20 m (Anselmetti et al., 2009), no identification of simultaneous mass-movement events and thus paleo-earthquakes is possible below. It is likely that repeated lake level fluctuations during the last glacial period as well as earthquakes have resulted in frequent slope collapses which have not yet been detected. However, the maximum in mass movement frequency dur-

ing the last glacial period is most likely the effect of environmental changes and not a paleo-earthquake signal. Probably, permafrost in combination with sea-level-controlled groundwater influence enforced lake level fluctuations. Frozen ground reduces infiltration and thus increases surface runoff and decreases groundwater recharge. Consequently, groundwater influence should be less important. Due to permafrost sealing of the ground, a much higher percentage of precipitation, regardless if related to rainfall or snowmelt runoff events, reaches the lake. Moreover, buffering of the lake level via groundwater is reduced for two reasons: (1) the groundwater level follows or at least responds to the global sea level and thus should be considerably deeper and (2) permafrost isolates the lake water body from groundwater influence although forming a talik. If both aspects are completely true, groundwater influence would have been eliminated by permafrost during the last glacial period. Then the typically high precipitation variability as observed in semiarid regions is not buffered any more by groundwater influence which consequently causes a much more direct link between precipitation, snowmelt and the lake level. Thus more pronounced lake level fluctuations can be expected under permafrost conditions. Moreover, a higher percentage of precipitation is transferred to the lake as infiltration is eliminated and also evaporation is less effective under the generally colder air temperatures of the glacial period. Relict permafrost features (sand-wedges) are actually widespread in southern Patagonia (Bockheim et al., 2009) and sand-wedges have also been detected in the catchment of Laguna Potrok Aike where they suggest permafrost conditions around 35 ka (Kliem et al., 2013a). The general decrease of mass movement deposits with time might also be related to a reduced subaquatic relief as the result of sediment accumulation and slope consolidation.

In addition to laminated pelagic sediments and mass movement deposits, tephra layers are the third dominant sediment feature. However, no tephras from local eruptions of the PAVF have been documented for the 51 ka record, although this volcanic area provides a huge source of volcaniclastic material and eruptions are ongoing until at least the early Holocene (Corbella, 2002). Since volcanic activities of the PAVF have developed towards the east, dominating west winds might have inhibited tephra accumulation from younger eruptions in Laguna Potrok Aike and only remote Andean tephras were recorded. Over- and underlain by lacustrine sediment, cohesionless tephra layers consisting of sorted silt may have acted as shear zones at the subaquatic slopes resulting in mass movements. This would explain that only one tephra layer exists between tephra layer t6-4 and t6-10 of PTA03/6 as the others probably have been eroded and are only preserved in the central deep site of 5022-2CP (Fig. 2.5). This also suggests unidentified hiatuses in PTA03/6 as no hiatus has been documented below 34

cal. ka BP (Haberzettl et al., 2009) which would explain that the proximal sedimentation rate at PTA03/6 is less than 1.0 mm/a compared to 0.6-2.4 mm/a in the profundal zone at 5022-2CP.

Chronology

The elaborated radiocarbon chronology (age-model 1) is hampered by several outliers representing ages considerably younger and older than the estimated age after the second iteration of the mixed-effect regression. Different reasons can be regarded as the cause for these results: Stratigraphical mixing, hard-water and reservoir effects, variations in ^{14}C production (plateau effects) as well as contamination by modern carbon can theoretically influence radiocarbon dates (Cohen, 2003). Stratigraphical mixing caused e.g. by bioturbation or dating of roots as well as the hard-water effect can be excluded for this record. The observed concentration of aquatic moss fragments in certain sediment layers point to sedimentation events during which these mosses are transported from littoral to profundal zones of the lake (Fig. 2.6). Hence, it is not surprising that some dates from pelagic sediments vary towards higher ages indicating the dating of reworked material. Offsets to younger ages occur at the transition from lithological unit C-2 to C-1 until ca. 30 cal. ka BP. These apparently too young dates might be explained by the sensibility of samples closer to the dating limit of the radiocarbon method for contamination by modern carbon (Olson and Eriksson, 1972). Contamination is known from fungi and bacterial activity as they assimilate modern CO_2 if stored for many years within sediment cores (Geyh et al., 1974) or under wet conditions after sampling (Wohlfarth et al., 1991). This explanation seems to be unlikely in our case as the cores were continuously stored under cool and dark conditions; samples were taken relatively fast after coring (10-12 months) and immediately dried after sampling. The most prominent too young dates (Poz-37075 with 34.4 cal. ka BP in 34.15 m cd-ec; Poz-32493 with 32.2 cal. ka BP in 33.88 m cd-ec) seem to be confirmed by the tephra layer 5022-2T35 if dated according to Haberzettl et al. (2009) and by one ^{230}Th-age dated to 29.4 ± 5.9 ka in 34.95 m cd-ec (Nuttin et al., 2013) which question age-model 1. Considering these younger dates as true ages would imply a hiatus to the next older date of 10.1 to 12.3 ka. However, in the lithology no indication for such a large hiatus has been observed. Mass movements within that depth interval suggest some degree of erosion, but applying the mean event-corrected sedimentation rate of 0.9 mm/a a sediment package between ~9 and ~11 m would have to be eroded. This seems to be very unlikely for the profundal zone of the lake. Another option would be an unidentified hiatus re-

lated to desiccation. However, a permanent water column is suggested by continuous lacustrine sedimentation on the subaquatic terrace and by seismic results between ~30 and 53.5 ka (Gebhardt et al., 2012b). Furthermore, the age of 5022-2T35 from Haberzettl et al. (2009) is questionable. Short term fluctuations of the atmospheric $^{14}C/^{12}C$ ratio caused by increased production of ^{14}C as a result of low paleomagnetic field intensity are another option to explain too young ages. Data available for calibrating ^{14}C ages vary up to 2000 years for the time window 30-50 cal. ka BP (Schramm et al., 2000) indicating short term fluctuations in atmospheric ^{14}C concentration. The two affected radiocarbon dates differ from the estimated age by ~11 ka and ~9 ka, respectively. It is conceivable that the short-living aquatic mosses might document fluctuations in the atmospheric $^{14}C/^{12}C$ ratio. Whether this is a realistic explanation and whether this effect is as large as ca 10 ka needs to be further investigated. At the older part of the record (>45 cal. ka BP) radiocarbon dates tend to show an asymptotic behavior, which can be a sign of underestimated ages close to the dating limit of the radiocarbon method (Chappell et al., 1996). Upcoming publications of high resolution radiocarbon dates for varve-dated sediments of Lake Suigetsu (Japan) might improve our understanding of the terrestrial radiocarbon calibration models and underlying ^{14}C variations back to the dating limit of this method (Nakagawa et al., 2012).

Age-model 2 as the conservative alternative for the age-depth modeling of sediments from Laguna Potrok Aike seems to be disproved by the two oldest tephra layers (Fig. 2.8B) and after comparison with global geomagnetic relative paleointensity data (Fig. 2.11). Therefore, we suggest following age-model 1 as the most likely chronology for the time being. Nevertheless, most radiocarbon dates approaching the limits of this dating method (30-45/50 ka BP) can be questioned and thus efforts have been undertaken to improve the reliability of our time control by additional and independent dating methods. As Ar/Ar dating of volcanic ashes turned out to be impossible due to the lack of suitable potassium feldspars (M. Storey, 2011, pers. comm.), our focus is now directed towards luminescence dating. Analyses of 38 samples from core 5022-1D have already been carried out and evaluated (Buylaert et al., 2013). However, before these dates can be compared to the age models presented here, a thorough correlation between the composite profile from Site 2 (radiocarbon chronology and most other stratigraphic investigations) with Site 1 (luminescence dating) needs to be carried out.

Sedimentation rates

Calculated sedimentation rates for the sediment record range between 0.37 and 8.5 mm/a (mean: 2.07 mm/a). However, the percentage of mass movement deposits increases downcore but no erosion at their respective bases was assumed for the compilation of the event-corrected composite profile 5022-2CP and thus this effect is not reflected in the sedimentation rates. Sharp contacts to underlying sediments document some degree of erosion of pelagic sediments. Therefore, calculated sedimentation rates have to be regarded as minimum values as it is impossible to estimate the degree of erosion.

During three time periods sedimentation rates exceed 1 mm/a (Fig. 2.8C: 6.6-9.4 cal. ka BP, 23.7-31.1 cal. ka BP and 46.3-51.2 cal. ka BP). The first of these periods correlates with the transition from lithological unit B to A which is described as having the lowest lake level (33 m below the lake level of 2003) since the last glacial period due to dry conditions caused by strengthening of the Southern Hemispheric Westerlies (Haberzettl et al., 2007; Haberzettl et al., 2008; Anselmetti et al., 2009). Profundal sedimentation increased probably because the lake level lowering exposed older terraces to erosion. Furthermore, a reduced water body would result in reduced accumulation space and therefore in increased sedimentation rates at the coring location. A more negative water balance of the lake between 9.2 and 8.7 cal. ka BP with considerable variations afterwards is based on pollen and geochemical evidence (Mayr et al., 2007b).

If low lake levels at Laguna Potrok Aike cause higher sedimentation rates, increased sedimentation rates during the last glacial period centered around 27.4 and 48.8 cal. ka BP may also document lower lake levels. For the younger glacial period with higher sedimentation rates from 31.1 to 23.7 cal. ka BP it would be plausible to assume that at the begin of the LGM a general decrease in precipitation occurred which might have caused a lake level lowering with enforced erosion of the then exposed former littoral zone. However, this assumption needs to be verified by additional future studies. In contrast, the record from PTA03/6 documents a higher lake level between 45 and 51 cal. ka BP (Haberzettl et al., 2009). This is much higher than the modern water level and supported by IRSL dating of tephra layers now exposed at terrace-outcrops that have been deposited in the lake between 44 and 48 ka suggesting overflow conditions (Kliem et al., 2013a). Based on this data, the hypothesis that higher sedimentation rates are linked to lake level low stands has either to be falsified or the temporal lake level variability was much higher than anticipated.

Formation of the lake basin

The expected base of lacustrine sediments inferred by a seismic survey is in 370 m blf (below lake floor which is presently at 13 m a.s.l.) (Gebhardt et al., 2011). Considering an overall mean sedimentation rate of 2.07 mm/a for the entire history of Laguna Potrok Aike, the start of lacustrine sedimentation can be estimated to ~180 ka. This represents also the approximate date of the maar eruption as the crater bottom filled-up rapidly with groundwater after the eruption. However, this date contradicts the Ar/Ar date of 770 ± 240 ka for a basaltic clast from the phreatomagmatic tephra of the maar eruption (Zolitschka et al., 2006). Explanations for this discrepancy could be unreliable dating or frequent desiccations of the lake basin which introduce periods without sedimentation and sediment removal by deflation as observed for this region today, e.g. for Laguna Maar Bismarck (Gebhardt et al., 2012b). Indeed, stacked sand dunes approximately 200 m below the present lake level in the eastern part of the lake basin, i.e. older than 51.2 cal. ka BP, have been inferred by seismic data and support desiccation and deflation just prior to the start of the sedimentary record discussed here (Gebhardt et al., 2012b). So far, no desiccation hiatus was identified lithologically. However, mass movements might have eroded such features at the coring location. Although high lake levels are documented for this record, low lake levels have not been determined prior to the Late Glacial. Furthermore, the presence of aquatic mosses throughout 5022-2CP supports at least ephemeral water bodies for the last 51.2 cal. ka BP confirming that no desiccation occurred during this time interval. But periods of desiccation accompanied by wind erosion most likely existed before (Gebhardt et al., 2012b) reducing the total amount of accumulated sediment and thus bringing the extrapolated age for the bedrock to sediment transition (using the mean sedimentation rate) and the Ar/Ar date for the maar formation into agreement.

Conclusions and outlook

The Holocene and the glacial periods of the 106.09 m long composite profile from Site 2 (5022-2CP) of Laguna Potrok Aike can be distinguished by dominance of laminated silts and the occurrence of carbonate crystals during the Holocene and by laminated silts intercalated with fine sand and coarse silt layers as well as mass movement deposits during the last glacial. The transition is characterized by a high content of plant macro remains, that started abruptly at 17.2 ± 0.5 cal. ka BP and continued until 12.2 ± 0.7 cal. ka BP. This period correlates with the first and second major deglacial warming step known from marine and Antarctic ice core climate records. Mass movement deposits are important for the sedimentation history of the

lake basin as they comprise over 50% of the record and increase downward in frequency. Rapid and frequent lake level changes might have enforced the collapse of slopes during the glacial period which increased the occurrence of mass movement deposits. Their general decrease with time is probably the effect of decreasing sub-aquatic relief energy, slope consolidation and a less inclined slope angle during basin development.

Prevailing permafrost conditions and a decreased sea level decoupled the lake water body from ground water which made the lake level more susceptible to variations in precipitation. Moreover, frozen ground inhibited infiltration. Together, these permafrost-related factors increased not only the amplitude but also the frequency of glacial lake level fluctuations.

The complete record was datable with the radiocarbon method. Sufficient amounts of carbon were found in layers containing organic macro remains. In most cases stems of aquatic mosses were analyzed, which apparently grew throughout the record. For age-depth modeling, an event-corrected composite profile of 45.80 m cd-ec was developed using the mixed-effect regression procedure. Two age-depth models consider two different interpretations of the same data and have been validated with tephra correlations and geomagnetic relative paleointensity records. For the favored age-model 1 several outliers of significantly older and younger ages have been removed. The age-model 2 includes ages strictly according to the law of superposition. However and based on a comparison of both models with the global geomagnetic relative paleointensity and tephrochronological data, age-model 1 is preferred.

Applying age-model 1, the bottom age of the record was dated to 51.2 cal. ka BP. Throughout this time range the lake basin was permanently filled with water; the water column distinctly exceeded modern water depth between 45 and 51 cal. ka BP and around 17 cal. ka BP (Kliem et al., 2013a) and was much lower between 9.4 and 7.3 cal. ka BP (Anselmetti et al., 2009). Considering the Ar/Ar age of the maar eruption and the extrapolation of sedimentation rates to the lacustrine base inferred by seismic data, the lake basin should be completely filled with sediment. Most likely, persistent desiccations causing erosion or at least no sedimentation have to have existed before 51.2 cal. ka BP to explain this discrepancy.

Acknowledgements

This research is supported by the International Continental Scientific Drilling Program (ICDP) in the framework of the "Potrok Aike Maar Lake Sediment Archive Drilling Project" (PASADO). Funding for drilling was provided by the ICDP, the German Science Foundation

(DFG ZO 102/11-1,2), the Swiss National Funds (SNF), the Natural Sciences and Engineering Research Council of Canada (NSERC), the Swedish Vetenskapsradet (VR) and the University of Bremen.

References

Anselmetti, F.S., Ariztegui, D., De Batist, M., Gebhardt, A.C., Haberzettl, T., Niessen, F., Ohlendorf, C. and Zolitschka, B., 2009. Environmental history of southern Patagonia unravelled by the seismic stratigraphy of Laguna Potrok Aike. Sedimentology 56, 873-892.

Baruth, B., Endlicher, W. and Hoppe, P., 1998. Climate and desertification processes in Patagonia. Bamberger Geographische Schriften 15, 307-320.

Bertrand, S., Charlet, F., Chapron, E., Fagel, N. and De Batist, M., 2008. Reconstruction of the Holocene seismotectonic activity of the Southern Andes from seismites recorded in Lago Icalma, Chile, 39°S. Palaeogeography, Palaeoclimatology, Palaeoecology 259, 301-322.

Bockheim, J., Coronato, A., Rabassa, J., Ercolano, B. and Ponce, J., 2009. Relict sand wedges in southern Patagonia and their stratigraphic and paleo-environmental significance. Quaternary Science Reviews 28, 1188-1199.

Buylaert, J.P., Murray, A.S., Gebhardt, C., Sohbati, R., Ohlendorf, C., Thiel, C., Zolitschka, B. and The PASADO science team, 2013. Luminescence dating of the PASADO core 5022-1D from Laguna Potrok Aike (Argentina) using IRSL signals from feldspar. Quaternary Science Reviews 71, 70-80.

Caldenius, C., 1932. Las glaciaciones cuarternarias en la Patagonia y Tierra del Fuego. Geografisker Annaler 22, 1-164.

Chappell, J., Head, J. and Magee, J., 1996. Beyond the radiocarbon limit in Australian archeology and Quaternary research. Antiquity 70, 543-552.

Cohen, A.S., 2003. Paleolimnology. The History and Evolution of Lake Systems. Oxford University Press, Oxford.

Conze, R., Wallrabe-Adams, H., Graham, C. and Krysiak, F., 2007. Joint Data Management in ICDP Projects and IODP Mission Specific Platform Expeditions. Scientific drilling 4, 32-34.

Corbella, H., 2002. El campo volcano-tectónico de Pali Aike. *In* "Geología y Recursos Naturales de Santa Cruz. Asociación Geológica Argentina." (M. Haller, Ed.), pp. 285-302, Buenos Aires.

Frey, K.E. and Smith, L.C., 2005. Amplified carbon release from vast West Siberian peatlands by 2100. Geophysical research letters 32.

Gebhardt, A.C., De Batist, M., Niessen, F., Anselmetti, F.S., Ariztegui, D., Haberzettl, T., Kopsch, C., Ohlendorf, C. and Zolitschka, B., 2011. Deciphering lake and maar geometries from seismic refraction and reflection surveys in Laguna Potrok Aike (southern Patagonia, Argentina). Journal of Volcanology and Geothermal Research 201, 357-363.

Gebhardt, A.C., Ohlendorf, C., Niessen, F., De Batist, M., Anselmetti, F.S., Ariztegui, D., Kliem, P., Wastegård, S. and Zolitschka, B., 2012. Seismic evidence of up to 200 m lake level change in Southern Patagonia since MIS4. Sedimentology 59, 1087-1100.

Geyh, M.A., Krumbein, W.E. and Kudrass, H.-R., 1974. Unreliable 14C dating of long-stored deep-sea sediments due to bacterial activity. Marine Geology 17, 45-50.

Gilli, A., Ariztegui, D., Anselmetti, F.S., McKenzie, J.A., Markgraf, V., Hajdas, I. and McCulloch, R.D., 2005. Mid-Holocene strengthening of the Southern Westerlies in South America - sedimentological evidences from Lago Cardiel, Argentina (49°S). Global and Planetary Change 49, 75-93.

Girardclos, S., Schmidt, O.T., Sturm, M., Ariztegui, D., Pugin, A. and Anselmetti, F.S., 2007. The 1996 AD delta collapse and large turbidite in Lake Brienz. Marine Geology 241.

Guillou, H., Singer, B.S., Laj, C., Kissel, C., Scaillet, S. and Jicha, B.R., 2004. On the age of the Laschamp geomagnetic excursion. Earth and Planetary Science Letters 227, 331.

Guyodo, Y. and Valet, J.-P., 1996. Relative variations in geomagnetic intensity from sedimentary records: the past 200,000 years. Earth and Planetary Science Letters 143, 23-36.

Haberzettl, T., Fey, M., Lücke, A., Maidana, N., Mayr, C., Ohlendorf, C., Schäbitz, F., Schleser, G.H., Wille, M. and Zolitschka, B., 2005. Climatically induced lake level changes during the last two millennia as reflected in sediments of Laguna Potrok Aike, southern Patagonia (Santa Cruz, Argentina). Journal of Paleolimnology 33, 283-302.

Haberzettl, T., Corbella, H., Fey, M., Janssen, S., Lücke, A., Mayr, C., Ohlendorf, C., Schäbitz, F., Schleser, G.H., Wille, M., Wulf, S. and Zolitschka, B., 2007. Lateglacial and Holocene wet-

dry cycles in southern Patagonia: chronology, sedimentology and geochemistry of a lacustrine record from Laguna Potrok Aike, Argentina. The Holocene 17, 297-310.

Haberzettl, T., Kück, B., Wulf, S., Anselmetti, F., Ariztegui, D., Corbella, H., Fey, M., Janssen, S., Lücke, A., Mayr, C., Ohlendorf, C., Schäbitz, F., Schleser, G.H., Wille, M. and Zolitschka, B., 2008. Hydrological variability in southeastern Patagonia and explosive volcanic activity in the southern Andean Cordillera during Oxygen Isotope Stage 3 and the Holocene inferred from lake sediments of Laguna Potrok Aike, Argentina. Palaeogeography, Palaeoclimatology, Palaeoecology 259, 213-229.

Haberzettl, T., Anselmetti, F.S., Bowen, S.W., Fey, M., Mayr, C., Zolitschka, B., Ariztegui, D., Mauz, B., Ohlendorf, C., Kastner, S., Lücke, A., Schäbitz, F. and Wille, M., 2009. Late Pleistocene dust deposition in the Patagonian steppe - extending and refining the paleoenvironmental and tephrochronological record from Laguna Potrok Aike back to 55 ka. Quaternary Science Reviews 28, 2927-2939.

Hahn, A., Kliem, P., Ohlendorf, C., Zolitschka, B., Rosen, P. and the PASADO science team, 2013. Climate induced changes as registered in inorganic and organic sediment components from Laguna Potrok Aike (Argentina) during the past 51 ka. Quaternary Science Reviews 71, 154-166.

Hampton, M.A., Lee, H.J. and Locat, J., 1996. Submarine landslides. Reviews of Geophysics 34, 33-59.

Heegaard, E., Birks, H.J.B. and Telford, R.J., 2005. Relationships between calibrated ages and depth in stratigraphical sequences: an estimation procedure by mixed-effect regression. The Holocene 15, 612-618.

Hein, A.S., Hulton, N.R.J., Dunai, T.J., Sugden, D.E., Kaplan, M.R. and Xu, S., 2010. The chronology of the Lasr Glacial Maximum and deglacial events in central Argentine Patagonia. Quaternary Science Reviews 29, 1212-1227.

Hughen, K.A., 2007. Radiocarbon dating of deep-sea sediment. In: Proxies in Late Cenozoic Paleoceanography, Hillaire-Marcel and A. de Vernal (Eds.), Elsevier, 99-138.

Jouve, G., Francus, P., Lamoureux, S., Provencher-Nolet, L., Hahn, A., Haberzettl, T., Fortin, D. and Nuttin, L., 2013. Microsedimentological characterization using image analysis and XRF as indicators of sedimentary processes and climate changes during Late Glacial at Laguna Potrok Aike, Santa Cruz, Argentina. Quaternary Science Reviews.

Kilian, R., Hohner, M., Biester, H., Wallrabe-Adams, H.J. and Stern, C.R., 2003. Holocene peat and lake sediment tephra record from the southernmost Chilean Andes (53-55°S). Revista Geológica de Chile 30, 23-37.

Kliem, P., Buylaert, J.P., Hahn, A., Mayr, C., Murray, A.S., Ohlendorf, C., Veres, D., Wastegård, S., Zolitschka, B. and the PASADO science team, 2013. Magnitude, geomorphologic response and climate links of lake level oscillations at Laguna Potrok Aike, Patagonian steppe (Argentina). Quaternary Science Reviews 71, 131-146.

Kokfelt, U., Rosén, P., Schoning, K., Christensen, T.R., Förster, J., Karlsson, J., Reuss, N., Rundgren, M., Callaghan, T.V., Jonasson, C. and Hammarlund, D., 2009. Ecosystem responses to increased precipitation and permafrost decay in subarctic Sweden inferred from peat and lake sediments. Global Change Biology 15, 1652-1663.

Lamy, F., Kaiser, J., Arz, H.W., Hebbeln, D., Ninnemann, U., Timm, O., Timmermann, A. and Toggweiler, J.R., 2007. Modulation of the bipolar seesaw in the Southeast Pacific during Termination 1. Earth and Planetary Science Letters 259, 400-413.

Lisé-Pronovost, A., St-Onge, G., Gogorza, C., Zolitschka, B. and the PASADO science team, 2013. High-resolution paleomagnetic secular variation and relative paleointensity since the Late Pleistocene and Southern South America. Quaternary Science Reviews.

Locat, J. and Lee, H.J., 2002. Submarine landslides: advances and challanges. Canadian Geotechnical Journal 39, 193-212.

Markgraf, V., Whitlock, C. and Haberle, S., 2007. Vegetation and fire history during the last 18,000 cal yr B.P. in Southern Patagonia: Mallin Pollux, Coyhaique, Province Aisen. Palaeogeography, Palaeoclimatology, Palaeoecology 254, 492-507.

Markgraf, V. and Huber, U.M., 2010. Late and postglacial vegetation and fire history in Southern Patagonia and Tierra del Fuego. Palaeogeography, Palaeoclimatology, Palaeoecology 297, 351-366.

Mayr, C., Lücke, A., Stichler, W., Trimborn, P., Ercolano, B., Oliva, G., Ohlendorf, C., Soto, J., Fey, M., Haberzettl, T., Janssen, S., Schäbitz, F., Schleser, G.H., Wille, M. and Zolitschka, B., 2007a. Precipitation origin and evaporation of lakes in semi-arid Patagonia (Argentina) inferred from stable isotopes ($d^{18}O$, $d^{2}H$). Journal of Hydrology 334, 53-63.

Mayr, C., Wille, M., Haberzettl, T., Fey, M., Janssen, S., Lücke, A., Ohlendorf, C., Oliva, G., Schäbitz, F., Schleser, G.H. and Zolitschka, B., 2007b. Holocene variability of the Southern Hemisphere westerlies in Argentinean Patagonia (52°S). Quaternary Science Reviews 26, 579-584.

Mayr, C., Lücke, A., Maidana, N.I., Wille, M., Haberzettl, T., Corbella, H., Ohlendorf, C., Schäbitz, F., Fey, M., Janssen, S. and Zolitschka, B., 2009. Isotopic fingerprints on lacustrine organic matter from Laguna Potrok Aike (southern Patagonia, Argentina) reflect environmental changes during the last 16,000 years. Journal of Paleolimnology 42, 81-102.

Mazzarini, F. and D`Orazio, M., 2003. Spatial distribution of cones and satellite-detected lineaments in the Pali Aike Volcanic Field (southernmost Patagonia): insights into the tectonic setting of a Neogene rift system. Journal of Volcanology & Geothermal Research 125, 291-305.

McCulloch, R.D., Fogwill, C.J., Sugden, D.E., Bentley, M.J. and Kubik, P.W., 2005. Chronology of the Last Glaciation in Central Strait of Magellan and Bahía Inútil, Southernmost South America. Geografiska Annaler, Series A: Physical Geography 87, 289-312.

Meglioli, A., 1992. Glacial geology and geochronology of southernmost Patagonia and Tierra del Fuego, Argentina and Chile. Ph.D. Dissertation, Leigh University, Bethlehem PA U.S.A., 216.

Mercer, J.H., 1976. Glacial history of southernmost South America. Quaternary Research 6, 125-166.

Meyer, I. and Wagner, S., 2008. The Little Ice Age in southern Patagonia: comparison between paleoecological reconstructions and downscaled model output of a GCM simulation. PAGES News 16, 12-13.

Meynadier, L., Valet, J.-P., Weeks, R., Shackleton, N.J. and Hagee, V.L., 1992. Relative geomagnetic intensity of the field during the last 140 Ka. Earth and Planetary Science Letters 114, 39-57.

Moy, C.M., Dunbar, R.B., Guilderson, T.P. and Waldmann, N., 2011. A geochemical and sedimentary record of high southern latitude Holocene climate evolution from Lago Fagnano, Tierra del Fuego. Earth and Planetary Science Letters 302, 1-13.

Muscheler, R., Beer, J., Kubik, P.W. and Synal, H.-A., 2005. Geomagnetic field intensity during the last 60,000 years based on ^{10}Be and ^{36}Cl from the Summit ice cores and ^{14}C. Quaternary Science Reviews 24, 1849-1860.

Myrbo, A., 2007. Smear slide identifications: the practical basics. Limnological Research Center Core Facility, SOP Series, draft v. 3.1; downloaded on 3.11.2010 from www.lrc.geo.umn.edu.

Nakagawa, T., Gotanda, K., Haraguchi, T., Danhara, T., Yonenobu, H., Brauer, A., Yokoyama, Y., Tada, R., Takemura, K., Staff, R.A., Payne, R., Ramsey, C.B., Bryant, C., Brock, F., Schlolaut, G., Marshall, M., Tarasov, P. and Lamb, H., 2012. SG06, a fully continuous and varved sediment core from Lake Suigetsu, Japan: stratigraphy and potential for improving the radiocarbon calibration model and understanding of late Quaternary climate changes. Quaternary Science Reviews 36, 164-176.

Nuttin, L., Francus, P., Preda, M., Ghaleb, B. and Hillaire-Marcel, C., 2013. Authigenic, detrital and diagenetic minerals in the Laguna Potrok Aike sedimentary sequence. Quaternary Science Reviews.

Ohlendorf, C., Gebhardt, C., Hahn, A., Kliem, P. and Zolitschka, B., 2011. The PASADO core processing strategy - A proposed new protocol for sediment core treatment in multidisciplinary lake drilling projects. Sedimentary Geology 239, 104-115.

Olson, I.U. and Eriksson, K.G., 1972. Fractionation studies of the shell of Foraminifera. Etudes sur la Quaternaire dans le Monde, 921-923.

Peck, J.A., King, J.W., Colman, S.M. and Kravchinsky, V.A., 1996. An 84-kyr paleomagnetic record from the sediments of Lake Baikal, Siberia. Journal of Geophysical Research 101 (B5), 11,365-11,385.

Rabassa, J. and Clapperton, C.M., 1990. Quaternary glaciations of the southern Andes. Quaternary Science Reviews 9, 153-174.

Schnurrenberger, D., Russell, J. and Kelts, K., 2003. Classification of lacustrine sediments based on sedimentary components. Journal of Paleolimnology 29, 141-154.

Schramm, A., Stein, M. and Goldstein, S.L., 2000. Calibration of the ^{14}C time scale to >40 ka by ^{234}U-^{230}Th dating of Lake Lisan sediments (last glacial Dead Sea). Earth and Planetary Science Letters 175, 27-40.

Stern, C.R., 2008. Holocene tephrochronology record of large explosive eruptions in the southernmost Patagonian Andes. Bulletin of Volcanology 70, 435-454.

Stoner, J.S., Laj, C., Channell, J.E.T. and Kissel, C., 2002. South Atlantic and North Atlantic geomagnetic paleointensity stacks (0-80 ka): implications for inter-hemispheric correlation. Quaternary Science Reviews 21, 1141-1151.

Strasser, M., Stegmann, S., Bussmann, F., Anselmetti, F.S., Rick, B. and Kopf, A., 2007. Quantifying subaqueous slope stability during seismic shaking: Lake Lucerne as model for ocean margins. Marine Geology 240, 77-97.

Sturm, M., Siegenthaler, C. and Pickrill, R.A., 1995. Turbidites and 'homogenites'. A conceptual model of flood and slide deposits. 5ème congrès de Sédimentologie. ASF, Livre des Résumés 22.

Sultan, N., Cochonat, P., Canals, M., Cattaneo, A., Dennielou, B., Haflidason, H., Laberg, J.S., Long, D. and Mienert, J., 2004. Triggering mechanisms of slope instability processes and sediment failures on continental margins: a geotechnical approach. Marine Geology 213, 291-321.

Uliana, M.A. and Biddle, T., 1988. Mesozoic-Cenozoic paleogeographic and geodynamic evolution of southern South America. Revista Brasileira de Geosciencas 18, 172-190.

Wagner, S., Widmann, M., Jones, J., Haberzettl, T., Lücke, A., Mayr, C., Ohlendorf, C., Schäbitz, F. and Zolitschka, B., 2007. Transient simulations, empirical reconstructions and forcing mechanisms for the Mid-Holocene hydrological climate in southern Patagonia. Climate Dynamics 29, 333-355.

Wastegård, S., Veres, D., Kliem, P., Ohlendorf, C. and Zolitschka, B., 2013. Towards a late Quaternary tephrochronological framework for the southernmost part of South America – the Laguna Potrok Aike tephra record. Quaternary Science Reviews.

Weischet, W., 1996. Regionale Klimatologie. Teil 1: Die Neue Welt: Amerika, Neuseeland, Australien. Teubner, Stuttgart.

Weninger, B. and Jöris, O., 2008. A 14C age calibration curve for the last 60 ka: the Greenland-Hulu U/Th timescale and its impact on understanding the Middle to Upper Paleolithic transition in Western Eurasia. Journal of Human Evolution 55, 772-781.

Weninger, B., Jöris, O. and Danzeglocke, U., 2010. 2010. CalPal-2007. Cologne Radiocarbon Calibration & Palaeoclimate Research Package. http://www.calpal.de/, accessed 2010-05-25.

Wille, M. and Schäbitz, F., 2009. Late-glacial and Holocene climate dynamics at the steppe/forest ecotone in southernmost Patagonia, Argentina: the pollen record from a fen near Brazo Sur, Lago Argentino. Vegetation History and Archaeobotany 18, 225-234.

Wohlfarth, B., Skog, G., Possnert, G. and Holmquist, B., 1991. Pitfalls in the AMS radiocarbon-dating of terrestrial macrofossils. Journal of Quaternary Science 13, 137-145.

Zolitschka, B., Schäbitz, F., Lücke, A., Corbella, H., Ercolano, B., Fey, M., Haberzettl, T., Janssen, S., Maidana, N., Mayr, C., Ohlendorf, C., Oliva, G., Paez, M.M., Schleser, G.H., Soto, J., Tiberi, P. and Wille, M., 2006. Crater lakes of the Pali Aike Volcanic Field as key sites for paleoclimatic and paleoecological reconstructions in southern Patagonia, Argentina. Journal of South American Earth Sciences 21, 294-309.

Chapter 3:

Magnitude, geomorphologic response and climate links of lake level oscillations at Laguna Potrok Aike, Patagonian steppe (Argentina)

Published in: Quaternary Science Reviews (2013) 71: 131-146

P. Kliem (1), J.P. Buylaert (2,3), A. Hahn (1), C. Mayr (4,5), A.S. Murray (2), C. Ohlendorf (1), D. Veres (6), S. Wastegård (7), B. Zolitschka (1) and the PASADO science team (8)

(1) Geomorphology and Polar Research (GEOPOLAR), Institute of Geography, University of Bremen, Celsiusstr. FVG-M, D-28359 Bremen, Germany. (kliem@uni-bremen.de)

(2) Nordic Laboratory for Luminescence Dating, Department of Geosciences, Aarhus University, Risø DTU, DK-4000 Roskilde, Denmark

(3) Radiation Research Division, Risø National Laboratory for Sustainable Energy, Technical University of Denmark (Risø DTU), DK-4000 Roskilde, Denmark

(4) Institute of Geography, University of Erlangen-Nürnberg, Kochstr. 4/4, D-91054 Erlangen, Germany

(5) Institute of Paleontology and Geobiology and GeoBio-Center, University of Munich, Richard-Wagner-Str. 10, D-80333 München, Germany

(6) Department of Geology, Babes-Bolyai University, 400084 Cluj-Napoca, and Institute of Speleology, Romanian Academy, 400006 Cluj-Napoca, Romania

(7) Department of Physical Geography and Quaternary Geology, Stockholm University, SE-106 91 Stockholm, Sweden

(8) PASADO science team as listed at http://www.icdp-online.org/front_content.php?idcatart=2794

Abstract

Laguna Potrok Aike is a large maar lake located in the semiarid steppe of southern Patagonia known for its Late-Glacial and Holocene lake level fluctuations. Based on sedimentary, seismic and geomorphological evidences, the lake level curve is updated and extended into the last glacial period and the geomorphological development of the lake basin and its catchment area is interpreted.

Abrasion and lake level oscillations since at least ~50 ka caused concentric erosion of the surrounding soft rocks of the Miocene Santa Cruz Formation and expanded the basin diameter by approximately 1 km. A high lake level and overflow conditions of the lake were dated by luminescence methods and tephra correlation to the early Late Glacial as well as to ~45 ka. The lowest lake level of record occurred during the mid-Holocene. A further lake level drop was probably prevented by groundwater supply. This low lake level eroded a distinct terrace into lacustrine sediments. Collapse of these terraces probably caused mass movement deposits in the profundal zone of the lake. After the mid-Holocene lake level low stand a general and successive transgression occurred until the Little Ice Age maximum; i.e. ca. 40 m above the local groundwater table. Frequent lake level oscillations caused deflation of emerged terraces only along the eastern shoreline due to prevailing westerly winds. Preservation of eolian deposits might be linked to relatively moist climate conditions during the past 2.5 ka.

Precisely dated lake level reconstructions in the rain-shadow of the Andes document high last glacial and low Holocene lake levels that could suggest increased precipitation during the last glacial period. As permafrost in semiarid Patagonia is documented and dated to the last glacial period we argue that the frozen ground might have increased surficial runoff from the catchment and thus influenced the water balance of the lake. This is important for investigating the glacial to Holocene latitudinal shift and/or strengthening of the Southern Hemispheric Westerlies by using lake level reconstructions as a means to assess the regional water balance. Our interpretation explains the contradiction with investigations based on pollen data indicating drier climatic conditions for the last glacial period.

Keywords: ICDP-project PASADO, lake terraces, Southern Hemispheric Westerlies, permafrost, Holocene, Glacial

Introduction

Lake level reconstructions are mostly aiming at hydrological, i.e. paleoclimatic reconstruction. However, prior to any paleoclimatic interpretation, non-climatic aspects of lake level oscillations need to be identified and excluded from any paleoclimatic scenario (Duck et al., 1998). Furthermore, multiple lines of evidence (sedimentary, geomorphological, and more recently anthropogenic causes) are an advantage. A robust indicator to infer the lake level history is the occurrence of wave-cuts, beach terraces and beach ridges as they are directly formed at the shoreline. These structures allow exact reconstructions of former water levels and can be identified in seismic, bathymetric and hypsometric profiles as well as in sediment cores. Furthermore, in combination with profundal sediment core data, reconstruction of former water depths becomes possible. Inherent disadvantages of using terraces as paleoenvironmental archives are their sensitivity to subaerial and subaquatic erosion and accumulation as well as to difficulties in dating. Additionally, terraces require a relatively stable water level for an extended period of time to be formed.

Reconstructions from Patagonian lakes east of the Andes reveal distinct lake level changes during the Holocene (Stine and Stine, 1990; Gilli, 2003; Haberzettl et al., 2007; Anselmetti et al., 2009; Fey et al., 2009). As most lakes at the foot of the Andes are of glacial origin, evidence for pre-Holocene lake levels can only be found in extra-Andean Patagonia. So far, geomorphology-based lake level reconstructions are only known from Lago Cardiel (Stine and Stine, 1990) and Laguna Cari-Laufquén (Cartwright et al., 2011). A third promising site for lake level reconstructions is the currently endorheic Laguna Potrok Aike (Zolitschka et al., 2006; Haberzettl et al., 2007; Haberzettl et al., 2009). Multiproxy sediment and seismic analyses suggest that it is an ephemeral water body for at least the last 51 ka (Recasens et al., 2011; Kliem et al., 2013b) and desiccated before, probably during Marine Isotope Stage (MIS) 4 (Gebhardt et al., 2012b). A previous study of the total inorganic carbon (TIC) contents suggested that this sediment parameter could be an important lake level proxy for the Holocene and the Late Glacial as carbonates precipitate from the calcium-supersaturated water body caused by lower lake levels (Haberzettl et al., 2007). Low concentrations of TIC during the last glacial cycle suggest high lake levels (Hahn et al., 2013). Therefore, a survey and dating of lacustrine terraces around Laguna Potrok Aike provides the opportunity to identify high lake levels in Patagonia during the last glacial period.

A pole to equator shift of the Southern Hemispheric Westerlies (SHW) versus a combination of temperature decrease and increased rainfall have been intensively discussed to explain high

lake levels during the Last Glacial Maximum (LGM) for Laguna Cari-Laufquén at 41°S in Patagonia (Cartwright et al., 2011). These authors concluded that well-dated shoreline reconstructions of higher latitudes are required to distinguish between both explanations. A further complication for large parts of Patagonia is the fact that the hydrology during glacial conditions additionally might have been affected by permafrost increasing surficial runoff. However, permafrost features in this region have not been dated precisely so far (Trombotto, 2000; Bockheim et al., 2009).

In this study we combine available seismic and sediment core data as well as geomorphological evidence obtained in the framework of the ICDP related "Potrok Aike Maar Lake Sediment Archive Drilling Project" (PASADO) to document range, shape and timing of lake level features at Laguna Potrok Aike. Lake levels were dated using luminescence dating and tephra layers as marker horizons. We also consider lake internal sedimentological processes and a range of external consequences and causes related to lake level changes, including evidences of basin expansion, terrace preservation and relict catchment permafrost. Dating of relict permafrost features contributes to the overall question whether such conditions have affected the amount of runoff from the catchment into the lake. This is of importance as it potentially could solve the contradiction of high Patagonian lake levels being in response to less precipitation during the last glacial period. Such dry climates were suggested by paleobiological evidences (Markgraf et al., 2007; Recasens et al., in press). Moreover, this approach helps to evaluate links between shifts in SHW and the regional water balance.

Site description

Laguna Potrok Aike is located in the older western part of the Pali Aike Volcanic Field (PAVF), a region in the Province of Santa Cruz (Argentina) characterized by extensive back-arc volcanism (Mazzarini and D`Orazio, 2003; Ross et al., 2011). Scoria cones, plateau lavas and maar volcanoes are common in the catchment area. A basaltic clast from the phreatomagmatic tephra outcropping east of the maar was dated by Ar/Ar technique to 0.77 ± 0.24 Ma (Zolitschka et al., 2006) and provides an age for its eruption. Outcrops of weakly compacted sandstone exist along the perimeter of the lake on subaerial terraces (Fig. 3.1). The sandstones belong to the fine-grained molasse-type fluvial deposits of the Lower Miocene Santa Cruz Formation, the youngest geological unit in the Magallanes Basin (Uliana and Biddle, 1988). The spatially extensive Pliocene and Pleistocene glaciations left behind glaciofluvial deposits and basal till in the catchment area. However, according to geomorphological

and stratigraphic evidences glaciers stopped beyond the catchment, and thus did not contribute to the lake water balance during at least the last five glacial periods (Caldenius, 1932; Mercer, 1976; Rabassa and Clapperton, 1990; Meglioli, 1992; Coronato et al., 2013).

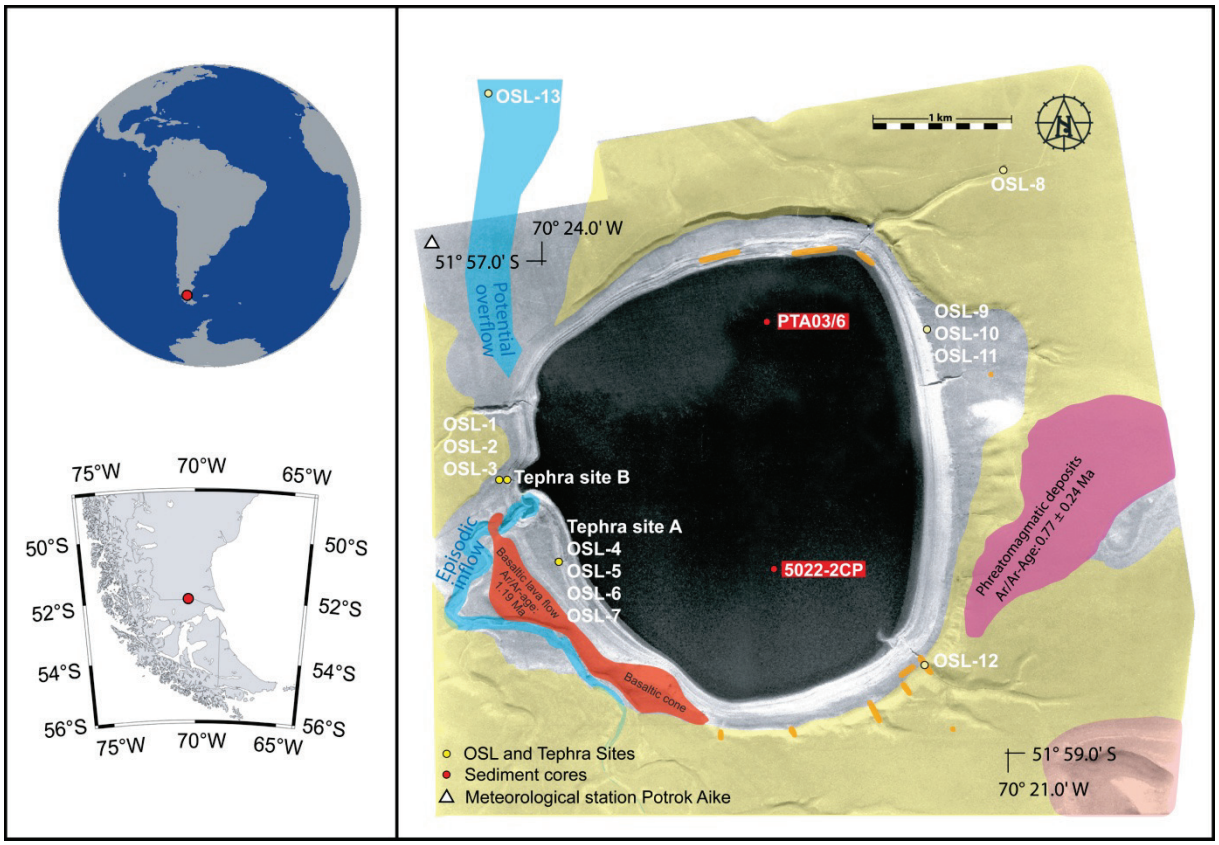

Fig. 3.1: Location of the investigated area, the position of drill sites and an aerial photograph merged with geological data (Corbella, 2002; Zolitschka et al., 2006). Color-coded young fluvial and lacustrine deposits (grey), a mid-Pleistocene basalt lava flow (red), phreatomagmatic tephra deposits (pink), moraine till (yellow), Miocene Santa Cruz Formation (orange). Due to the large catchment and valley morphology, the main water supply is expected by the episodic western inflow, minor inflow comes from SE, NE and NW-arroyos.

Due to the proximity of the Antarctic continent and its small land mass, southern Patagonia does not warm up during austral summers like comparable latitudes in the northern hemisphere (Weischet, 1996). The mean annual air temperature at Rio Gallegos (6 m a.s.l., 85 km north-east of the study site) is 7.4 ± 0.7 °C, with a July (winter) minimum of 1.0 ± 1.5 °C and a January (summer) maximum of 13.0 ± 1.2 °C (Zolitschka et al., 2006). Mean annual wind speeds of 7.4 m/s occur at Rio Gallegos from a primarily western direction (Weischet, 1996; Baruth et al., 1998). Indeed, the regional climate is strongly affected by the SHW, but the rain shadow effect east of the Andean mountain chain decreases precipitation to less than 300 mm/a in the PAVF (Mayr et al., 2007b). An annual precipitation sum of 150 mm has been

observed at the meteorological station near Laguna Potrok Aike (Zolitschka et al., 2006). A more recent series of precipitation measurements (1999-2005) at Laguna Potrok Aike shows that easterly wind directions are often combined with precipitation whereas west winds generally carry no considerable amounts of moisture per rainfall event (Mayr et al., 2007b).

Steppe vegetation covers the entire catchment area of Laguna Potrok Aike between the Andean forest ecotones located about 80 km to the west and the coast of the Atlantic Ocean about 100 km to the east (Wille et al., 2007; Schäbitz et al., 2013). Sheep farming activities of early European settlers altered the natural vegetation and are likely the main factor causing higher erosion rates since the 19th century (Liss, 1979; Aagesen, 2000).

In a limnological context, Laguna Potrok Aike today is a polymictic and subsaline maar lake at an elevation of 113 m a.s.l. (Fig. 3.1). It has a maximum diameter of 3.5 km, and a present-day water depth of 100 m with a water volume of 0.41 km^3 (Zolitschka et al., 2006). There is extensive geomorphological evidence for rapid and sizable past hydrological variations, including numerous subaerial and subaqueous lake level terraces, sediment mass movements and a possible Late Glacial paleo-outflow channel related to an exceptional high lake level (Haberzettl et al., 2005; Haberzettl et al., 2007; Anselmetti et al., 2009). Today the lake has neither a permanent tributary nor a surficial outflow. Thus, the episodic or ephemeral surface runoff which occurs mainly after spring snowmelt rapidly enters the lake through gullies (arroyos) deeply cut into the surrounding subaerial terraces (Haberzettl et al., 2005; Mayr et al., 2007a).

Methods

To construct a precise topographic map, a differential GPS survey with a dense grid was carried out using the Trimble R3 GPS System. Data were post-processed with the Trimble Business Center software (Version 1.0.2076.14363). The bathymetric dataset comprises 8146 depth measurements conducted with an echosounder (Apelco 560) coupled to a conventional GPS (MLR SP24). Bathymetric and differential GPS data were combined and modeled into a digital elevation grid by triangulation.

Littoral, eolian and relict periglacial sediments were sampled in lightproof tubes for optically stimulated luminescence (OSL) dating and analyzed at the Nordic Laboratory for Luminescence Dating (Aarhus University, Denmark). In the laboratory, sediment from the ends of the tubes was taken for measurement using high resolution gamma spectrometry (Murray et al., 1987). The remaining material was wet sieved before treating the 180-250 µm grain size fraction with HCl, H_2O_2 and 10% HF (40 min) to give clean sand-sized grains. A K-rich feldspar

fraction was then density separated (<2.58 g cm^{-3}) using an aqueous solution of sodium heteropolytungstate (LST Fastfloat). Grains were mounted on 9.8 mm diameter stainless steel discs using silicone oil before measurement using a Risø TL/OSL reader model DA-20 (Bøtter-Jensen et al., 2010) with infrared (IR; 870 nm, 130 mW cm^{-2}) light stimulation and optical detection through a Schott BG-39 and Corning 7-59 glass filter combination. Each aliquot contained several thousands of grains. A single-aliquot regenerative-dose (SAR) protocol (Murray and Wintle, 2000; Thiel et al., 2011; Buylaert et al., submitted) was used for dose measurement with thermal pretreatment at 320°C for 60 s, and each IR stimulation at 50°C followed by a subsequent IR stimulation at 290°C ($pIRIR_{290}$). A final IR stimulation with the sample held at 325°C was applied to ensure there was no residual signal left at the end of each SAR cycle. The doses measured using a single IR stimulation at 50°C (IR_{50}) were measured with a separate SAR protocol using lower preheats of 250°C for 60 s both for dose and test dose, and an elevated temperature IR stimulation at 290°C at the end of each SAR cycle (Buylaert et al., 2008; Buylaert et al., submitted). The duration of all IR stimulations was 200 s. For calculations the initial 2 s of the decay curve minus a background derived from the last 50 s was used. We examined the overall performance of this protocol by measuring the dose recovery ratio using aliquots of the two young samples OSL-10 and OSL-13 (natural dose ~5 Gy). In this experiment the ratio of the dose, measured after giving a known dose (57 Gy) before any thermal treatment, to the known dose (i.e. the measured/given dose ratio) was 1.00±0.03 (n=12) for the dosimetric $pIRIR_{290}$ signal, confirming that our protocol is applicable to this material.

The elemental geochemical composition of glass shards from volcanic tephra layers sampled in outcrops and sediment cores was obtained at the Tephrochronology Analytical Unit of the University of Edinburgh, UK. Analyses were performed on polished thin-sections using a five-spectrometer Cameca SX-100 electron microprobe with a beam diameter of 5 µm and an accelerating voltage (beam current) of 15 keV (2 nA) for major elements, and 15 keV (80 nA) for minor elements. Standard calibration blocks and glass standards were used for calibration and control of accuracy during analyses. Based on geochemical data, a local tephrostratigraphic framework is proposed, linking tephra layers from sediment outcrops with the lacustrine sediment record (5022-2CP) from the lake center (the composite profile of site 2 of ICDP expedition 5022 “PASADO”; Kliem et al.; 2013) and from a core with a littoral position in the lake basin (PTA03/6 (Haberzettl et al., 2008)).

Estimates of past water column variations were inferred from correlation of tephra layers as well as temporal correlation between geomorphological lake level signals and respective core

depths. Tephra correlations yield minimum water depths as their preservation in a sedimentary record requires some meters of water column above, e.g. the respective water depth must have been deeper than the erosive wave base.

Mass movement events were identified and dated using magnetic susceptibility profiles to link the current radiocarbon based age-model of 5022-2CP (Kliem et al., 2013b) to the previously investigated record of PTA03/12+13 (Haberzettl et al., 2007; Anselmetti et al., 2009).

Results

Luminescence dating

It is important to be confident that the feldspar infrared stimulated luminescence (IRSL) signal is stable over the relevant timescales. Fortunately, the oldest sample examined here is beyond the dating range of our technique and can be used for a test. Figure 3.2A shows the $pIRIR_{290}$ laboratory dose response curve for an aliquot of sample OSL-12. The data have been fitted by the sum of two saturating exponentials and this fit suggests that we could measure a dose up to ~1300 Gy with an acceptable accuracy based on 86% of the final signal intensity (Wintle and Murray, 2006). Note that data have been normalized to this final intensity for ease of interpretation. The sensitivity-corrected natural signal (1.04) is shown as a dashed line on Figure 3.2A. It is within uncertainty of the saturated value, strongly suggesting that any instability in the $pIRIR_{290}$ signal during burial is insignificant. The mean natural to saturation intensity ratio is 0.98±0.02 (n=5). For comparison, the corresponding data for the IR_{50} data are shown as inset, and these show the effect of the well-known instability in this signal (Huntley and Lamothe, 2001). The natural signal has reached only ~70% of the laboratory saturation value before the rate of loss of stored charge in this mineral equals the rate of charge build up from the environmental dose rate (Lamothe et al., 2003; Huntley and Lian, 2006).

Tab. 3.1: Summary of burial depths, radionuclide concentrations, field water contents (% dry weight), total dose rates, IR_{50} and $pIRIR_{290}$ D_e values and $pIRIR_{290}$ ages (n denotes the number of aliquots contributing to the D_e value).

Sample code	Lab no.	Depth (cm)	^{226}Ra (Bq/kg)	^{232}Th (Bq/kg)	^{40}K (Bq/kg)	w.c. (%)	Total dose rate (Gy/ka)	IR_{50} D_e (Gy)	(n)	$pIRIR_{290}$ D_e (Gy)	(n)	$pIRIR_{290}$ Age (ka)
OSL-1	09 57 01	132	16.3 ± 0.4	22.0 ± 0.5	393 ± 9	19	2.62 ± 0.08	32.7 ± 4.4	3	44 ± 2	8	16.9 ± 1.1
OSL-2	09 57 02	146	17.3 ± 0.4	22.7 ± 0.5	401 ± 10	21	2.37 ± 0.08	27.2 ± 0.4	3	40.2 ± 1.4	10	16.9 ± 0.9
OSL-3	09 57 03	139	16.6 ± 0.5	20.9 ± 0.5	392 ± 11	8	2.54 ± 0.09	26.7 ± 0.4	6	45 ± 3	8	17.6 ± 1.3
OSL-4	09 57 04	70	17.0 ± 0.6	21.6 ± 0.6	350 ± 10	15	2.68 ± 0.09	80.8 ± 3.5	6	128 ± 5	13	48 ± 3
OSL-5	09 57 05	50	N.A. (did not yield K-feldspar rich extract)									
OSL-6	09 57 06	25	21.2 ± 0.6	23.0 ± 0.7	317 ± 9	38	2.30 ± 0.07	74.0 ± 3.4	3	101 ± 4	10	44 ± 2
OSL-7	09 57 07	15	17.1 ± 0.6	23.5 ± 0.6	348 ± 11	17	2.57 ± 0.08	52.7 ± 2.3	3	87 ± 3	13	34 ± 2
OSL-8	09 57 08	55	15.6 ± 0.6	22.1 ± 0.6	340 ± 10	8	2.70 ± 0.09	63.2 ± 8.1	3	95 ± 6	7	35 ± 3
OSL-9	09 57 09	30	14.7 ± 0.5	19.6 ± 0.6	363 ± 10	2	2.84 ± 0.10	1.1 ± 0.2	2	3.7 ± 0.2	9	1.3 ± 0.1
OSL-10	09 57 10	60	14.3 ± 0.5	20.9 ± 0.6	390 ± 10	3	2.81 ± 0.10	1.2 ± 0.1	3	4.3 ± 0.4	16	1.5 ± 0.2
OSL-11	09 57 11	90	15.3 ± 0.5	19.9 ± 0.5	396 ± 12	5	2.84 ± 0.10	3.2 ± 0.2	3	7.0 ± 0.7	9	2.5 ± 0.3
OSL-12	09 57 12	210	18.5 ± 0.8	29.1 ± 0.9	459 ± 14	10	3.12 ± 0.11			>1300	6	>400
OSL-13	09 57 13	25	15.4 ± 0.5	21.6 ± 0.6	376 ± 9	13	2.71 ± 0.09	2.8 ± 0.4	3	5.2 ± 0.4	16	1.9 ± 0.2

Note: Grain size K-feldspar rich extract is 180-250 µm except for samples 095702 and -03 (90-180 µm)

The external beta and gamma dose rates for our samples were calculated from the gamma spectrometry data using the data of Olley et al. (1996). These dose rates were modified to take into account the observed water contents (given in Tab. 3.1). A cosmic ray contribution was also derived based on the sample burial depth (Prescott and Hutton, 1994). The internal dose rate assumed a K concentration of 12.5±0.5% (Huntley and Baril, 1997). The resulting total dose rates are given in Table 3.1, together with the doses estimated from $pIRIR_{290}$ signals and the resulting ages. Note that the apparent doses from the IR_{50} signals are presented, but not used to calculate ages because of the instability referred to above.

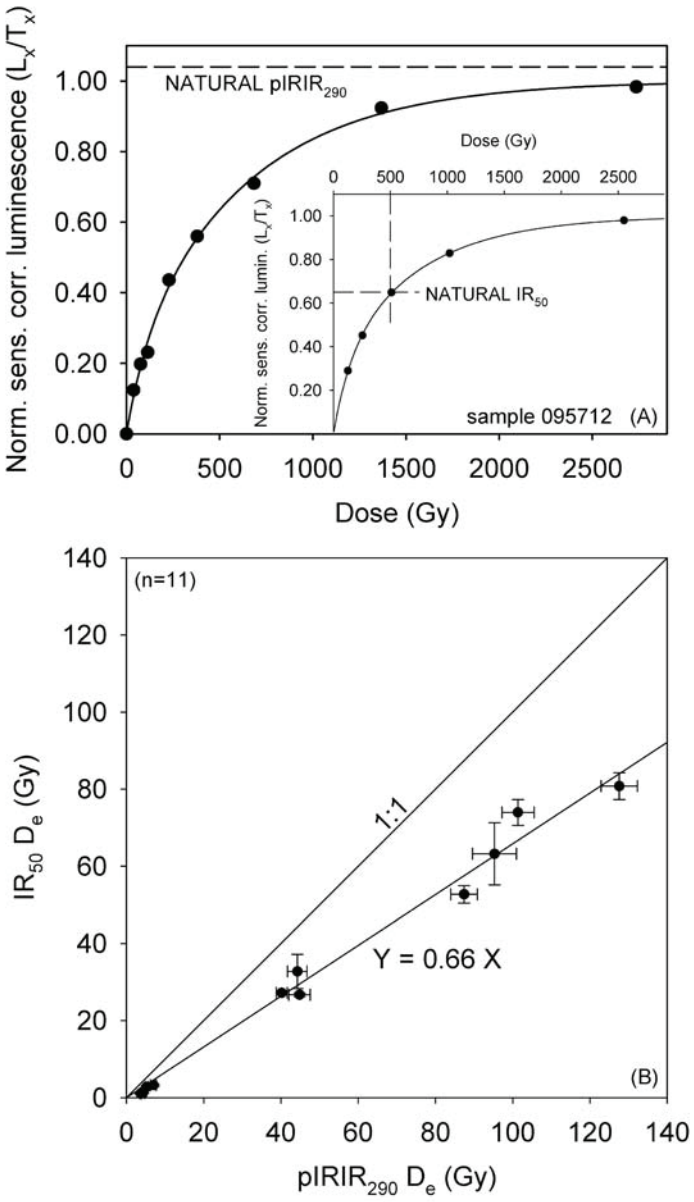

Fig. 3.2: A) Typical $pIRIR_{290}$ dose response curve of sample OSL-12 (inset shows dose response curve for the IR_{50} signal. Dashed lines indicate the sensitivity corrected natural signal intensity. B) IR_{50} D_e values plotted against $pIRIR_{290}$ D_e values for all samples in this study.

It is important to have confidence that these samples were exposed to sufficient light before burial and that any residual luminescence signal was negligible compared to the subsequent

burial dose. It is known that the IR_{50} signal bleaches more readily than the $pIRIR_{290}$ signal when exposed to sunlight (Thomsen et al., 2008; Buylaert et al., submitted; Murray et al., submitted). Thus, we expect that a plot of dose derived from the IR_{50} signal against that from the $pIRIR_{290}$ should reveal samples with a different bleaching history by the scatter in the trend line. Buylaert et al. (2013) have shown how this relationship can be used successfully to identify samples which are less likely to have been well bleached at deposition. We present a corresponding plot for the catchment samples in Figure 3.2B. The data are all consistent with a straight slope of 0.66, very similar to the ratio of the IR_{50} signal to the predicted saturation value (see inset to Figure 3.2A) of 0.65. The absence of outliers in these data which is in contrast with Figure 6a of Buylaert et al. (2013) strongly suggests that all these samples have had a similar bleaching history. It is very unlikely that this can be the result of significant incomplete bleaching. We conclude that the $pIRIR_{290}$ ages presented in Table 3.1 are based on stable signals and that these signals were probably adequately reset before burial.

Tephra correlation and dating

A succession of two macroscopically similar tephra layers has been identified in two sedimentary outcrops ca. 750 m apart (A, B), both located in a distance of ca. 100 m from the western shoreline of Laguna Potrok Aike (Fig. 3.1, Fig. 3.3A). The upper (131.2 m a.s.l.) and the lower tephra (129.1 m a.s.l.) at site B occur in gravels. The upper tephra layer (PAS77A) is 8 cm in thickness and consists of a white fine sand-sized base and a light-brownish silt-sized upper part. The lower tephra layer (PAS78A) is 48 cm in thickness with distinct wavy structures and ripples. The wavy structures of PAS78A contain a few fragments of clastic sediment suggesting minor reworking in the former littoral zone, whereas PAS77A reflects fall out deposits. The upper (126.8 m a.s.l.) and lower tephra layer (126.4 m a.s.l.) in outcrop A occur within laminated lacustrine silts which have been dated by luminescence techniques (Fig. 3.3B, Tab. 3.1). The upper tephra is 4 cm in thickness with a sand-sized whitish base and a silt-sized light-brownish upper part and reflects fall out deposits. The lower tephra is massive, 13 cm thick with wavy structures of silt and fine sand. It contains a few clastic grains suggesting minor reworking in the littoral zone of the lake. Based on the macroscopic appearance of tephra layers from both outcrops a correlation between sites seems very likely.

Tab. 3.2: Mean major element oxide concentration of glass shards (wt %) from tephra layers PAS77A and PAS78A and 1σ standard deviation in parentheses. Only analyses above 94% are included in the means (n: number of analyses).

Tephra	PAS77A	PAS78A
SiO_2	74.37 (1.51)	72.90 (0.96)
TiO_2	0.32 (0.02)	0.34 (0.02)
Al_2O_3	12.61 (0.19)	13.10 (0.38)
FeO_{tot}	1.63 (0.13)	1.74 (0.11)
MnO	0.05 (0.01)	0.05 (0.01)
MgO	0.42 (0.02)	0.49 (0.05)
CaO	2.00 (0.07)	2.26 (0.18)
Na_2O	4.23 (0.32)	4.54 (0.16)
K_2O	1.69 (0.04)	1.62 (0.07)
P_2O_5	0.04 (0.01)	0.05 (0.01)
Cl	n.a.	n.a.
Total	97.36	97.09
n=	8	10

The chemical composition of the glass shards from both tephras is rhyolithic (Tab. 3.2). Comparisons with possible sources identify their provenance as Mt. Burney volcano (Fig. 3.4A). For discrimination between different eruptions, mean major element oxide concentrations were compared with all Mt. Burney ash layers of sediment record 5022-2CP (Fig. 3.4B, C) characterized by Wastegård et al. (Wastegård et al., 2013). Based on their geochemical characterization, the tephra layer PAS78A correlates with tephra 5022-2T39 in 72.13 m cd (composite depth) of 5022-2CP and thus is considered as 49 ± 5 cal. ka BP in age (Fig. 3.4, Fig. 3.5), while tephra layer PAS77A correlates geochemically with 5022T38 in 69.99 m cd dated to 48 ± 5 cal. ka BP.

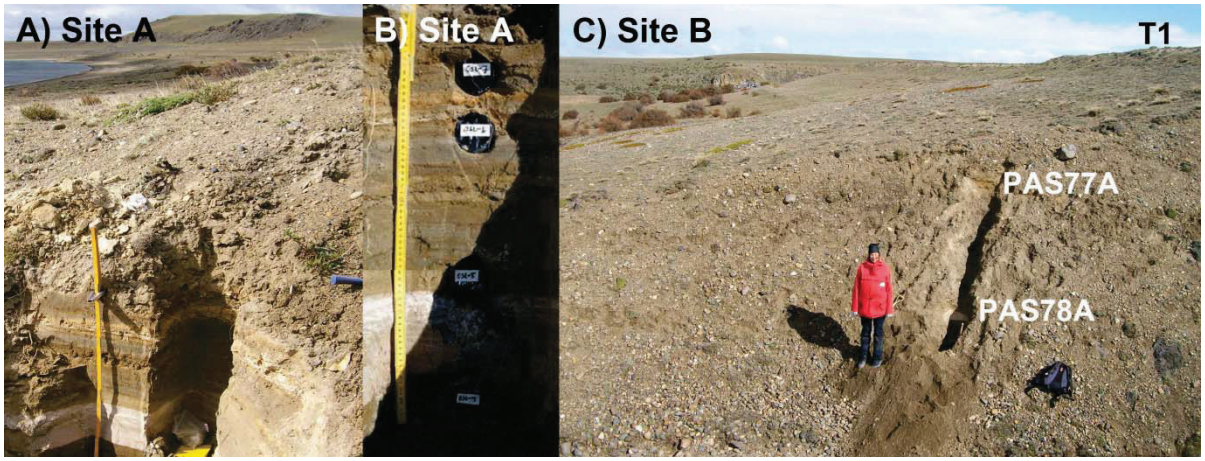

Fig. 3.3: A) Location of tephra site A ca. 10 m above the modern lake level with a young gravel beach-terrace on top. B) Tephra site A: OSL samples 4 (48 ± 3 ka), 5 (no K-feldspar rich extract), 6 (44 ± 2 ka) and 7 (34 ± 2 ka) (from bottom to top) obtained from lacustrine silts intercalated with tephra layers. C) Tephra site B a few meters below uppermost major-tread T1 as well as tephra layers PAS77A and PAS78A that correlate with those from site A.

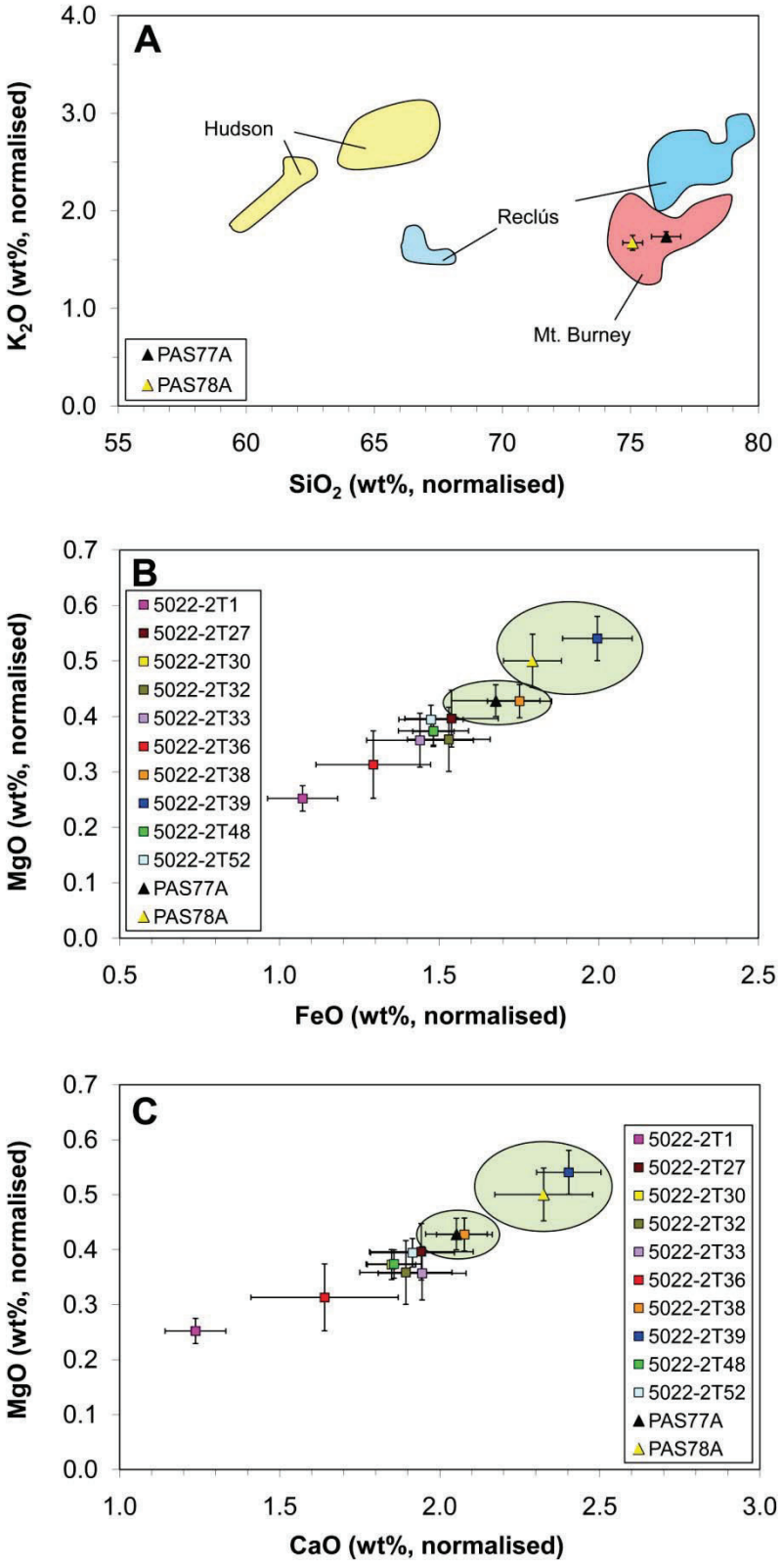

Fig. 3.4: A) Geochemical characterization of ash layers PAS77A and PAS78A compared with possible regional source volcanoes (Stern, 1990; Naranjo and Stern, 1998; Kilian et al., 2003; Haberzettl et al., 2007; Haberzettl et al., 2009). B and C) All Mt. Burney ash layers obtained from sediment record 5022-2CP compared with PAS77A and PAS78A.

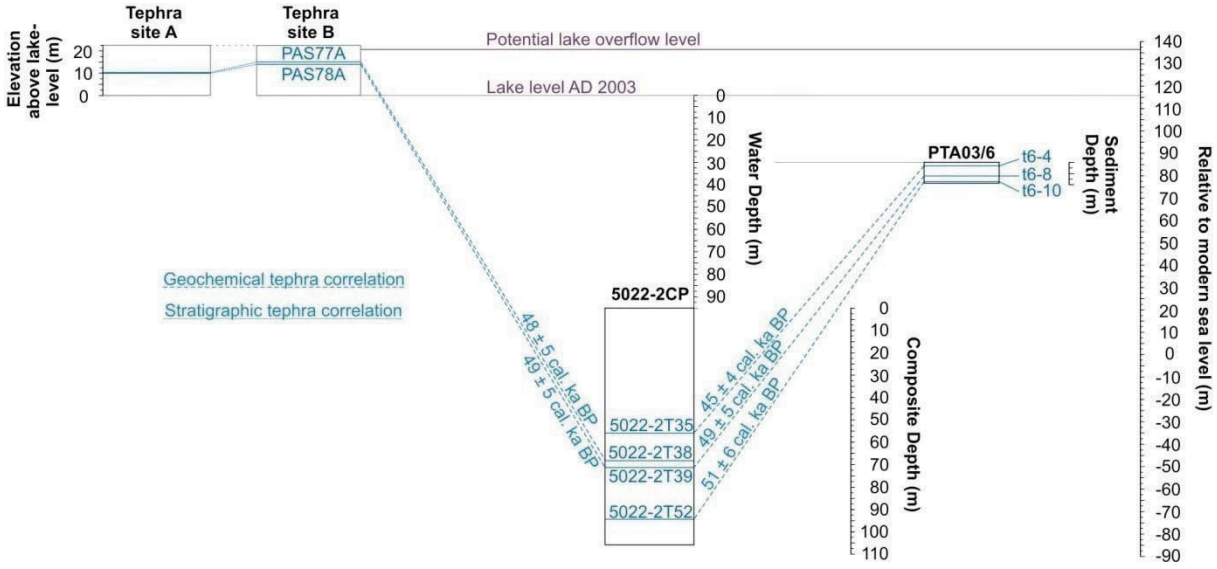

Fig. 3.5: Correlation between lacustrine sediment profiles 5022-2CP and PTA03/6 (after Kliem et al.; 2013) as well as tephra sites A and B. Ages transferred from the radiocarbon-based age-model of 5022-2CP.

OSL dating yields ages between 34 ± 2 (OSL-7) and 48 ± 3 ka (OSL-4) bracketing the two tephras at site A (Tab. 3.1). Unfortunately, one sample did not yield useful results: OSL-5 is a pure tephra sample (no crystalline quartz or K-feldspar grains were extracted) and no luminescence measurements could be made. Sample OSL-7 immediately above the upper tephra is younger than expected. It may be that there has been a phase of erosion after tephra deposition. The lower tephra is bracketed between 48±3 ka (OSL-4) and 44±2 ka (OSL-6) and supports that this ash layer correlates with the lower tephra at site B due to consistent ages. The upper tephra layers of both sites very likely correlate as OSL-6 immediately underlies the upper tephra and covers the radiocarbon age range of PAS77A obtained by correlation with 5022-2CP (Fig. 3.5).

Lake level features

Field survey, digital elevation modeling as well as seismic and sediment core data identified five distinct lake level signals (T1-T5) at Laguna Potrok Aike. The most prominent levels (T1, T4, T5) are represented by well-marked terraces (see elevation map and cross-section, Fig. 3.6, Fig. 3.7), whereas the two minor levels (T2, T3) have only been identified on aerial images and during geomorphological field surveys. Nevertheless, the signal is more complex as many minor terrace-like features modify the relief of the prominent terraces. These very likely document a persistent lake level or lake levels oscillating within a certain low-

amplitude range, whereas the minor features might refer to short-lived lake level variations. The prominent lake levels complicate the traditional discrimination in a low oblique "tread" below and a steep oblique "riser" above the shoreline according to Bowman (1971), who documented one distinct lake level per terrace. Therefore, the terms "major-tread" and "major-riser" are introduced here to describe features related to the prominent terraces identified at Laguna Potrok Aike.

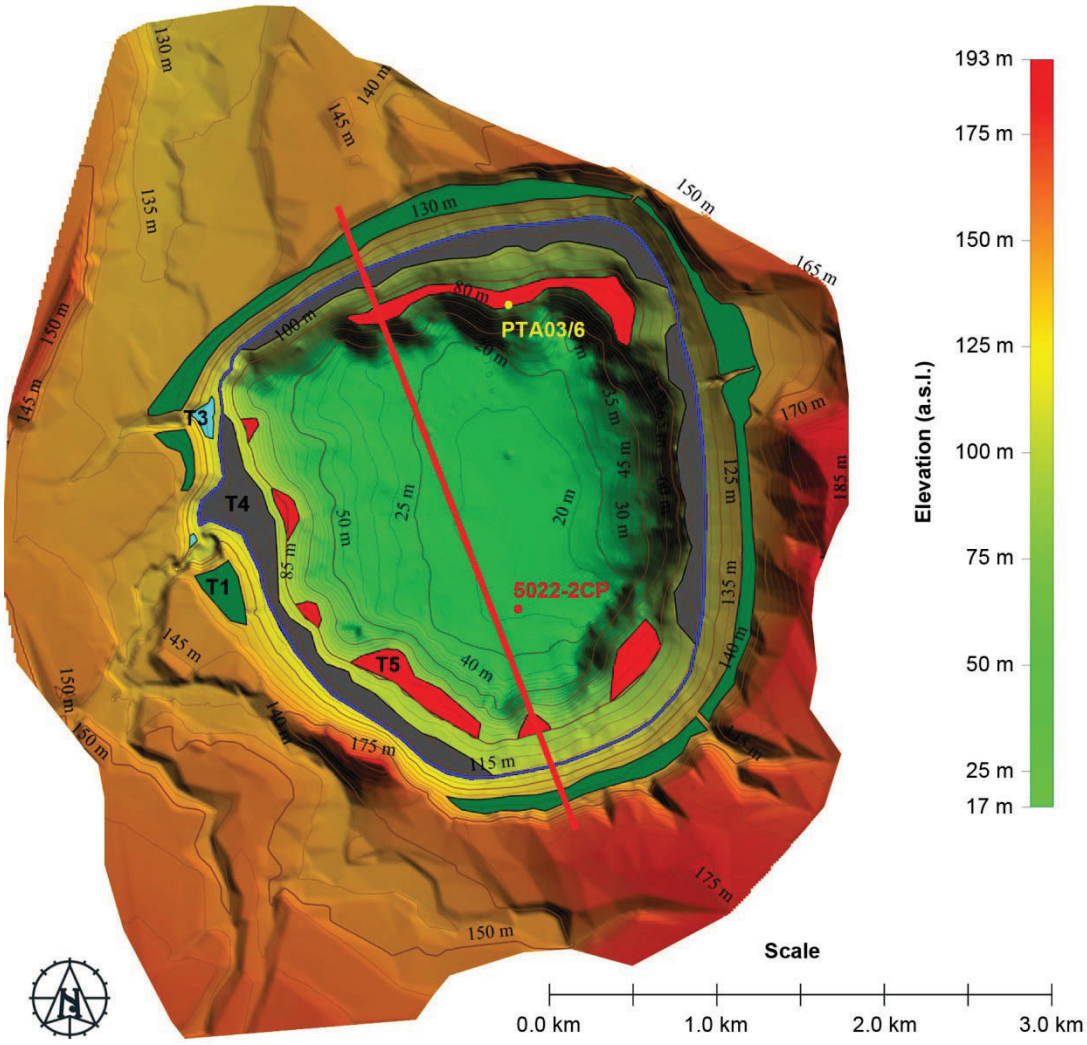

Fig. 3.6: Bathymetry and digital elevation model of the proximal catchment of Laguna Potrok Aike. The red line shows the cross section (Fig. 3.7). Color coded major-treads T1 (green), T4 (grey) and T5 (red) as well as T3 (cyan). The blue line at 116 m a.s.l. marks the lake level of 2003.

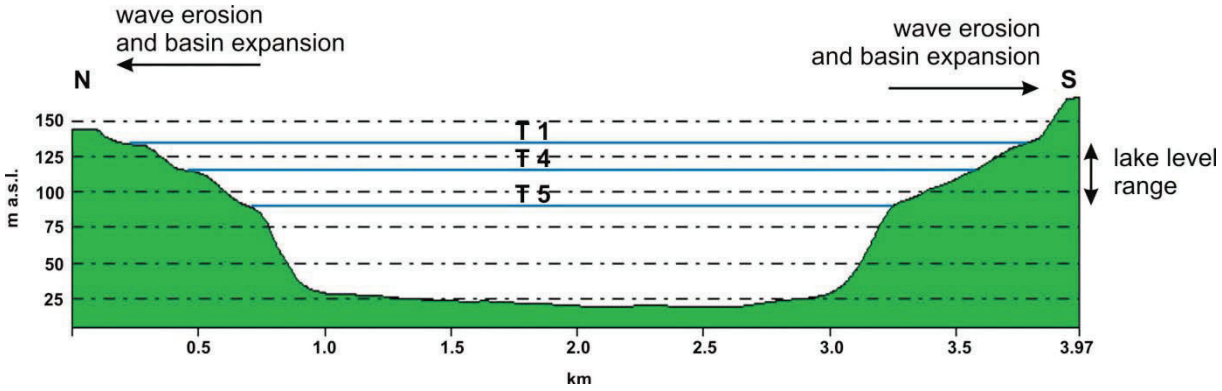

Fig. 3.7: Cross-section (Fig. 3.6) with three distinct major-treads reflecting the range of major lake level changes. Within this range mainly wave erosion caused a basin expansion of more than 700 m.

T1

The major-tread T1 (Figs. 3.6, 3.7) ranges between 131 and 140 m a.s.l. around the entire lake basin and is very wide on the northern (up to 160 m), southern (up to 120 m) and western slopes (up to 220 m) and, apart from the small eastern sub-basin of unknown origin with a diameter of ca. 800 m, relatively narrow on eastern slopes (up to 90 m). Near the basaltic cone (south-western slope; cf. Fig. 3.1) T1 is only documented by a slope angle between the steep basalt wall and gentle slope angles of the beach gravel downwards.

At northern, eastern and western slopes the major-riser primarily occurs in till and glaciofluvial outwash, while sandstone underlying till and glaciofluvial deposits outcrop at the southern slopes. Only a few outcrops allow insights into the major-tread below the cover of lacustrine sediments and beach gravel but suggest sandstone at northern, southern and eastern slopes. The related lacustrine sediments and beach gravels are covered on the northern, southern and western treads by several centimeters to decimeter-thick eolian sands, while on the eastern major-tread eolian deposits reach >1 m in thickness. The major-risers of the relatively steep northern, eastern (apart from the sub-basin) and southern slopes mainly consist of till and sandstone as well as basalt on the southwestern slope. Due to the lower topography the western slopes show only a moderate major-riser. Both, major-tread and major-riser, are covered by steppe vegetation and soils but locally incised by gullies related to the erosive action of episodic inflow events.

Three luminescence samples (OSL-1, 2, 3) at two sites, separated 20 m from each other, were obtained from lacustrine sediments immediately below the surface of T1 (Fig. 3.1, Fig. 3.8; Tab. 3.1). Samples OSL-1 (16.9 ± 1.1 ka) and OSL-2 (16.9 ± 0.9 ka), vertically separated by

14 cm from each other, yield consistent ages. Additionally, OSL-3 (17.6 ± 1.3 ka) confirms these ages.

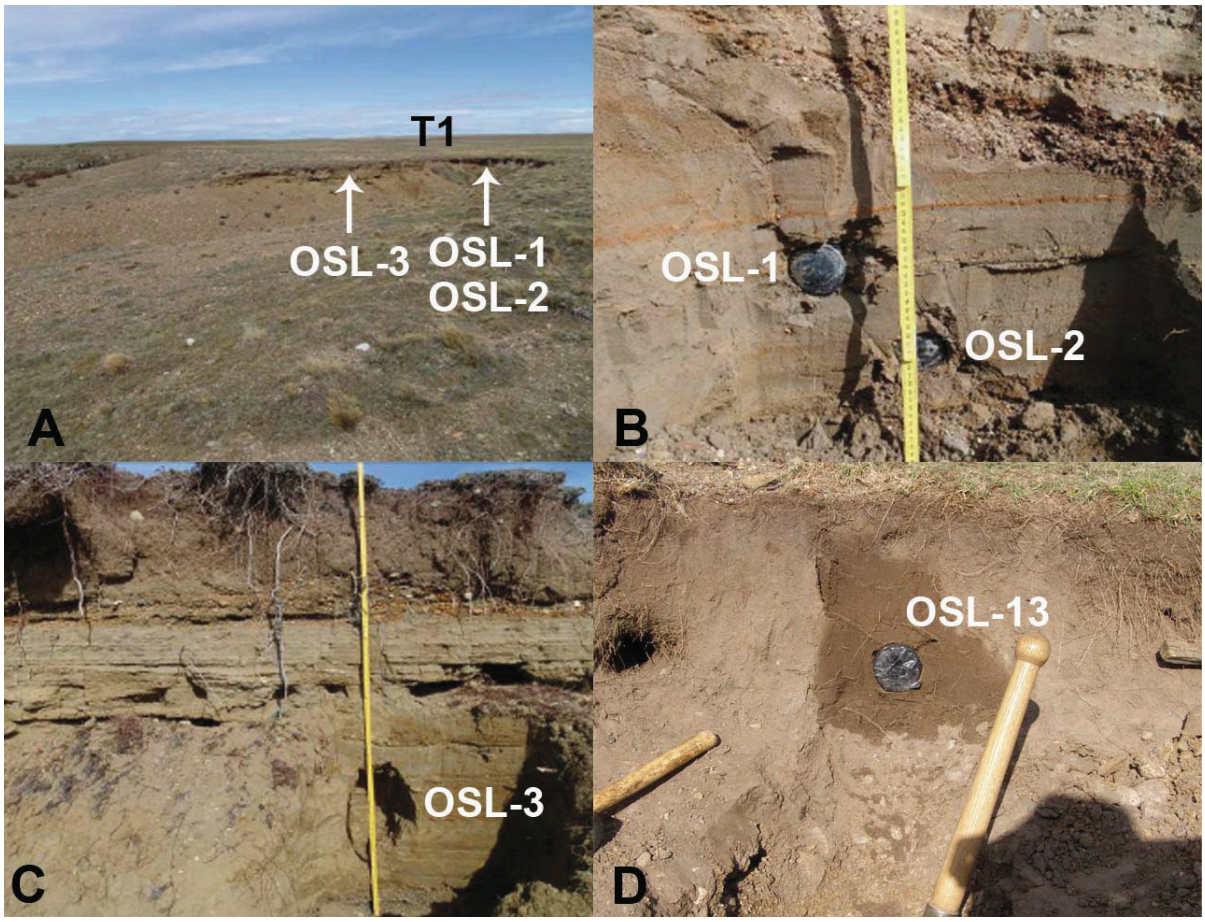

Fig. 3.8: A) Location and B, C) sediment outcrops of OSL-1 (132 cm below T1; 16.9 ± 1.1 ka), OSL-2 (146 cm below T1; 16.9 ± 0.9 ka) and OSL-3 (139 cm below T1; 17.6 ± 1.3 ka) within lacustrine silts. Soil developed in eolian sand cover on top. D) OSL-13 (1.9 ± 0.2 ka) sampled at the base of ca. 20 cm thick eolian sediments overlying fluvial gravel.

As the highest lake level T1 probably relates to overflow conditions of the lake, OSL-13 (Fig. 3.1, Fig. 3.8D) was sampled from eolian sediments overlying fluvial gravels in the potential outflow drainage pathway and thus should yield a minimum age of the latest drainage. Unfortunately, this luminescence age (1.9 ± 0.2 ka) should not be regarded as true depositional age. Using a variety of modern samples, Buylaert et al. (2011) have shown that residual $pIRIR_{290}$ doses of sediments expected to be well-bleached range between ~2 Gy and ~15 Gy. The $pIRIR_{290}$ D_e value for OSL-13 (Tab. 3.1) is of the same order which implies that this age should be considered as upper limit but that the true age of the sediment can be much younger.

T2

T2 is a wave-cut at the eastern shore, where a ~1.2 m thick eolian sand cover (with some fine gravel) on top of beach gravel has been eroded by a transgression event reaching up to ~134 m a.s.l. (Fig. 3.1, Fig. 3.9A). The wave-cut is absent at northern, southern and western shores. A vertical sand cliff face modeled by wave erosion (and locally by wind-carvings) marks the upper limit of this transgression. Wind-deflation exposes the underlying beach gravel. A poorly developed soil is found on the eolian sand cover.

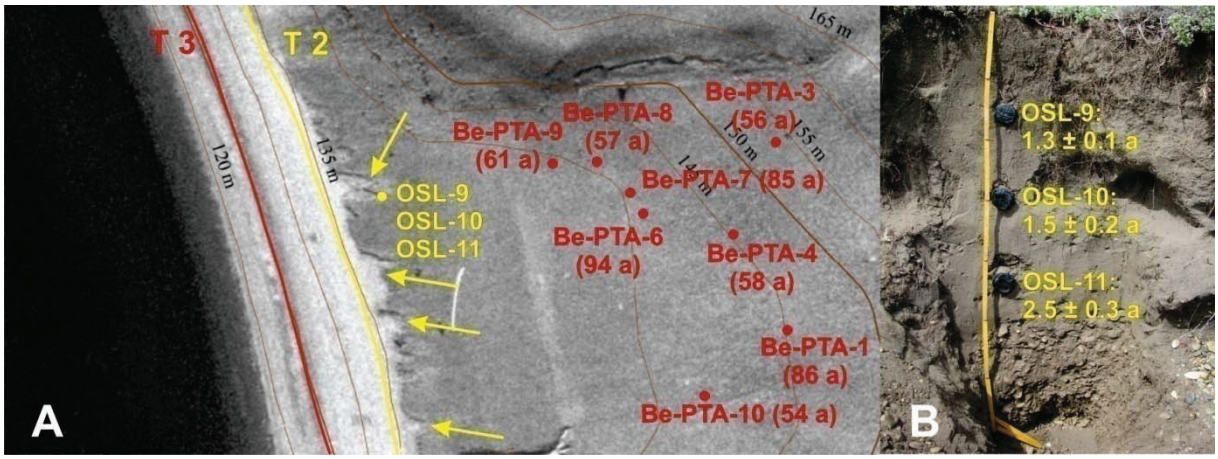

Fig. 3.9: A) Two lake levels (T2 and T3) preserved at the eastern shore. OSL-sites (yellow dots) as well as *Berberis*-sites (red dots) with tree ring ages in brackets. The straight line of T2 is interrupted by wind-carvings (arrows) due to intensive westerly winds. B) Sediment outcrop of OSL-site shows eolian sediments on top of beach gravels at the eastern lake shore.

Luminescence samples of the eolian sediment at the eastern shore sampled between 30 cm (OSL-9) and 90 cm (OSL-11) sediment depth yield ages between 1.3 ± 0.1 ka and 2.5 ± 0.3 ka (Tab. 3.1; Fig. 3.9B). As the case for OSL-13, luminescence ages of OSL-9, 10, 11 show upper limits as the residual $pIRIR_{290}$ D_e range between ~2 Gy and ~15 Gy. Thus, OSL-9 documents the maximum age of the T2 transgression at ca. 1.3 ± 0.1 ka (AD 700 ± 100) as eolian sediments were eroded during the transgression up to T2 and left beach gravel behind on emerged terraces after regression. A minimum age for T2 is provided by tree ring counting of *Berberis* wood sampled in AD 2003 on the eastern slope. Unfortunately, *Berberis* are only available from T2 upwards (Fig. 3.9A). However, above T3 (see below) the largest *Berberis* shrubs reach similar dimensions of trunks and habits suggesting that they are of a similar age. Therefore, samples between T2 and T3 are suitable as well to date a minimum age of T2 and yield ages between 54 and 94 years. Thus, AD ~1930 ± 20 is the minimum age for the T2

transgression. Furthermore, *Berberis* shrubs yield a minimum age for the top of the eolian sediment cover.

T3

A distinct tread of T3 occurs only at the mouth of the main tributary (western shore) as well as at the gully immediately north of it between 117 and 125 m a.s.l. (Fig. 3.1, Fig. 3.6). In aerial images this level is identified by a relatively dark surface at the northeastern and western shore at ca. 125 m a.s.l. (Fig. 3.9A). It coincides with the lower limit of large and apparently relatively old *Berberis* shrub stands, rooted at ca. 125 m a.s.l. Below this level, only small and consequently younger *Berberis* have been observed. It might be a transgression or lake level stagnation of the general regression from T2 to the modern lake level.

We consider that the *Berberis* tree ring count provided a minimum age for T2 (AD ~1930 ± 20) which is the maximum age for the T3. Thus, it is very plausible that a lake level regression of ~9 m occurred between AD ~1930 ± 20 and AD 2003.

T4

The major-tread of T4 occurs between 110-116 m a.s.l. almost all around the lake and coincides with the current lake level (Fig. 3.6, Fig. 3.7). However, due its large size, it is unlikely that T4 was exclusively sculptured in the short time after the regression from the T3 level. Apart from the delta of the main tributary on the western shore, where the tread is ca. 300 m wide, the major-tread reaches ca. 100 m in lateral extension. The major-tread of T4 is not documented along the south-eastern shore where only a basal angle exists to the major-riser.

T5

The T5 feature is inferred from bathymetric echo-sounding data and thus its identification is not as straightforward compared to using ground-based data. Furthermore, this major-tread has been covered by lacustrine sediments deposited during successive transgressions as documented by the presence of several beach terraces easily observable on the seismic data (Anselmetti et al., 2009). The sediment record of PTA03/6 (Fig. 3.1, Fig. 3.5) comprises 311 cm of lacustrine sediments above the discontinuity (Haberzettl et al., 2008). Nonetheless, a fragmented major-tread can be identified at certain locations between 85 and 95 m a.s.l. (Fig. 3.6).

It consists of single platforms with a distinct major-tread and a major-riser on northern and north-eastern slopes and is absent on the eastern slope where steep slopes prevail. Between south-western and south-eastern slopes no distinct terrace is identifiable. Instead, relatively low slope angles occur upwards from 85 m to the T4 level at 116 m a.s.l. On the western slope the major-tread occurs on the delta fan of the main tributary as well as close to the basaltic cone (Fig. 3.6). Apart from the clear evidence from these locations, elsewhere between 85 and 95 m a.s.l. only steep slopes occur.

By integrating sediment core and seismic data it can be deduced that this terrace originated from a low lake level immediately before 6.8 cal. ka BP (Anselmetti et al., 2009). The successive transgression that followed was interrupted by a minor regression and continued until 3.4 cal. ka BP according to the updated age model (Kliem et al., 2013b).

Permafrost features

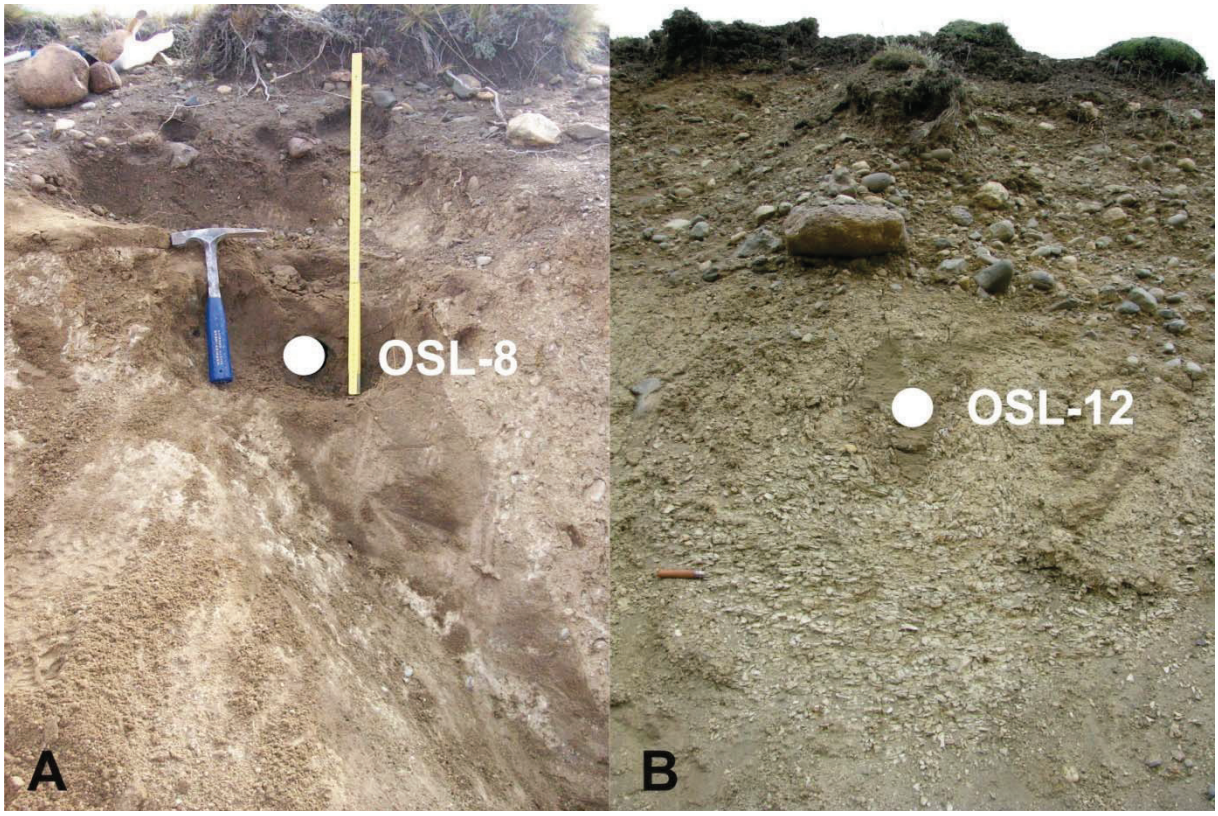

Fig. 3.10: Relict sand-wedges in proximity of the lake (cf. Fig. 3.1) document permafrost conditions at A) 35 ± 3 ka (OSL-8) and B) prior to 400 ka (OSL-12).

Close to the lake two relict sand-wedges were sampled for luminescence dating (Fig. 3.1). Basal till is the host sediment of the first sand-wedge (OSL-8; 35 ± 3 ka; Tab. 3.1) which is located on a plain north-east of the lake (Fig. 3.1, Fig. 3.10). A sandy gravel cover overlies both the sand-wedge and the embedding till deposits. The second sand-wedge (OSL-12; >400 ka; Tab. 3.1) is located in the terrace of a south-eastern gully. The host sediment is composed of aggregates of clay, silt and some sand. The sand-wedge is covered by ca. 1 m of fluvial to periglacial sediments composed mainly of boulders and gravel of a fluvial terrace connected with T1 (Fig. 3.10). Both sand-wedges consist of sand and occasionally fine gravel, which is typical for Patagonian sand-wedges filled with eolian sand (Bockheim et al., 2009).

Interpretation and discussion

Overflow conditions at Laguna Potrok Aike

The major-tread of T1 has been mapped between 131 and 140 m a.s.l., values that overlap with the presumed overflow condition of the lake, considering that today an overflow spill would be active at a lake level of 136.9 m a.s.l. (Fig. 3.1, Fig. 3.6). The fact that the major-tread can be identified up to 140 m a.s.l. at the eastern slope of the lake probably reflects the enhanced accumulation of eolian sands on this shore, masking the underlying relief of the original morphological feature. When active, the overflow water drained into the old terrace system that drained meltwater from a former ice margin south of the lake to the Rio Gallegos valley located ca. 16.5 km north of Laguna Potrok Aike (Coronato et al., 2013). This high lake level has to have persisted for a long time or was reached several times because of the distinct shape of the major-tread all around the lake.

Luminescence ages obtained from lacustrine sediments sampled immediately below T1 (OSL-1, 2, 3) suggest high lake levels and lake overflow at ~17 ka. This is consistent with multi-proxy analyses of lacustrine sediments supporting high lake levels prior to 13.2 cal. ka BP (Haberzettl et al., 2007; Anselmetti et al., 2009; Hahn et al., 2013). Lacustrine sediments underlying these samples suggest a high lake level also during the LGM.

Furthermore, overflow conditions are suggested by tephra of site B reflecting minimum elevations of the lake level as water cover is necessary for their accumulation and preservation. As the difference between PAS77A and the overflow level (136.9 m a.s.l.) is 5.7 m as well as 7.8 m for PAS78A, overflow is likely around 48-49 ± 5 cal. ka BP according to stratigraphic correlation with 5022-2CP (Fig. 3.5). A water column of ca. 190 m can be inferred for this

time (Fig. 3.11): The lake level itself was 20 m higher than today and the sediment record lacked ca. 70 m of deposits postdating this event. Thus the lake was 90 m deeper at that time.

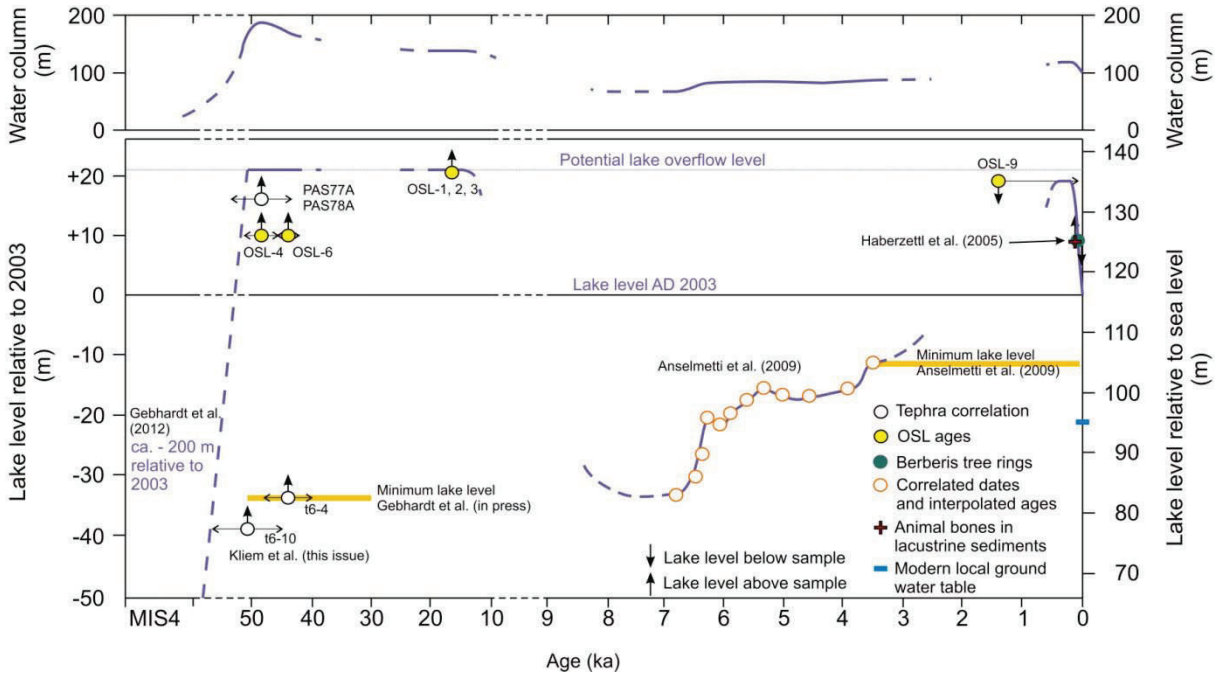

Fig. 3.11: Lake level reconstruction and inferred water columns since MIS 4. Desiccation estimated during MIS 4 after seismic interpretation (Gebhardt et al., 2012b). Radiocarbon ages of Anselmetti et al. (2009) were recalibrated with CALPAL and the calibration curve CALPAL_2007_HULU. Horizontal bars show 1 σ errors of OSL-ages or 95% confidence intervals of tephra ages in the 5022-2CP radiocarbon chronology (Kliem et al, 2013). Due to dating accuracy OSL-9 is regarded as maximum age.

Knowledge about the timing and extent of overflow conditions is important for validation of the sediment TIC record as lake level indicator and paleoclimate proxy (Haberzettl et al., 2005; Haberzettl et al., 2007; Haberzettl et al., 2008; Hahn et al., 2013) considering that carbonate supersaturation is unlikely for an open lake system. Interestingly, no or very low TIC contents are documented for the sediments of Laguna Potrok Aike during the last glacial period, a fact that suggests dominantly cold and wet conditions and/or a permanent lake overflow. In contrast, several organic geochemical sediment proxies indicate significant climatic variations during this time interval (Hahn et al., 2013).

High lake levels during the last glacial period in semi-arid Patagonia

The results indicate high lake levels at Laguna Potrok Aike around 17 ka as well as between 44 and 48 ka (Fig. 3.11). Between both ages high lake levels with overflow conditions are a possibility; likewise the lake level could have dropped or fluctuated during this rather long period. In contrast, seismic results suggest a desiccation of the lake basin estimated for the time frame of MIS 4 (Gebhardt et al., 2012b), just prior to our lake level maximum. According to this study, the desiccated lake floor was roughly 200 m below the modern lake level and a successive lake level transgression followed afterwards. As tephra layers PAS77A and PAS78A document high lake levels, the water column increased up to 190 m between the time frame of MIS 4 and 48 ka (Fig. 3.11). Gebhardt et al. (2012b) suggest a climatic connection with the general weakening or latitudinal shift of the SHW as postulated by several authors (Lamy et al., 2001; Hebbeln et al., 2007; Kaiser et al., 2008). A weakening of the SHW by the occurrence of blocking situations can result in a higher frequency of relatively moist easterly winds which would increase precipitation in south-eastern Patagonia (Mayr et al., 2007b).

In this context it is interesting to note the synchronism between high lake levels at Laguna Cari-Laufquén (located at 41°S in central Argentina) and at Laguna Potrok Aike suggesting no latitudinal shift of the SHW. Moreover, considering recent synoptic meteorological results Laguna Cari-Laufquén and Laguna Potrok Aike are located in two independent precipitation regions (Berman et al., in press). At Laguna Cari-Laufquén shoreline and deep-lake sediments demonstrate a high lake level during the LGM (between 19 and 28 cal. ka BP). Radiocarbon ages that would document an even higher lake level between 40 and 45 cal. ka BP – and thus match overflow conditions at Laguna Potrok between 44 and 48 ka – were interpreted as infinite ages (Cartwright et al., 2011). Nevertheless, almost synchronous high lake levels occurred during the LGM to Late Glacial transition. In contrast, at Lago Cardiel (49° S at the eastern foothills of the Andes) pre-Holocene desiccation (Gilli et al., 2005a) and a low lake level at least from 35 cal. ka BP (bottom of lacustrine sediments) until ca. 11 ka BP (Gilli et al., 2007) have been inferred from seismic data and lacustrine sediments. However, two pre-Holocene transgressions above the modern lake level have been reported based on geomorphic and sedimentary evidences, but only minimum radiocarbon ages have been obtained and date them prior to 31.4 and prior to 20.7 ka BP (Stine and Stine, 1990). The late Pleistocene lake level history of Lago Cardiel might be more complicated, maybe due to the occurrence of significant catchment glaciations (Wenzens, 2007).

An alkenone based sea surface temperature record ca. 40 km offshore Chile (41°S) and Antarctic ice-core records suggest the start of deglacial warming immediately after 19 cal. BP (Lamy et al., 2007). This is supported by the pollen record of Mallin Pollux (Chile, 46°S) documenting a warming after 18.6 cal. ka BP (Markgraf et al., 2007). Lake levels of Laguna Cari-Laufquén recede after a high stand at ca. 19 ka (Cartwright et al., 2011). At Laguna Potrok Aike high lake levels existed slightly longer than at Laguna Cari-Laufquén, as overflow conditions at Laguna Potrok Aike were dated to ~17 ka. Lacustrine sediment data support a high lake level until 13.2 cal. ka BP (Haberzettl et al., 2007). However, an overflow situation only documents a positive water balance for a lake without information about the lake level trend and maximum, whereas shoreline reconstructions give information about transgression, regression and maximum lake level. Consequently, the overflow and high lake level between 17 and 13.2 ka does not indicate synchronism with the largest subtropical lake expansions of South America which occurred between 10-17 ka (Grosjean, 1994; Mourguiart et al., 1997; Seltzer et al., 2002; Jennerjahn et al., 2004; Placzek et al., 2006; Weng et al., 2006). Moreover, it is impossible to claim that there is a time lag between lake level maxima at Laguna Cari-Laufquén and Laguna Potrok Aike that could indicate a shifted SHW between 41°S and 52°S. Nevertheless, overflow at 17 ka at Laguna Potrok Aike and a high LGM lake level at Laguna Cari-Laufquén seem to contradict the hypothesis of dry conditions in Patagonia at 17 ka caused by a distinct northward shift of SHW storm tracks (Markgraf et al., 2007). Cartwright et al. (2011) suggest a combination of temperature depression and rainfall increase in the SHW to explain high LGM lake levels at Laguna Cari-Laufquén. This would be in accordance with modeling simulations showing decreased SHW wind strengths during the LGM as well as increased storm activity at 25-45°S but no SHW shift. This might have decreased the blocking of Atlantic wet air (Rojas et al., 2009; Cartwright et al., 2011). Water balance calculations suggest that among the four meteorological parameters (relative humidity, precipitation, wind speed and temperature) wind direction is the important influence for the hydrological balance of Laguna Potrok Aike (Ohlendorf, 2013). A decrease in temperature would additionally cause a seasonal ice cover and thus distinctly reduced evaporation.

Apart from these direct climatic effects for Patagonian lake levels during the last glacial period, paleoclimatic interpretations based on lake level reconstruction should consider the effect of permafrost. Permafrost is documented south of 40° S between the Patagonian Ice Sheet in the west and – apart from low altitudes in the north-east – the Atlantic Ocean in the east (Trombotto, 2000). The presence of permafrost in the catchment of Laguna Potrok Aike is supported for the last glacial period (OSL-8, 35 ± 3 ka) and before (OSL-12, >400 ka). No-

wadays, episodic surface runoff occurs mainly after spring snowmelt or following occasional extreme rainfall events (Haberzettl et al., 2005; Ohlendorf, 2013). However, permafrost might have enhanced surficial runoff because of reduced infiltration and therefore especially affected lakes with relatively large catchment areas compared to the lake surface area. Relict sand-wedges document former permafrost and cold (mean annual air temperature of -4 to -8°C or colder) and arid (mean annual precipitation <100 mm) climate conditions (Péwé, 1959; Mackay, 1974; Karte, 1983). Hence, the occurrence of sand-wedges indicates permafrost and shows that the climate around 35 ka was drier than today at Laguna Potrok Aike and probably this was contemporaneous with the occurrence of high lake levels. This supports climate interpretations based on pollen suggesting that dry conditions prevailed during the last glacial period in southernmost Patagonia (Markgraf et al., 2007; Recasens et al., 2011), as regional permafrost might have distinctly enhanced surficial runoff and increased lake levels – not related to a precipitation increase – in contrast to the permafrost-free Holocene. Additionally, seasonal ice cover, increased relative humidity and precipitation, low temperature and decreased wind speed likely reduced evaporation from the lake surface.

However, seismic data suggest desiccation at Laguna Potrok Aike during MIS 4 (Gebhardt et al., 2012b) and during the last glacial cycle at Lago Cardiel (Gilli et al., 2005a) probably under permafrost conditions. Hence, despite the presence of permafrost conditions, significant lake level changes might have occurred during the last glacial period. One explanation for desiccation despite the presence of permafrost might be that the lake level was affected by an aquifer-sea level coupling (Ohlendorf, 2013). The decreased sea level (ca. 80 m during MIS 4) of the Atlantic Ocean in a distance of ca. 100 km to the east, might have lowered the local aquifer accordingly, increasing the infiltration of lake water to groundwater. Groundwater loss stopped when permafrost reached a sufficient depth during MIS 4. Moreover, groundwater production might have been reduced, caused by permafrost sealing the surface, thus decreasing the depth of the groundwater table. Further studies are required to explain these links between sea level, lake level and groundwater level.

Holocene lake level changes

The lake level related to T2 results from a transgression up to 134 m a.s.l. (18 m above modern lake level and less than 3 m below overflow) and prevailed only for a short time as no distinct tread can be identified in uncompacted beach gravels. As the time window of T2 ranges between AD 700 ± 100 and the AD 1930 ± 20, it likely reflects the high lake level dur-

ing the LIA which is also supported by radiocarbon-dated horse and guanaco bones in fluvio-lacustrine sediments 9 m above the AD 2003 lake level. Ages obtained are AD 1820 (+135/-150) and AD 1870 (+95/-165) (Haberzettl et al., 2005). Furthermore, according to low TIC values in lacustrine sediments the LIA was the most persistent moist and/or cold period after the early Holocene (Haberzettl et al., 2005; Haberzettl et al., 2007).

Unfortunately, two OSL dates (OSL-11, -13) have to be regarded as maximum ages. Eolian sediments of OSL-11 would document that the lake level never increased 134 m a.s.l. after 2.5 ± 0.3 ka. Moreover, eolian deposits in the potential drainage path of the outflow river would have been easily eroded (Fig. 3.1, Fig. 3.7D; Tab. 3.1) and would exclude overflow at least since 1.9 ± 0.2 ka. Nevertheless, it is likely that the lake level never increased 134 m a.s.l. after 2.5 ± 0.3 ka as the T2 transgression results from the LIA, according to multiproxy analyses of the lacustrine sediments from the center of the lake the most persistent period of high lake levels after the early Holocene (Haberzettl et al., 2007). Consequently, the highest lake level since the early Holocene occurred during the LIA.

The lake level regression from T2 via T3 to the modern lake level (AD 2003: 116 m a.s.l.) correlates with increased TIC precipitation starting around AD 1940 (Haberzettl et al., 2005). This regression coincides with the temperature increase since the LIA with colder and moister climatic conditions which is documented by different Patagonian climate archives (Stine and Stine, 1990; Glasser et al., 2002; Villalba et al., 2003). Increased precipitation caused by a higher frequency of rain-bringing easterly winds might have resulted in a high lake level for the LIA, subsequently followed by the present period of intensified dry westerly circulation (Mayr et al., 2007b). A decreased wind strength would also indicate a reduced evaporation which has been revealed as important for the hydrological balance of Laguna Potrok Aike (Ohlendorf, 2013). Furthermore, closed-basin lakes at large distances from rivers – as is the case for Laguna Potrok Aike – are very susceptible to hydrological forcing linked to variations of the groundwater table (Almendinger, 1990). However, there is no information to estimate recent ground water variation in the area. Wells in a distance of 1.3 km (NW) and 4.2 km (N) from the lake shore suggest a modern local groundwater table at ca. 95 m a.s.l. (Jose Larosa, pers. communication). This is supported by the fact that no perennial tributaries or springs exist in the vicinity of the lake. Consequently, the modern lake level is ca. 21 m higher than the local groundwater table (Fig. 3.11) and a significant loss of lake water to the groundwater must be assumed. This is supported by water isotope data, which document an infiltration of 42% from Laguna Potrok Aike to the groundwater (Mayr et al., 2007a).

Recent climate data and lake level monitoring at Laguna Potrok Aike suggest an immediate lake level and isotopic response of the lake water to precipitation events (Mayr et al., 2007a; Ohlendorf, 2013). The lake level rose during each winter half year between 2003 and 2007 by an equivalent of at least 400 mm which contrasts the annual sum of precipitation that never exceeded 300 mm (Ohlendorf, 2013). As the groundwater table is 21 m below the lake level, surficial water supply is necessary for such a seasonal lake level increase. Deeply incised gullies, eroded into the emerged lake terraces below T2, document the highly dynamic superficial runoff. Generally, enhanced surficial runoff can be explained because the dominantly fine-grained matrix of till delays infiltration. Seasonally frozen ground during winter and early spring might additionally increase surficial inflow from the catchment. Such conditions might also have been common during the LIA because winter and early spring snow melt occurred and only a moderate decrease of the mean winter minimum temperature of today 1.5 ± 1.5 °C for July is necessary to obtain monthly mean temperatures below freezing.

In the geomorphological context, the rapid lake level lowering caused young lacustrine sediment to emerge that is prone to wind erosion, given the high wind speeds prevailing in this region. The maximum accumulation of eolian sands on top of eastern T1 suggests a preferred deflation of emerged terraces which were perpendicularly exposed to the prevailing westerly wind direction. The OSL date (OSL-11) overlying the eolian base documents that wind erosion and accumulation occurred within the last 2.5 ± 0.3 ka. Similarly, accumulation of eolian sediments north of the lake occurred almost in the same time range (OSL-13, 1.9 ± 0.2 ka). Probably, no preceding lake overflow eroded older eolian sediments and these deposits likely correlate with relatively young (>1 ka) eolian sand sheets widespread in southern Patagonia and Tierra del Fuego (Favier-Dubois, 2007). However, as the lowest Holocene lake level occurred around 6.8 cal. BP ka (Fig. 3.11) and intensified westerly winds were suggested thereafter (Mayr et al., 2007b; Anselmetti et al., 2009), a greater age near the eolian base would be expected. Interestingly, regional pollen data suggest increasingly humid conditions and a changed floristic composition after 2500-2300 cal. BP (Huber et al., 2004; Wille et al., 2007). Geochemical data suggest moisture variability for this period (Haberzettl et al., 2007). A humid pulse ca. 1000 years ago might has started the development of a Mollisol often over- and underlain by eolian deposits (Favier-Dubois, 2007). Increased humidity since ca. 2500 cal. BP as well as moisture variability might have promoted the interaction of wind deflation, eolian accumulation and preservation of eolian deposits. At Laguna Potrok Aike frequent lake level changes might have caused periodical emergence and thus deflation of unconsolidated littoral sediment at the easterly shore and increased accumulation in the steppe above. Wind-carvings

at the T2 wave-cut demonstrate the susceptibility of eolian sands to wind erosion if exposed and uncovered from vegetation (Fig. 3.9A). A slightly sparser vegetation and increased wind strength prior to 2.5 ka might have prevented the regional preservation of older eolian sediments.

Collapse of sub-aquatic terraces

In contrast to major-tread T1 and T4, the sub-aquatic major-tread T5 is separated into individual platforms, apparently of quite similar lateral extent. One reason for this geomorphological discrepancy might have been the partial collapse of some terrace sections. The collapse of sub-aquatic slopes resulting in mass movement deposits throughout the lake basin was already known from seismic and sediment core data (Haberzettl et al., 2007; Haberzettl et al., 2008; Anselmetti et al., 2009). Seismic activity as well as a very low lake level during the early Holocene might have triggered these events. Low lake levels can decrease slope stability because of increased sedimentation on tilted subaquatic strata (Hampton et al., 1996; Locat and Lee, 2002; Strasser et al., 2007) in combination with pore-fluid overpressure (Sultan et al., 2004). The latter might be the effect of a reduced water column in combination with increased deposition of fine-grained sediments on subaquatic slopes potentially closing-off pore water for undrained conditions (Anselmetti et al., 2009). As most mass movement deposits show lobate shapes immediately below the steep sub-aquatic slopes, the collapse zone can be restricted to the slopes above. In areas with frequent and/or large collapses no T5 major-treads exist anymore (Fig. 3.12). The relative position between mass movement deposits and terrace gaps suggests a successive collapse of subaquatic terraces, which have been eroded by wave action of a preceding or persisting low lake level. In contrast to T5 no collapses were identified for T1 and T4. Steep slope angles below T5 might have enforced slope collapses, whereas minor slope angles below T1 and T4 prevented slopes from collapsing and from destruction of these levels. Additionally, due to their elevation, slopes underlying T5 are permanently water-saturated which increases the probability of slope collapses as friction is reduced in subaqueous sediments. Furthermore, T1 is abraded mainly into till and sandstones, and these sedimentary deposits provide more stable slope conditions compared to unconsolidated lacustrine sediments of T5. The cohesionless tephra layers underlying T5 and intercalated in lacustrine slopes sediments (Haberzettl et al., 2008) might have additionally acted as collapse-supporting agents.

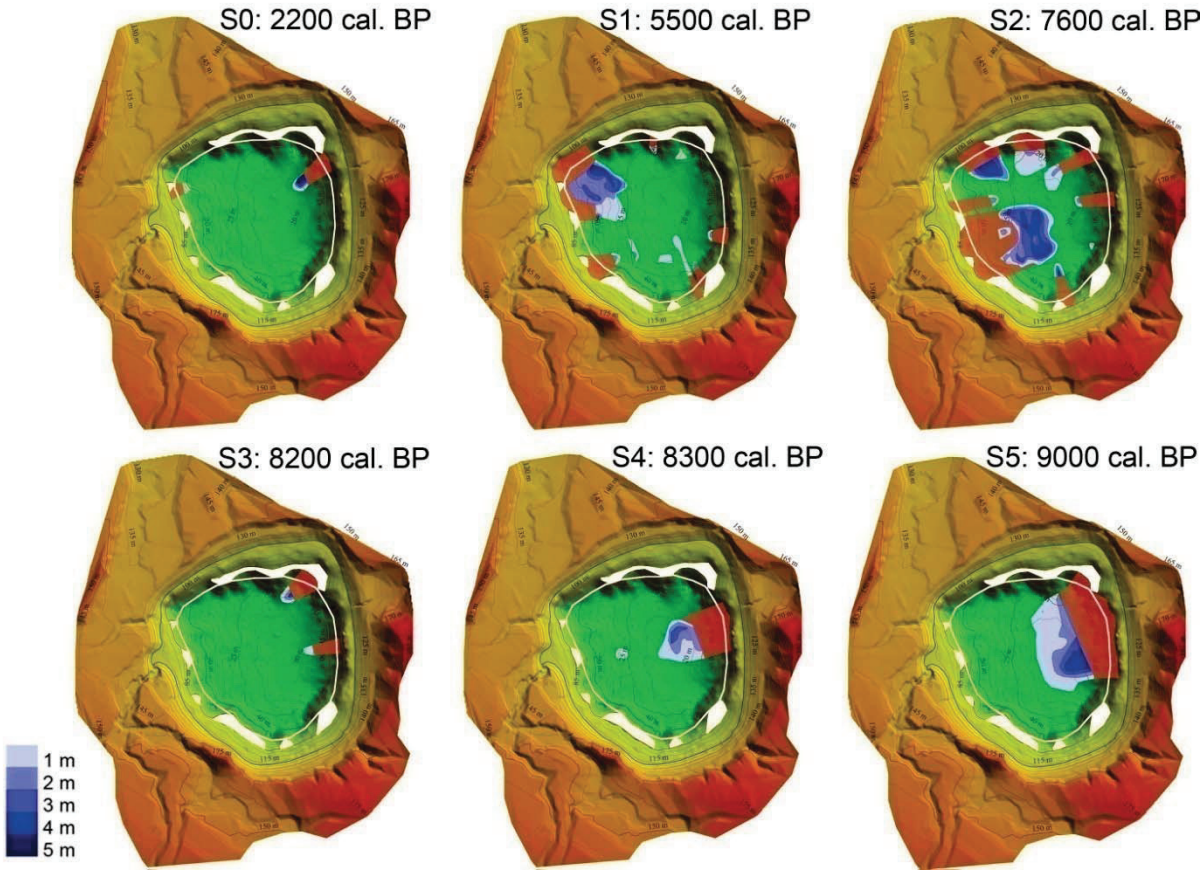

Fig. 3.12: Collapse of sub-aquatic terraces resulted in lobate mass movement deposits running down sub-aquatic slopes. Red shadings indicate the probable collapse areas. White areas show relicts of the T5 level and the white line indicates the inner limit of the original T5 level prior to collapse. T5 is missing where many collapses occurred. Distribution and thickness of mass movements are according to Anselmetti et al (2009).

Basin-diameter expansion and range of lake level oscillations

At least since ~50 ka, the lake level seems to have been oscillating between major-tread T1 and T5. No other major-treads have been identified above and below. Overflow probably occurred between 44 and 48 ka as well as around 17 ka. T5 indicates the lower limit of lake level oscillations and might relate to the local groundwater table, which prevented a further lake level lowering due to water supply from the aquifer during this distinct mid-Holocene dry period in southern Patagonia (Gilli et al., 2005b; Mancini et al., 2005; Haberzettl et al., 2007; Wille et al., 2007; Mayr et al., 2007b). Furthermore, based on seismic data, a persistent high lake level is estimated to between ca. 51 and 30 ka, inferred from well-layered deposits below the erosive discontinuity of T5, suggesting continuous lacustrine deposition for this time range (Gebhardt et al., 2012b). This is supported by sediment data of PTA03/6 (Haberzettl et al., 2009). Considering the profundal sediment of 5022-2CP (Kliem et al., 2013b), lacustrine

sedimentation above the discontinuity indicates deeper water than today (Fig. 3.11, Fig. 3.5). Moreover, the sediments of 5022-2CP accumulated during the last glacial period contain no TIC, also suggesting a high lake level or even overflow (Hahn et al., 2013).

Wave abrasion caused significant expansion of the diameter of the lake basin above the lowest major-tread T5 at 85 m a.s.l. (Fig. 3.6, Fig. 3.7). Immediately after maar eruption, inner crater slopes decreased within decades by gravitational processes expanding the lake basin (Pirrung et al., 2008). However, no debris cones occur on the subaerial terraces and slope angles between T1 and T5 remain below 10° suggesting that gravitational processes had no influence during later episodes of lake-basin evolution. In the early phase of lake basin development, supposed permafrost conditions (Corbella et al., 1990; Corbella et al., 2011) and the presence of unconsolidated basement deposits may have contributed to the formation of a larger crater by immediate slope collapses due to steep slope angles following the maar eruption (Coronato et al., 2013). Thereafter, weakly consolidated sandstones of the Santa Cruz Formation and the widespread occurrence of unconsolidated till, gravel and eolian sands certainly facilitated wave abrasion and promoted basin expansion. Therefore, mostly wave erosion enlarged the initial crater diameter of ca. 2.2 km, as inferred by seismic extrapolation of the crater wall discordance (Gebhardt et al., 2011), to a ca. 3.8 km wide basin.

Consequently, the diameter/depth (D/d) ratio of >30:1 for Laguna Potrok Aike is an indicator of the soft rock maar environment (Coronato et al., 2013) enforcing wave abrasion of the weakly consolidated deposits surrounding the maar crater. The combination of wave abrasion and soft rock environment might have affected other maars of the PAVF with a high D/d ratio. Additionally, the D/d ratio is a morphometric indicator of the age of a maar as depth decreases due to sedimentation and diameter increases due to lateral erosion (Cas and Wright, 1987; Carn, 2000; Ross et al., 2011). However, this process is much faster in a soft rock compared to a hard rock environment.

The major-treads (Fig. 3.6) document a concentric wave abrasion typical for maar lakes (Pirrung et al., 2008). This is probably the reason that no tephra wall persists. Only the pyroclastic hill accumulated east of the lake is preserved partially, another indication that prevailing westerly winds were dominant during the eruption as they are today and resulted in a massive accumulation of pyroclastic material east of the lake.

Conclusion

Based on an extensive geomorphological survey and on evidence from sediment records, seismic surveys, bathymetry and topographic GPS data of the lake site of Laguna Potrok Aike, lake level signals of the past ca. 50 ka have been described, dated and interpreted. Five lake levels have been identified (T1-T5). Two of three prominent lake levels (T1 and T4) occur without gaps around the lake. The lowest of them is interrupted as the result of intensive terrace collapses. The upper minor level is restricted to erosion of eolian sediments accumulated at the eastern lake shore due to prevailing westerly winds. The lower minor level is indicated by the distribution of *Berberis* that has been eroded by a transgression or indicates stagnation.

Wave action eroded the soft rocks of the Santa Cruz Formation and unconsolidated till within an elevation range of 85 and 136 m a.s.l. expanding the diameter of the depression from the initial crater (2.2 km) to 3.8 km. At least since ~50 ka the lake level oscillated within this range. The lake level maximum occurred during the last glacial period and was limited to this elevation because of overflow conditions. The lake level minimum during the mid-Holocene might have been limited against further regression by the local groundwater table. A subsequent Holocene transgression culminated in the LIA with a lake level ca. 40 m above the local groundwater table and 18 m above the present lake level.

Apart from climatic considerations, permafrost during the glacial period might have enforced superficial runoff and caused lake levels distinctly higher than those of the Holocene in semiarid Patagonia. Therefore, high lake levels are not necessarily related to increased precipitation or decreased evaporation during glacial periods. This complicates any attempts to identify glacial to Holocene SHW shifts, strengthening or weakening from lake level reconstruction. Seasonally frozen ground can be expected for the LIA and might have enforced the highest lake level since the early Holocene during this time interval.

Deflation of emerged lacustrine sediments by the prevailing westerly winds caused a leeside accumulation of eolian sediments of at least 1 m in thickness. The preservation of these eolian sediments might correlate with a regional moisture increase and floristic changes since ~2.5 ka.

Acknowledgements

This research is supported by the International Continental Scientific Drilling Program (ICDP) in the framework of the "Potrok Aike Maar Lake Sediment Archive Drilling Project" (PASADO). Funding for drilling was provided by the ICDP, the German Science Foundation (DFG ZO 102/11-1,2), the Swiss National Funds (SNF), the Natural Sciences and Engineering Research Council of Canada (NSERC), the Swedish Vetenskapsradet (VR) and the University of Bremen. For their invaluable help in field logistics and drilling we thank the staff of INTA Santa Cruz and Rio Dulce Catering as well as the Moreteau family and the DOSECC crew.

References

Aagesen, D., 2000. Crisis and conservation at the end of the world: sheep ranching in Argentine Patagonia. Environmental Conservation 27, 208-215.

Almendinger, J.E., 1990. Groundwater control of closed-basin lake-levels under steady-state conditions. Journal of Hydrology 112, 293-318.

Anselmetti, F.S., Ariztegui, D., De Batist, M., Gebhardt, A.C., Haberzettl, T., Niessen, F., Ohlendorf, C. and Zolitschka, B., 2009. Environmental history of southern Patagonia unravelled by the seismic stratigraphy of Laguna Potrok Aike. Sedimentology 56, 873-892.

Baruth, B., Endlicher, W. and Hoppe, P., 1998. Climate and desertification processes in Patagonia. Bamberger Geographische Schriften 15, 307-320.

Berman, A.L., Silvestri, G. and Compagnucci, R., in press. Eastern Patagonia seasonal precipitation: influence of Southern Hemisphere circulation and links with subtropical South American precipitation. Journal of Climate.

Bockheim, J., Coronato, A., Rabassa, J., Ercolano, B. and Ponce, J., 2009. Relict sand wedges in southern Patagonia and their stratigraphic and paleo-environmental significance. Quaternary Science Reviews 28, 1188-1199.

Bøtter-Jensen, L., Thomsen, K.J. and Jain, M., 2010. Review of optically stimulated luminescence (OSL) instrumental developments for retrospective dosimetry. Radiation Measurements 45, 253-257.

Bowman, D., 1971. Geomorphology of the shore terraces of the Late Pleistocene Lisan Lake (Israel). Palaeogeography, Palaeoclimatology, Palaeoecology 9, 183-209.

Buylaert, J.P., Murray, A.S. and Huot, S., 2008. Optical dating of an Eemian site in Northern Russia using K-feldspar. Radiation Measurements 43, 715-720.

Buylaert, J.P., Thiel, C., Murray, A.S., Vandenberghe, D.A.G., Yi, S. and Lu, H., 2011. IRSL and post-IR IRSL residual doses recorded in modern dust samples from the Chinese Loess Plateau. Geochronometria 38, 432-440.

Buylaert, J.P., Murray, A.S., Gebhardt, C., Sohbati, R., Ohlendorf, C., Thiel, C., Zolitschka, B. and The PASADO science team, 2013. Luminescence dating of the PASADO core 5022-1D from Laguna Potrok Aike (Argentina) using IRSL signals from feldspar. Quaternary Science Reviews 71, 70-80.

Buylaert, J.P., Jain, M., Murray, A.S., Thomsen, K.J., Thiel, C. and Sohbati, R., submitted. A robust method for increasing the age range of feldspar IRSL dating. Boreas.

Caldenius, C., 1932. Las glaciaciones cuarternarias en la Patagonia y Tierra del Fuego. Geografisker Annaler 22, 1-164.

Carn, S.A., 2000. The Lamongan volcanic field, East Java, Indonesia: physical volcanology, historic activity and hazards. Journal of Volcanology and Geothermal Research 95, 81-108.

Cartwright, A., Quade, J., Stine, S., Adams, K.D., Broecker, W. and Cheng, H., 2011. Chronostratigraphy and lake-level changes of Laguna Cari-Laufquén, Río Negro, Argentina. Quaternary Research 76, 430-440.

Cas, R.F. and Wright, J.V., 1987. Volcanic Successions: Modern and Ancient. A geological approach to processes, products and successions.

Corbella, H., Pomposiello, M.C., Malagnino, E., Trinchero, E., Alonso, M.S., Chelotti, L. and Firpo, L., 1990. Volcanismo lávico y freatomagmático post-glacial asociado al campo de fracturación Austral, Provincia de Santa Cruz, Argentina, Patagonia Extrandina. *In* "XI Congreso Geológico Argentino, San Juan, Argentina." pp. 39-42.

Corbella, H., 2002. El campo volcano-tectónico de Pali Aike. *In* "Geología y Recursos Naturales de Santa Cruz. Asociación Geológica Argentina." (M. Haller, Ed.), pp. 285-302, Buenos Aires.

Corbella, H., Coronato, A., Ercolano, B., Tiberi, P. and Echazú, D., 2011. Geological aperçu of the Potrok Aike lake area, southern Patagonia, Argentina. Abstracts of the 22nd Colloquium on Latin America Earth Science, Heidelberg, Alemania, pp:58.

Coronato, A., Ercolano, B., Corbella, H. and Tiberi, P., 2013. Glacial, fluvial and volcanic landscape evolution in the Laguna Potrok Aike maar area, southernmost Patagonia, Argentina. Quaternary Science Reviews 71, 13-26.

Duck, R.W., Dearing, J.A., Zolitschka, B., Renberg, I., Frenzel, B., Negendank, J.F.W., Merkt, J., Giraudi, C. and Dahl, S.-O., 1998. Physical records from lakes: the discrimination between signals due to changes in lake water depth and those due to changes in catchment processes. Palaeoclimate Research 25.

Favier-Dubois, C.M., 2007. Soil genesis related to medieval climatic fluctuations in southern Patagonia and Tierra del Fuego (Argentina): Chronological and paleoclimatic considerations. Quaternary International 162-163, 158-165.

Fey, M., Korr, C., Maidana, N.I., Carrevedo, M.L., Corbella, H., Dietrich, S., Haberzettl, T., Kuhn, G., Lücke, A., Mayr, C., Ohlendorf, C., Paez, M.M., Quintana, F.A., Schäbitz, F. and Zolitschka, B., 2009. Palaeoenvironmental changes during the last 1600 years inferred from the sediment record of a cirque lake in southern Patagonia (Laguna Las Vizcachas, Argentina). Palaeogeography, Palaeoclimatology, Palaeoecology 281, 363-375.

Gebhardt, A.C., De Batist, M., Niessen, F., Anselmetti, F.S., Ariztegui, D., Haberzettl, T., Kopsch, C., Ohlendorf, C. and Zolitschka, B., 2011. Deciphering lake and maar geometries from seismic refraction and reflection surveys in Laguna Potrok Aike (southern Patagonia, Argentina). Journal of Volcanology and Geothermal Research 201, 357-363.

Gebhardt, A.C., Ohlendorf, C., Niessen, F., De Batist, M., Anselmetti, F.S., Ariztegui, D., Kliem, P., Wastegård, S. and Zolitschka, B., 2012. Seismic evidence of up to 200 m lake level change in Southern Patagonia since MIS4. Sedimentology 59, 1087-1100.

Gilli, A., 2003. Tracking late Quaternary environmental change in southernmost South America using lake sediments of Lago Cardiel (49°S), Patagonia, Argentina (=DISS ETH No. 15307). Zurich.

Gilli, A., Anselmetti, F.S., Ariztegui, D., Beres, M., McKenzie, J.A. and Markgraf, V., 2005a. Seismic stratigraphy, buried beach ridges and contourite drifts: the Late Quaternary history of the closed Lago Cardiel basin, Argentina (49°S). Sedimentology 52, 1-23.

Gilli, A., Ariztegui, D., Anselmetti, F.S., McKenzie, J.A., Markgraf, V., Hajdas, I. and McCulloch, R.D., 2005b. Mid-Holocene strengthening of the Southern Westerlies in South America - sedimentological evidences from Lago Cardiel, Argentina (49°S). Global and Planetary Change 49, 75-93.

Gilli, A., Markgraf, V., Anselmetti, F.S. and Aristegui, D., 2007. Comment on: G. Wenzens 2005: Glaciar advances east of the Southern Andes between the Last Glacial Maximum and 5,000 BP compared with lake terraces of the endorrheic Lago Cardiel (49 S, Patagonia, Argentina). Zeitschrift für Geomorphologie N.F. 49:433-454 51, 135-137.

Glasser, N.F., Hambrey, M.J. and Aniya, M., 2002. An advance of Soler Glacier, North Patagonian Icefield, at c. AD 1222-1342. The Holocene 12, 113-120.

Grosjean, M., 1994. Paleohydrology of Laguna Lejía (north Chilean Altiplano) and climatic implications for late-glacial times. Palaeogeography, Palaeoclimatology, Palaeoecology 109, 89-100.

Haberzettl, T., Fey, M., Lücke, A., Maidana, N., Mayr, C., Ohlendorf, C., Schäbitz, F., Schleser, G.H., Wille, M. and Zolitschka, B., 2005. Climatically induced lake level changes during the last two millennia as reflected in sediments of Laguna Potrok Aike, southern Patagonia (Santa Cruz, Argentina). Journal of Paleolimnology 33, 283-302.

Haberzettl, T., Corbella, H., Fey, M., Janssen, S., Lücke, A., Mayr, C., Ohlendorf, C., Schäbitz, F., Schleser, G.H., Wille, M., Wulf, S. and Zolitschka, B., 2007. Lateglacial and Holocene wet-dry cycles in southern Patagonia: chronology, sedimentology and geochemistry of a lacustrine record from Laguna Potrok Aike, Argentina. The Holocene 17, 297-310.

Haberzettl, T., Kück, B., Wulf, S., Anselmetti, F., Ariztegui, D., Corbella, H., Fey, M., Janssen, S., Lücke, A., Mayr, C., Ohlendorf, C., Schäbitz, F., Schleser, G.H., Wille, M. and Zolitschka, B., 2008. Hydrological variability in southeastern Patagonia and explosive volcanic activity in the southern Andean Cordillera during Oxygen Isotope Stage 3 and the Holocene inferred from lake sediments of Laguna Potrok Aike, Argentina. Palaeogeography, Palaeoclimatology, Palaeoecology 259, 213-229.

Haberzettl, T., Anselmetti, F.S., Bowen, S.W., Fey, M., Mayr, C., Zolitschka, B., Ariztegui, D., Mauz, B., Ohlendorf, C., Kastner, S., Lücke, A., Schäbitz, F. and Wille, M., 2009. Late Pleistocene dust deposition in the Patagonian steppe - extending and refining the paleoenvironmental and tephrochronological record from Laguna Potrok Aike back to 55 ka. Quaternary Science Reviews 28, 2927-2939.

Hahn, A., Kliem, P., Ohlendorf, C., Zolitschka, B., Rosen, P. and the PASADO science team, 2013. Climate induced changes as registered in inorganic and organic sediment components from Laguna Potrok Aike (Argentina) during the past 51 ka. Quaternary Science Reviews 71, 154-166.

Hampton, M.A., Lee, H.J. and Locat, J., 1996. Submarine landslides. Reviews of Geophysics 34, 33-59.

Hebbeln, D., Lamy, F., Mohtadi, M. and Echtler, H., 2007. Tracing the impact of glacial-interglacial climate variability on erosion of the southern Andes. Geology 35, 131-134.

Huber, U.M., Markgraf, V. and Schäbitz, F., 2004. Geographical and temporal trends in Late Quaternary fire histories of Fuego-Patagonia, South America. Quaternary Science Reviews 23, 1079-1097.

Huntley, D.J. and Baril, M.R., 1997. The K content of the K-feldspars being measured in optical dating or in thermoluminescence dating. Ancient TL 15, 11-13.

Huntley, D.J. and Lamothe, M., 2001. Ubiquity of anomalous fading in K-feldspars and the measurement and correction for it in optical dating. Canadian Journal of Earth Sciences 38, 1093-1106.

Huntley, D.J. and Lian, O.B., 2006. Some observations on tunnelling of trapped electrons in feldspars and their implications for optical dating. Quaternary Science Reviews 25, 2503-2512.

Jennerjahn, T., Ittekkot, V., Arz, H., Behling, H., Patzold, J. and Wefer, G., 2004. Asynchronous terrestrial and marine signals of climate change during Heinrich events. Science 306, 2236-2239.

Kaiser, J., Schefuss, E., Lamy, F., Mohtadi, M. and Hebbeln, D., 2008. Glacial to Holocene changes in sea surface temperature and coastal vegetation in north central Chile: high versus low latitude forcing. Quaternary Science Reviews 27, 2064-2075.

Karte, J., 1983. Periglacial Phenomena and their significance as climatic and edaphic indicators. Geojournal 7, 329-340.

Kilian, R., Hohner, M., Biester, H., Wallrabe-Adams, H.J. and Stern, C.R., 2003. Holocene peat and lake sediment tephra record from the southernmost Chilean Andes (53-55°S). Revista Geológica de Chile 30, 23-37.

Kliem, P., Enters, D., Hahn, A., Ohlendorf, C., Lisé-Pronovost, A., St-Onge, G., Wastegård, S., Zolitschka, B. and the PASADO science team, 2013. Lithology, radiocarbon chronology and sedimentological interpretation of the lacustrine record from Laguna Potrok Aike, southern Patagonia. Quaternary Science Reviews 71, 54-69.

Lamothe, M., Auclair, M., Hamzaoui, C. and Huot, S., 2003. Towards a prediction of long-termanomalous fading of feldspar IRSL. Radiation Measurements 37, 493-498.

Lamy, F., Hebbeln, D., Röhl, U. and Wefer, G., 2001. Holocene rainfall variability in southern Chile: a marine record of latitudinal shifts of the Southern Westerlies. Earth and Planetary Science Letters 185, 369-382.

Lamy, F., Kaiser, J., Arz, H.W., Hebbeln, D., Ninnemann, U., Timm, O., Timmermann, A. and Toggweiler, J.R., 2007. Modulation of the bipolar seesaw in the Southeast Pacific during Termination 1. Earth and Planetary Science Letters 259, 400-413.

Liss, C.-C., 1979. Die Besiedlung und Landnutzung Ostpatagoniens. Göttinger Geographische Abhandlungen 73, 240.

Locat, J. and Lee, H.J., 2002. Submarine landslides: advances and challanges. Canadian Geotechnical Journal 39, 193-212.

Mackay, J.R., 1974. Ice-wedge cracks, Garry Island, Northwest Territories. Canadian Journal of Earth Sciences 11, 1366-1383.

Mancini, M.V., Paez, M.M., Prieto, A.R., Stutz, S., Tonello, M. and Vilanova, I., 2005. Mid-Holocene climatic variability reconstruction from pollen records (32°-52°S, Argentina). Quaternary International 132, 47-59.

Markgraf, V., Whitlock, C. and Haberle, S., 2007. Vegetation and fire history during the last 18,000 cal yr B.P. in Southern Patagonia: Mallin Pollux, Coyhaique, Province Aisen. Palaeogeography, Palaeoclimatology, Palaeoecology 254, 492-507.

Mayr, C., Lücke, A., Stichler, W., Trimborn, P., Ercolano, B., Oliva, G., Ohlendorf, C., Soto, J., Fey, M., Haberzettl, T., Janssen, S., Schäbitz, F., Schleser, G.H., Wille, M. and Zolitschka, B., 2007a. Precipitation origin and evaporation of lakes in semi-arid Patagonia (Argentina) inferred from stable isotopes ($d^{18}O$, $d^{2}H$). Journal of Hydrology 334, 53-63.

Mayr, C., Wille, M., Haberzettl, T., Fey, M., Janssen, S., Lücke, A., Ohlendorf, C., Oliva, G., Schäbitz, F., Schleser, G.H. and Zolitschka, B., 2007b. Holocene variability of the Southern Hemisphere westerlies in Argentinean Patagonia (52°S). Quaternary Science Reviews 26, 579-584.

Mazzarini, F. and D`Orazio, M., 2003. Spatial distribution of cones and satellite-detected lineaments in the Pali Aike Volcanic Field (southernmost Patagonia): insights into the tectonic setting of a Neogene rift system. Journal of Volcanology & Geothermal Research 125, 291-305.

Meglioli, A., 1992. Glacial geology and geochronology of southernmost Patagonia and Tierra del Fuego, Argentina and Chile. Ph.D. Dissertation, Leigh University, Bethlehem PA U.S.A., 216.

Mercer, J.H., 1976. Glacial history of southernmost South America. Quaternary Research 6, 125-166.

Mourguiart, P., Argollo, J., Correge, T., Martin, L., Montenegro, M., Sifeddine, A. and Wirrmann, D., 1997. Changements limnologiques et climatologiques dans le basin du lac Titicaca (Bolivie) depuis 30 000 ans. Earth and Planetary Sciences 325, 139-146.

Murray, A.S., Marten, R., Johnston, A. and Martin, P., 1987. Analysis for naturally occurring radionuclides at environmental concentrations by gamma spectrometry. Journal of Radioanalytical and Nuclear Chemistry 115, 263-288.

Murray, A.S. and Wintle, A.G., 2000. Luminescence dating of quartz using an improved single-aliquot regenerative-dose protocol. Radiation Measurements 32, 57-73.

Murray, A.S., Thomsen, K.J., Masuda, N., Buylaert, J.P. and Jain, M., submitted. Identifying well-bleached quartz using the different bleaching rates of quartz and feldspar luminescence signals. Radiation Measurements.

Naranjo, J.A. and Stern, C.R., 1998. Holocene explosive activity of Hudson Volcano, southern Andes. Bulletin of Volcanology 59, 291-306.

Ohlendorf, C., 2013. A comparison of hydrological balance calculations with instrumental lake level data for Laguna Potrok Aike (Argentina).

Olley, J.M., Murray, A.S. and Roberts, R.G., 1996. The effects of disequilibria in the uranium and thorium decay chains on the burial dose rates in fluvial sediments. Quaternary Science Reviews 15, 751-760.

Péwé, T.L., 1959. Sand-wedge polgons (tessellations) an the McMurdo Sound region, Antarctica-a progress report. American Journal of Science 257, 545-552.

Pirrung, M., Büchel, G., Lorenz, V. and Treutler, H.-C., 2008. Post-eruptive development of the Ukinrek East Maar since its eruption in 1977 A.D. in the periglacial area of south-west Alaska. Sedimentology 55, 305-334.

Placzek, C., Quade, J. and Patchett, P.J., 2006. Geochronology and stratigraphy of late Pleistocene lake cycles on the southern Bolivian Altiplano: implications for causes of tropical climate change. Geological Society of America Bulletin 118, 515-532.

Prescott, J.R. and Hutton, J.T., 1994. Cosmic ray contributions to dose rates for luminescence and ESR dating: large depths and long-term variations. Radiation Measurements 23, 497-500.

Rabassa, J. and Clapperton, C.M., 1990. Quaternary glaciations of the southern Andes. Quaternary Science Reviews 9, 153-174.

Recasens, C., Ariztegui, D., Gebhardt, C., Gogorza, C., Haberzettl, T., Hahn, A., Kliem, P., Lisé-Pronovost, A., Lücke, A., Maidana, N., Mayr, C., Ohlendorf, C., Schäbitz, F., St-Onge, G., Wille, M., Zolitschka, B. and the PASADO Science Team, 2011. New insights into paleoenvironmental changes in Laguna Potrok Aike, Southern Patagonia, since the Late Pleistocene: the PASADO multiproxy record. The Holocene.

Recasens, C., Ariztegui, D., Gebhardt, C., Gogorza, C., Haberzettl, T., Hahn, A., Kliem, P., Lisé-Pronovost, A., Lücke, A., Maidana, N., Mayr, C., Ohlendorf, C., Schäbitz, F., St-Onge, G., Wille, M., Zolitschka, B. and Team, t.P.S., in press. New insights into paleoenvironmental changes in Laguna Potrok Aike, Southern Patagonia, since the Late Pleistocene: the PASADO multiproxy record. The Holocene.

Rojas, M., Moreno, P., Kageyama, M., Crucifix, M., Hewitt, C., Abe-Ouchi, A., Ohgaito, R., Brady, C. and Hope, P., 2009. The Southern Westerlies during the last glacial maximum in PMIP2 simulations. Climate Dynamics 32, 525-548.

Ross, P.S., Delpit, S., Haller, M.J., Nemeth, K. and Corbella, H., 2011. Influence of the substrate on maar-diatreme volcanoes - An example of a mixed setting from Pali Aike volcanic field, Argentina. Journal of Volcanology and Geothermal Research 201, 253-271.

Schäbitz, F., Wille, M., Haberzettl, T., Mayr, C., Lücke, A., Ohlendorf, C., Mancini, V., Paez, M. and Zolitschka, B., 2013. Palaeoclimate reconstruction for Laguna Potrok Aike, southern Patagonia, based on pollen transfer functions.

Seltzer, G., Rodbell, D., Baker, P., Fritz, S., Tapia, P., Rowe, H. and Dunbar, R., 2002. Early warming of tropical South America at the last glacial–interglacial transition. Science 31, 1685-1686.

Stern, C.R., 1990. Tephrochronology of southernmost Patagonia. National Geographic Research 6, 110-126.

Stine, S. and Stine, M., 1990. A record from Lake Cardiel of climate change in southern South America. Nature 345, 705-708.

Strasser, M., Stegmann, S., Bussmann, F., Anselmetti, F.S., Rick, B. and Kopf, A., 2007. Quantifying subaqueous slope stability during seismic shaking: Lake Lucerne as model for ocean margins. Marine Geology 240, 77-97.

Sultan, N., Cochonat, P., Canals, M., Cattaneo, A., Dennielou, B., Haflidason, H., Laberg, J.S., Long, D. and Mienert, J., 2004. Triggering mechanisms of slope instability processes and sediment failures on continental margins: a geotechnical approach. Marine Geology 213, 291-321.

Thiel, C., Buylaert, J.P., Murray, A.S., Terhorst, B., Hofer, I., Tsukamoto, S. and Frechen, M., 2011. Luminescence dating of the Stratzing loess profile (Austria) - Testing the potential of an elevated temperature post-IR IRSL protocol. Quaternary International 234, 23-31.

Thomsen, K.J., Murray, A.S., Jain, M. and Bøtter-Jensen, L., 2008. Laboratory fading rates of various luminescence signals from feldspar-rich sediment extracts. Radiation Measurements 43, 1474-1486.

Trombotto, D., 2000. Survey of cryogenic processes, periglacial forms and permafrost conditions in south america. Revista do Instituto Geológico, 21 (1/2), 33-55.

Uliana, M.A. and Biddle, T., 1988. Mesozoic-Cenozoic paleogeographic and geodynamic evolution of southern South America. Revista Brasileira de Geosciencas 18, 172-190.

Villalba, R., Lara, A., Boninsegna, J.A., Masiokas, M., Delgado, S., Aravena, J.C., Roig, F.A., Schmelter, A., Wolodarsky, A. and Ripalta, A., 2003. Large-Scale Temperature Changes Across the Southern Andes: 20th-Century Variations in the Context of the Past. Climatic Change 59, 177-232.

Wastegård, S., Veres, D., Kliem, P., Ohlendorf, C. and Zolitschka, B., 2013. Towards a late Quaternary tephrochronological framework for the southernmost part of South America – the Laguna Potrok Aike tephra record. Quaternary Science Reviews.

Weischet, W., 1996. Regionale Klimatologie. Teil 1: Die Neue Welt: Amerika, Neuseeland, Australien. Teubner, Stuttgart.

Weng, C., Bush, M., Curtis, J., Kolata, A., Dillehay, T. and Binford, M., 2006. Deglaciation and Holocene climate change in the western Peruvian Andes. Quaternary Research 66, 87-96.

Wenzens, G., 2007. Author's response to the comments by A. Gilli, V. Markgraf, F. Anselmetti and D. Aristegui. Zeitschrift für Geomorphologie N.F. 51, 139-140.

Wille, M., Maidana, N.I., Schäbitz, F., Fey, M., Haberzettl, T., Janssen, S., Lücke, A., Mayr, C., Ohlendorf, C., Schleser, G.H. and Zolitschka, B., 2007. Vegetation and climate dynamics in southern South America: the microfossil record of Laguna Potrok Aike, Santa Cruz, Argentina. Review of Palaeobotany and Palynology 146, 234-246.

Wintle, A.G. and Murray, A.S., 2006. A review of quartz optically stimulated luminescence characteristics and their relevance in single-aliquot regeneration dating protocols. Radiation Measurements 41, 369-391.

Zolitschka, B., Schäbitz, F., Lücke, A., Corbella, H., Ercolano, B., Fey, M., Haberzettl, T., Janssen, S., Maidana, N., Mayr, C., Ohlendorf, C., Oliva, G., Paez, M.M., Schleser, G.H., Soto, J., Tiberi, P. and Wille, M., 2006. Crater lakes of the Pali Aike Volcanic Field as key sites for paleoclimatic and paleoecological reconstructions in southern Patagonia, Argentina. Journal of South American Earth Sciences 21, 294-309.

Chapter 4:

Periodic 1.5 ka climate variations during MIS 2 in the belt of Southern Hemispheric westerlies

Published in: Quaternary Research (2017) 88: 110-120

P. Kliem (1), H. Baumgarten (2), C. Gebhardt (3) A. Hahn (4), C. Ohlendorf (1) and B. Zolitschka (1)

(1) *University of Bremen, Institute of Geography, Geomorphology and Polar Research (GEOPOLAR), Wiener Strasse 9, D-28359 Bremen, Germany. (kliemp@gmx.de)*
(2) *Leibniz Institute for Applied Geophysics (LIAG), Stilleweg 2, D-30655 Hannover*
(3) *Alfred Wegener Institute (AWI), Van-Ronzelen-Str. 2, D-27568 Bremerhaven*
(4) *University of Bremen, Center for Marine Environmental Sciences (MARUM), Loebener Straße, D-28359 Bremen, Germany*

Abstract

Lacustrine sediments retrieved from Laguna Potrok Aike in the framework of the Potrok Aike Maar Lake Sediment Archive Drilling Project (PASADO) offer the possibility to investigate climate variations of the past ~51 cal ka BP in southern hemispheric mid-latitudes, Argentinean Patagonia. This study focuses on short-term cyclicities in the Ca and magnetic susceptibility datasets between 51-15 cal ka BP. The record yields a climate pattern with a periodicity of 1.5 ka during marine isotope stage 2 detected in the Southern Hemisphere from 31-17 cal ka BP for the first time. Marine isotope stage (MIS) 2 is known for constantly cold temperatures whereas prominent climate variations paced by a 1.5-ka periodicity occurred during MIS 3. Our study documents that minor latitudinal oscillations of the Southern Hemispheric Westerlies and the Polar Easterlies with a 1.5-ka periodicity also took place during MIS 2. However, we assume that due to a major northward displacement of the Southern Hemispheric Westerlies these oscillations did not sufficiently affect the zone of Circumpolar Deep Waters and an increased greenhouse effect by upwelling of CO_2-rich deep waters did not occur. This mechanism illustrates why prominent climate events fail to appear during MIS 2.

Keywords: Patagonia, Laguna Potrok Aike, Lake sediments, Frequency analysis, Bond cycles, Dansgaard-Oeschger events; PASADO

Introduction

Patagonia has been in the focus of paleoclimate research since Caldenius (1932) started to reconstruct past glacier advances in the 1930s. Since then, the number of climate archives and proxies applied to unravel the regional climate history increased distinctly (cf. review of Kilian and Lamy, 2012). During the last decades studies concentrated on the reconstruction of latitudinal shifts of the Southern Hemispheric Westerlies (SHW) at the Pleistocene-to-Holocene transition (Mayr et al., 2013) as well as on the role of Patagonia as a dust source for the Southern Hemisphere (Petit et al., 1999).

With the discovery of significant variations of dust in Antarctic ice cores during the last 800 ka, Patagonia was suggested as the main dust source (Petit et al., 1999; EPICA community members, 2004, 2006). This hypothesis is supported by data from geochemical fingerprinting (Grousset et al., 1992; Basile et al., 1997; Gaiero, 2007; Sugden et al., 2009; Delmonte et al., 2010).

Increased Patagonian dust production during the glacial period is related to several factors, e.g. increased glacial and fluvial erosion in mountain regions (Petit et al., 1999), exposure of the South American shelf as a potential source area for continental dust (Kaiser and Lamy, 2010), increased proglacial meltwater dynamic (Sugden et al., 2009), intensified foehn winds increasing aridity (Kaiser and Lamy, 2010) and reducing atmospheric dust outwash (Lambert et al., 2008).

After mobilization at the surface, cyclones elevate aerosols to the upper troposphere where they move to the east and to the southeast as far as 80 °S (Iriondo, 2000). Here dust transporting air masses sink to the ground under the influence of the Antarctic Anticyclone. Trajectory studies demonstrate that dust is transported eastwards by moving low-pressure systems. Today, this takes about seven days from Patagonia to East Antarctica (Li et al., 2010) on pathways crossing the Scotia Sea (Fig. 4.1, Reijmer et al., 2002). Consequently, marine dust records from the Scotia Sea (Fig. 4.1), located midway between the source region (Patagonia) and East Antarctica, correlate with Antarctic dust variations (Hofmann, 1997; Weber et al., 2012).

Suitable proxies to compare records are the nss (non-sea-salt) Ca flux established as an indicator for atmospheric dust variations during glacial times for Antarctic ice cores (Lambert et al., 2011) as well as the magnetic susceptibility (MS) obtained for the marine record from the Scotia Sea (Hofmann, 1997; Weber et al., 2012). These two proxies have also been suggested to document dust activity for sediments of Laguna Potrok Aike (LPA) at 52 °S, located at the

southern limit of the Patagonian dust source-region (Haberzettl et al., 2009; Hahn et al., 2014; Lisé-Pronovost et al., 2015).

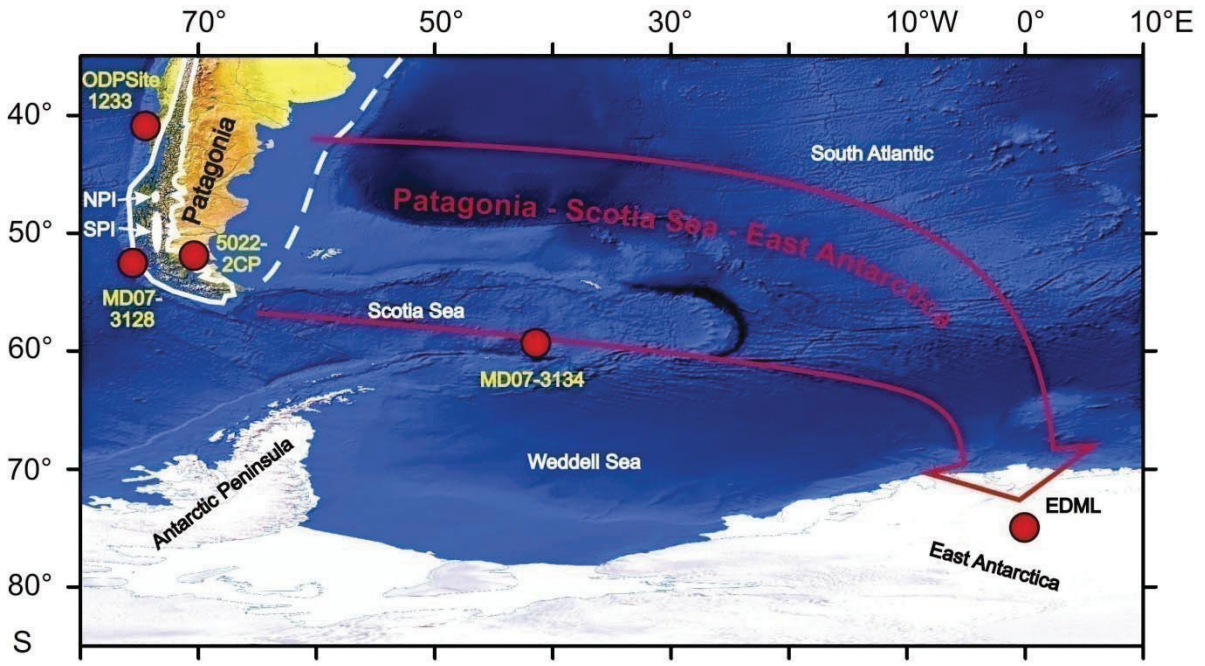

Fig. 4.1: Map with sites mentioned in Fig. 4.3 along the dust trajectory from the South Pacific coast (ODP Site 1233, MD07-3128) and Patagonia (5022-2CP) via the Scotia Sea (MD07-3134) to Antarctica (East Antarctic Dronning Maud Land, EDML). The red arrow indicates the pathway of dust based on a 5-day backward air-parcel trajectory for EDML after Reijmer et al. (2002). Additionally, the extent of the Patagonian shelf during the sea-level lowstand of the LGM (Iriondo, 2000) and the limit of the Patagonian Icefield during the LGM (Hein et al., 2010) are indicated. NPI: Modern Northern Patagonian Icefield; SPI: Modern Southern Patagonian Icefield.

The main argument for using Ca and MS as LPA dust proxies is the long-term correlation with regional dust proxies of the Scotia Sea and Antarctica (Haberzettl et al., 2009; Hahn et al., 2014; Lisé-Pronovost et al., 2015). However, the interpretation of MS is complicated due to several confounding factors (Lisé-Pronovost et al., 2015). Ca reflects the dust activity of LPA shore sediments (Hahn et al., 2014). During the Holocene and the late glacial period autochthonous carbonates were precipitated in the lake (Hahn et al., 2014). For these time intervals Ca cannot be used as an indicator for clastic input. However, the glacial sediments deposited between 51-15 cal ka BP are carbonate-free (Hahn et al. 2013). Therefore, we focus our study on this time window. Regarding individual limitations, this study analyzed both parameters together. The Ca record is based on XRF-detection and was published by Hahn et

al. (2014). The new MS record was obtained by point sensor detection on split cores. For further characterization of the parameters Ca and MS the new dry density (DD) record is presented.

This study focuses on the frequency analysis of Ca and MS records. The analyzed time window from 51 to 15 ka is well-known for rapid warming events: Dansgaard-Oeschger (DO) cycles (Dansgaard et al., 1993) from the North Greenland $\delta^{18}O$ record (NGRIP) and the Southern Hemisphere (Alley et al., 2001). The location of LPA offers the opportunity to identify short-term climate cycles within the dust source area. Furthermore, Quaternary climate variations, probably expressed as displacements of the SHW, can be tracked at southern hemispheric mid-latitudes (Anderson et al., 2009; Toggweiler, 2009).

Site description

Laguna Potrok Aike is located on the leeside of the Andes in south-eastern Patagonia (85 km south-west of the city of Rio Gallegos and ~80 km north of the Strait of Magellan), Argentina. South of 40 °S low-level westerly winds prevail over the continent throughout the year (Garreaud 2009). The upper-level jet stream moves between 45 °S and 55 °S during austral summer and between 20 °S and 40 °S in winter. Regionally, the amount of precipitation and the strength of westerly winds correlate at the Pacific coast and the western slope of the Andes. This correlation decreases dramatically towards the east and reaches negative values across the Patagonian steppe (Garreaud et al., 2013). Consequently, the west-east precipitation gradient is less prominent in years with weak westerly winds.

Within the c. 200 km² semiarid catchment area of LPA (Zolitschka et al., 2006) annual precipitation is < 300 mm (Mayr et al., 2007b) and reaches 150 mm at a local meteorological station near LPA (Zolitschka et al., 2006). A recent time series of precipitation measurements (1999-2005) at Laguna Potrok Aike shows that easterly wind directions (from the South Atlantic) are often combined with precipitation whereas west winds carry considerable less moisture per rainfall event (Mayr et al., 2007b). Easterly wind directions can be caused by atmospheric blocking of the SHW, which are more likely during winter seasons (Schneider et al., 2003; Garreaud et al., 2013). Furthermore, blocking of SHW enables cold Antarctic air masses to migrate into Patagonia from the South. The mean annual air temperature at Rio Gallegos (6 m a.s.l., 85 km north-east of the study site) is 7.4 ± 0.7 °C, with a July (winter) minimum of 1.0 ± 1.5 °C and a January (summer) maximum of 13.0 ± 1.2 °C (Zolitschka et

al., 2006). Mean annual wind speeds of 7.4 m/s occur at Rio Gallegos with a dominantly western direction (Weischet, 1996; Baruth et al., 1998).

The sediment basin containing LPA is of volcanic origin and resulted from a phreatomagmatic eruption dated to 0.77 ± 0.24 Ma by $^{40}Ar/^{39}Ar$ (Zolitschka et al., 2006). The area is characterized by extensive backarc volcanism and belongs to the Pali Aike Volcanic Field (Mazzarini and D`Orazio, 2003; Ross et al., 2011). Scoria cones, plateau lavas and maar volcanoes are common. They are covered by glaciofluvial deposits and basal till of Pliocene to middle Pleistocene glaciations. However, according to geomorphological and stratigraphic evidence, glaciers did not reach the catchment area of LPA at least for the last five glacial periods (Caldenius, 1932; Mercer, 1976; Rabassa and Clapperton, 1990; Meglioli, 1992; Coronato et al., 2013). Widespread sand sheets are the youngest deposits and demonstrate Late Holocene eolian dynamics (Favier-Dubois, 2007; Kliem et al., 2013a).

In a limnological context, Laguna Potrok Aike is a polymictic and subsaline maar lake (Zolitschka et al., 2006) and clastic sedimentation dominated throughout the past 51 ka (Hahn et al., 2014). In 2003 the lake level was at an elevation of 116 m a.s.l., had a maximum diameter of 3.5 km and a water depth of 100 m (Zolitschka et al., 2006). Numerous subaerial and subaqueous lake-level terraces demonstrate rapid and sizable past hydrological variations and a paleo-outflow channel related to an exceptional high lake level (Haberzettl et al., 2005; Haberzettl et al., 2007; Anselmetti et al., 2009; Kliem et al., 2013a). Presently, the lake has neither a permanent tributary nor a surficial outflow. Episodic or ephemeral surface runoff enters the lake through gullies mainly after spring snowmelt that deeply eroded into the subaerial terraces (Haberzettl et al., 2005; Mayr et al., 2007a).

Methods

Lithology and Chronology

The sediment record of LPA (5022-2CP) with a length of 106.08 m cd (meter composite depth) was the key site of the ICDP lake deep drilling expedition 5022 (PASADO) performed from August to November 2008 (Zolitschka et al., 2009). Site 5022-2CP consists of three different sediment types: pelagic sediments, mass movement deposits and tephra layers (Kliem et al., 2013b).

Three main lithostratigraphic units (A, B and C) were distinguished by Kliem et al. (2013b). Sediments of unit A are characterized by laminated silts with inorganic carbonate contents of

up to 2 % that were deposited from 8.3 cal ka BP to the present day. Highest concentration of plant macro remains occurs in lithostratigraphic unit B, which is characterized by an abrupt onset at 17.2 cal ka BP; this unit represents the transition from the last glacial period to the early Holocene. Unit C comprises the glacial time slice of the record from 51.2 to 17.2 cal ka BP. This unit is composed of pelagic sediments with a downcore increase of mass-movement deposits (MMD).

The sediments were radiocarbon (^{14}C) dated and ages were calibrated applying the Cal-Pal_2007_HULU dataset (Weninger and Jöris, 2008). For age-modeling mass-movement deposits and tephra layers were excluded from the profile (Fig. 4.2). The age-model of the event-corrected record is based on a mixed-effect regression procedure (Heegaard et al., 2005; Kliem et al., 2013b). The age-depth relationship for the investigated time interval (51.2 to 15 cal ka BP) is based on 22 AMS (accelerator mass spectrometry) ^{14}C dates. However, preliminary correlation of OSL dates from drill site 1 (Gebhardt et al., 2012a; Buylaert et al., 2013) and results from diatom studies (Recasens et al., 2014) support that the record may extent into an older Antarctic warm period, i.e. Antarctic Isotope Maximum (AIM) 14 (Fig. 4.3).

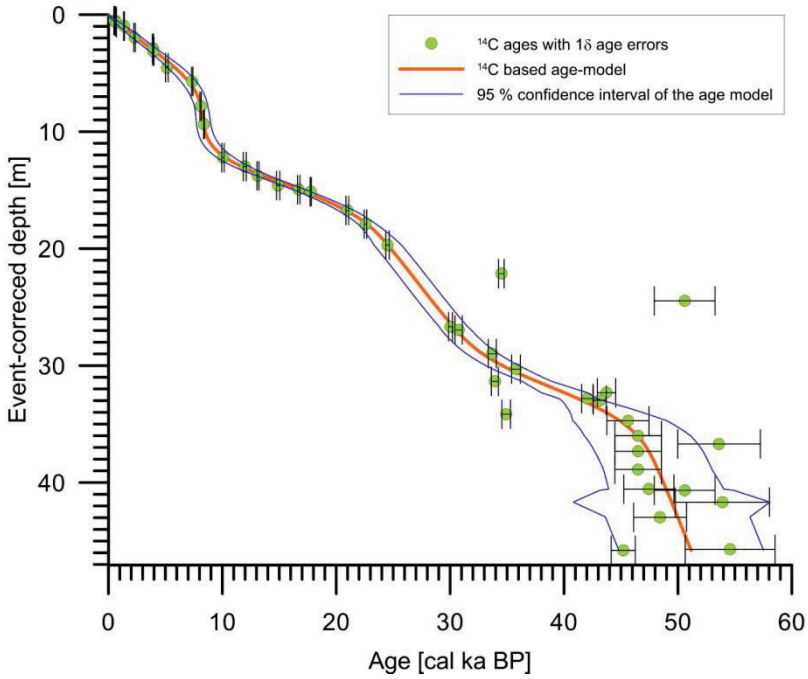

Fig. 4.2: Radiocarbon-based age model for the event-corrected (after removal of event deposits with a thickness >2 cm) sediment record of PASADO site 5022-2CP (modified after Kliem et al, 2013b).

Magnetic susceptibility and dry density

MS was measured non-destructively at 0.5-cm increments on split core halves using a Bartington point-sensor (MS2F) mounted on an automated scanner as described by Funk et al.

(2004). In contrast, the dataset published by Lisé-Pronovost et al. (2015) was measured on U-channels. Dry density was calculated from volumetric subsamples that were taken in consecutive 2-cm increments for the entire sediment sequence. Each subsample was weighed, freeze-dried and weighed again to obtain dry density values.

Spectral analysis

Cycles in sediment records can be studied by cyclostratigraphic methods (Prokopenko et al., 2001; Weedon, 2003; Lenz et al., 2011). The cyclic nature of a sedimentary sequence is investigated by spectral analysis. The spectral analysis is calculated for a certain interval that is defined by the window size. After the interval was analyzed, the window is shifted downwards continuously at a specific step size. The calculation is repeated, and the results are displayed at the centre of each window, resulting in a three-dimensional spectral plot (Molinie and Ogg, 1990; Wonik, 2001; Weedon, 2003; Baumgarten and Wonik, 2014).

For MS and Ca of the LPA sediment record a spectral analysis is calculated for an interval of specific duration (window size = 14 ka) and the window is moved downwards continuously with a step size of 1 ka. The analysis is repeated at consecutive intervals and spectra are displayed at the central depth of each window. Results are presented in a three-dimensional spectral plot. The optimal window size was determined by empirical testing.

Generally, a small window size maximizes the length of the resulting plot. However, the contained signal needs to be covered and cannot be determined if a window size was chosen that is too small, e. g. only half of the signal length. Based on the age-depth relationship (Kliem et al., 2013b), the data was analyzed from 51.2 to 15 cal ka BP. For this study 200-year running means of the new MS and published Ca (Hahn et al., 2014) data were analyzed.

As spectral analysis by sliding window method can be applied on evenly spaced data only, the unevenly spaced datasets were resampled by linear interpolation prior to further analysis. Spectral analysis for identification of characteristic periodicities (Jenkins and Watts, 1969; Priestley, 1981) was performed as fast Fourier Transform using MATLAB (MathWorks®).

Results

To detect sedimentary cycles, continuous sedimentation is required. Therefore, all presented data are based on the event-corrected composite profile of LPA (Kliem et al., 2013b). Because of the location of the drill site within the flat profundal zone of the lake (accumulation area of

mass-movement deposits), a neglectable erosion of pelagic sediments by mass-movement events is assumed.

Dry density, Ca and magnetic susceptibility

The DD record of LPA sediments reflects a minor compaction trend and ranges from 0.6 g/cm³ at ~16 cal ka BP to 1.5 g/cm³ at ~48 cal ka BP (Fig. 4.3d). This trend is interrupted by decreases in DD of ~0.5 g/cm³ for four periods: 1) 51.0-49.0 cal ka BP; 2) 46.9-45.1 cal ka BP; 3) 40.5-37.1 cal ka BP and 4) 17.5-15 cal ka BP. The same intervals are characterized by increased biogenic silica (BSi) values (Fig. 4.3c) published by Hahn et al. (2013). Both parameters exhibit an anti-correlation ($r = -0.62$).

The records of DD and MS correlate weakly ($r = 0.51$ for a 200-year running mean). Moreover, DD shows no correlation with Ca ($r = 0.33$). A good correlation was only identified between Ca and MS ($r = 0.78$).

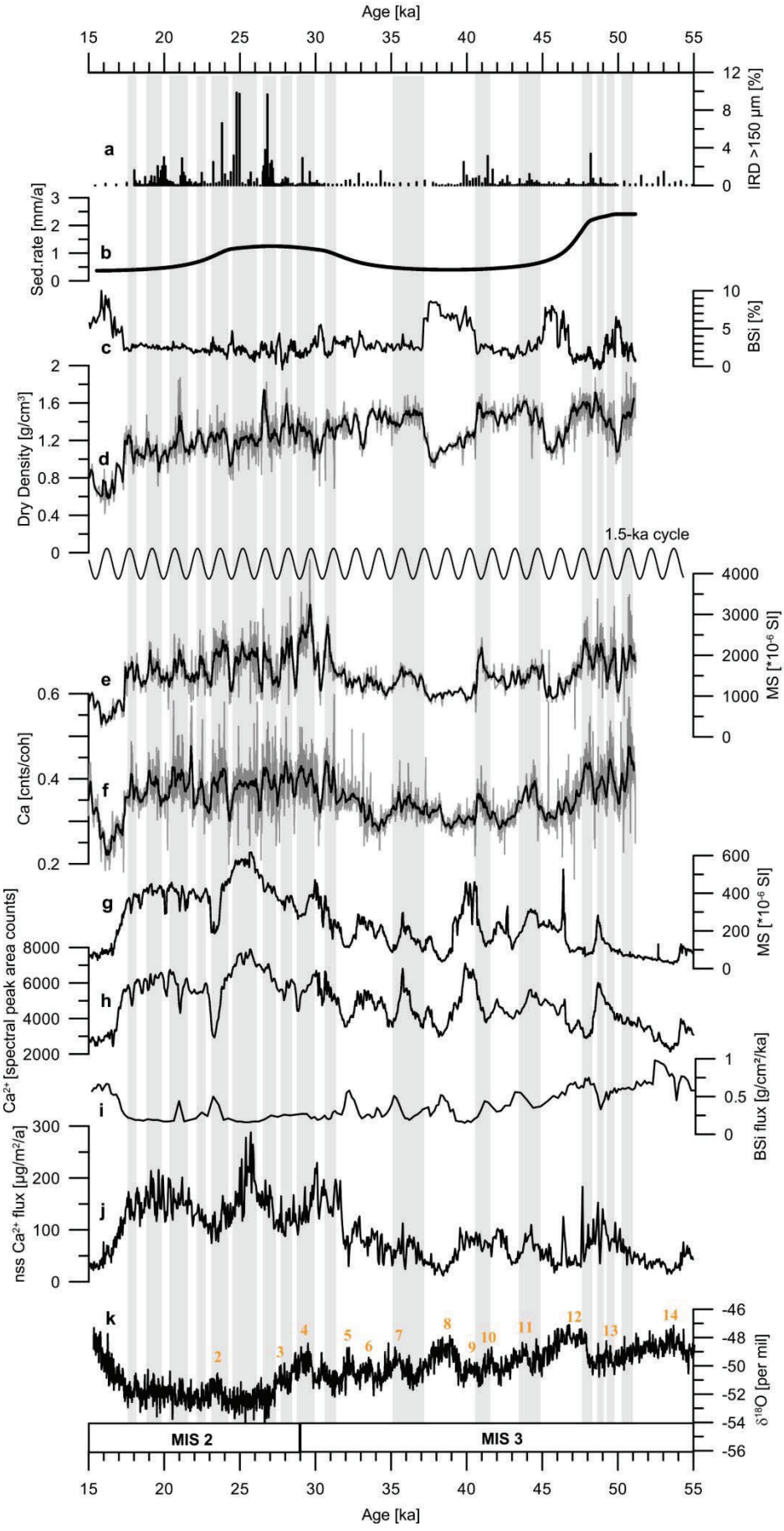
Age [ka]
15 20 25 30 35 40 45 50 55
a
IRD >150 µm [%]
0 4 8 12
b
Sed.rate [mm/a]
0 1 2 3
c
BSi [%]
0 5 10
d
Dry Density [g/cm³]
0 0.4 0.8 1.2 1.6 2
1.5-ka cycle
e
MS [*10⁻⁶ SI]
0 1000 2000 3000 4000
f
Ca [cnts/coh]
0.2 0.4 0.6
g
MS [*10⁻⁶ SI]
0 200 400 600
h
Ca²⁺ [spectral peak area counts]
2000 4000 6000 8000
i
BSi flux [g/cm²/ka]
0 0.5 1
j
nss Ca²⁺ flux [µg/m²/a]
0 100 200 300
k
δ¹⁸O [per mil]
-46 -48 -50 -52 -54 -56
2 3 4 5 6 7 8 9 10 11 12 13 14
MIS 2
MIS 3
Age [ka]

Fig. 4.3: Northwest-southeast transect from the South Pacific entrance of the Magellan Strait to East Antarctica (for location of sites: cf. Fig. 4.1): a) Ice-rafted debris at the Pacific entrance of the Magellan Strait (Caniupán et al., 2011). Records from LPA (5022-2CP) are displayed from b to f with individual data points and the 200-year running mean as a bold line: b) sedimentation rate (Kliem et al., 2013b), c) biogenic silica (BSi), d) dry density, e) magnetic susceptibility (MS), f) XRF calcium (Ca) (c and f: Hahn et al., 2014), g-i) are from Scotia Sea sediment core MD07-3134 (g and h: Weber et al., 2012) with g) magnetic susceptibility (MS) and h) XRF-Ca and i) biogenic silica (BSi) flux (Sprenk et al., 2013), j) EDML non sea salt (nss) Ca flux (Fischer, 2008) and k) EDML $\delta^{18}O$ including orange numbered Antarctic Isotope Maxima (EPICA Community Members, 2006, 2010). Intervals with increased Ca and MS for 5022-2CP are shaded. An ideal 1.5-ka cycle is represented by the sinusoidal curve between d) and e) for comparison.

Spectral analysis

The 3D spectral plots of Ca and MS range from 44 to 22 cal ka BP, because half of the window length of 14 ka cannot be displayed. For both records, different high amplitudes have been detected whereas the frequency of 1.5 ka occurs in both datasets.

The 3D spectral plot of the MS data (Fig. 4.4a) documents the 1.5 ka cycle starting at c. 36 cal ka BP with an increased amplitude towards the top. An additional cycle of 6 ka occurs in the youngest section, establishes with increasing energy and persists towards the top.

The sliding window plot of the Ca data (Fig. 4.4b) shows that the 1.5 ka cycle establishes around 36 cal ka BP with an increasing energy level towards the top of the analyzed time interval. The amplitude of 3.0 ka has high energy prior to 36 cal ka BP, weakens afterwards and reoccurs around 25 ka.

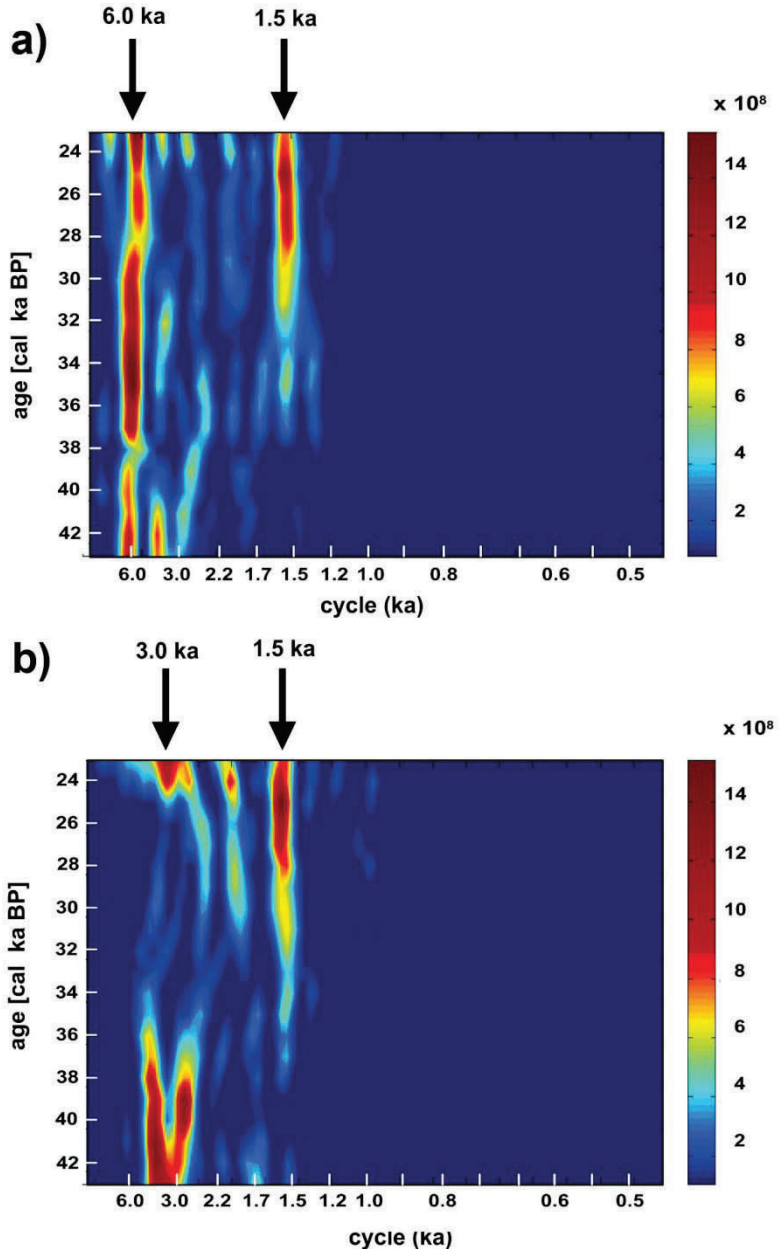

Fig. 4.4: 3D spectral plots of MS (a) and Ca (b) data for the last glacial period (51.2 to 15 cal ka BP). Dominant cycles are labeled with their frequency.

Discussion

Ca and magnetic susceptibility

Ca and MS records of LPA reflect chemical/magnetic changes of the clastic input during the glacial period (Hahn et al., 2014; Lisé-Pronovost et al., 2015). Ca is mainly derived from eroded local basaltic rocks and accumulates as shore sediment (Hahn et al., 2014). During low lake levels, strong winds triggered the transport of basaltic sand from the lake shore to the lake centre. The identification of the source of clastic input with high values of MS is complicated due to several confounding factors (Lisé-Pronovost et al., 2015). However, due to a good visual coincidence (Fig. 4.3e and f) and a good correlation between Ca and MS

(r = 0.78), MS very likely also reflects dust input blown out by strong winds from basaltic shore sediments.

Strong winds (deduced from high levels of Ca and MS) likely result from intensified catabatic winds due to glacier advances of the Southern Patagonian Ice Field (SPI; Fig. 4.1) covering large areas of the eastern Andean Foreland. Data from a record of ice-rafted debris in the Pacific support a coincidence of SPI dynamics (Fig. 4.3a) with Ca and MS records (Fig. 4.3e and f). The glacier dynamics of the SPI likely reflect climate variations due to shifts of the atmospheric circulation (Caniupán et al., 2011). Glacier advances were associated with the influence of the Polar Easterlies, while glacier retreats reflect intensified SHW.

Very strong SHW during AIM 12 and AIM 8 were also inferred from high levels of the lacustrine paleo-productivity indicator BSi (Fig. 4.3c; Hahn et al., (2013) and coincide with very low Ca and MS levels, i.e. with a glacier retreat. The DD of the sediment likely decreased due to the high content of BSi (r = -0.62). Thus, low Ca and MS levels due to dilution effects by high BSi content or other non-clastic compounds cannot be excluded during these periods.

Ca and MS variations of the clastic component in the LPA sediment record are indirectly linked to shifts of the Polar Easterlies and the SHW. Increased Ca and MS levels reflect intensified Easterlies, whereas decreased Ca and MS reflect intensified SHW.

A robust 1.5 ka periodicity dominates MIS 2

The parameters MS and Ca document a 1.5 ka cycle from 36-22 cal ka BP (Fig. 4.4). However, due to the 14 ka spectral time window the center of the spectral analysis is limited to 22 cal ka BP, even if including data up to 15 cal ka BP. Indeed, the distinct 1.5 ka signal is visually traceable between 31 and 17 cal ka BP (Fig. 4.3e and f).

Persistent 1-2 ka climate cyclicities during MIS 3 and MIS 2 show a mean periodicity of 1476 a ± 585 a (1σ) between 65 and 15 ka at site DSDP 609. They were inferred from hematite stained grains of ice-rafted debris (IRD-HSG) records recovered from the North Atlantic (50 °N) and were suggested to pace DO events known from Greenland ice cores (Bond et al., 1999). A chronology update and statistical analysis on the classic DSDP 609 datasets revised earlier results and showed that the original ~1.5 ka periodicity is a mixture of two cyclicities (~1000 a and ~2000 a; Obrochta et al., 2012). Moreover and not corresponding to LPA, a ~2 ka cyclicity prevails between 30-22 ka.

The difference between LPA and the reinterpreted DSDP 609 record is of major scientific interest regarding ongoing discussions about the origin of this 1-2 ka periodicity. A combination of different solar frequencies (Braun et al., 2005; Clemens, 2005) might be an explanation for the origin of a 1.5-ka periodicity. However, Holocene atmospheric ^{14}C production rates and ice core ^{10}Be fluxes suggest solar variations with periodicities of ~1000 and ~2000 years (Obrochta et al., 2012). It is possible that variations of the geomagnetic field modified this pattern at least for the Holocene (St-Onge et al., 2003; Snowball and Muscheler, 2007).

The LPA record reveals a robust ~ 1.5 ka climate periodicity prevailing during MIS 2. If the reinterpretation of DSDP 609 reports the same climate signal, differences might result from climate cycles not recovered at the North Atlantic IRD-HSG sites or from chronological uncertainties (Fig. 4.2). For comparison, expected 1.5 ka paced DO events often fail during MIS 3 (Schulz, 2002). Alley et al. (2001) explained this property of Arctic and Antarctic ice-core records with stochastic resonance, i.e. the climate switches between warm and cold if a combination of a weak periodicity plus noise reach a certain threshold (the noise characteristic is of importance and summarizes all relevant factors).

Implications for atmospheric circulations

The 1.5-ka periodicity dominates MIS 2 and occurs with diminished power during the late MIS 3 at LPA. In contrast, distinct climate variations paced by a ~1.5 periodicity were only dominant during MIS 3 in the polar regions (Grootes and Stuiver, 1997) and not during the constantly cold temperatures of MIS 2 (Fig. 4.5a and e). Why did the 1.5-ka paced climate variations not occur during MIS 2 in the Antarctic?

Recently, the displacement of the SHW was linked with Quaternary climate variations. As a poleward shift of the SHW increases upwelling of the circumpolar deep waters, the released CO_2-rich deep waters influence the greenhouse effect (Anderson et al., 2009; Toggweiler, 2009). Increased upwelling identified in the Southern Ocean coincides with the distinct warm events of AIM 8 and AIM 12 (Anderson et al., 2009). Frequent upwelling during MIS 3 has also been inferred from Scotia Sea BSi fluxes (Fig. 4.5i; Sprenk et al., 2013). In contrast, upwelling in the Scotia Sea was distinctly reduced during MIS 2. With the SHW in a much more northerly position during MIS 2, it is possible that the (minor) latitudinal shifts paced by a 1.5-ka periodicity of this wind system did not reach the required latitude to release CO_2-rich deep waters into the atmosphere. Therefore, an increased greenhouse effect did not occur and thus the prominent climate signals disappeared.

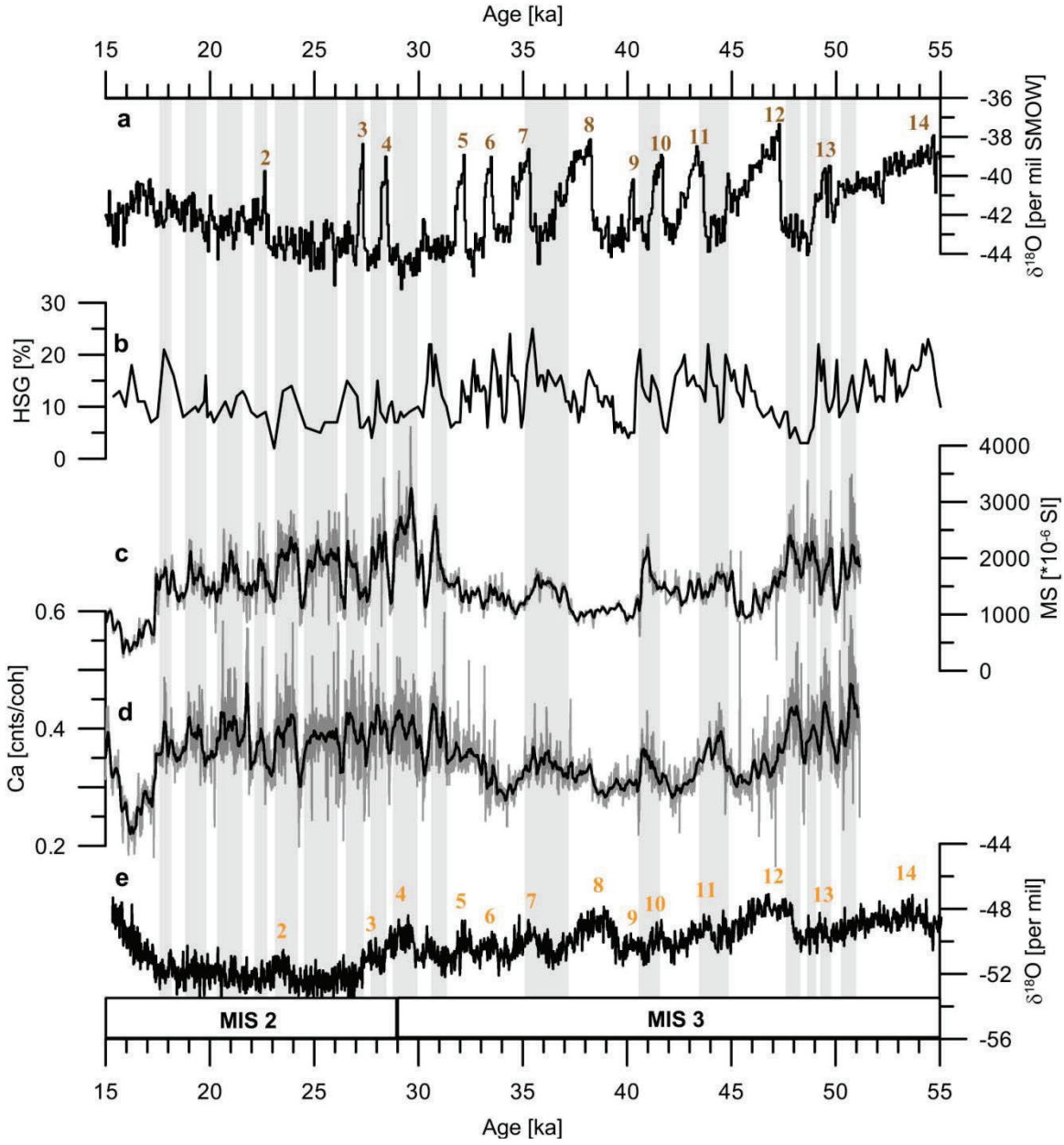

Fig. 4.5: North-south transect from Greenland via the Atlantic Ocean to East Antarctica. Records from: a) Northern Hemisphere (North Greenland – NGRIP) $\delta^{18}O$ including brown numbered Dansgaard-Oeschger Cycles (North Greenland Ice Core Project members, 2004), b) hematite-stained grains of ice-rafted debris (IRD-HSG) records recovered from the North Atlantic at 50 °N (Bond et al., 1999) with updated chronology (Obrochta et al., 2012), c) and d) LPA (5022-2CP) with individual magnetic susceptibility (MS) and Ca data points and the respective 200-year running means as bold lines and e) EDML $\delta^{18}O$ including orange numbered Antarctic Isotope Maxima (EPICA Community Members, 2006, 2010). Intervals with increased Ca and MS for 5022-2CP are shaded.

In contrast, the provenance changes of the detrital input at LPA reflect a climate signal with a 1.5-ka periodicity during MIS 2. Glacier advances of the SPI suggest a northward displacement of the SHW that probably increased the influence of Polar Easterlies delivering cold and/or wet air masses to Southern Patagonia. The influence of Polar Easterlies decreased during minor southward displacements with a 1.5-ka periodicity, resulting in temporary temperature increases and/or precipitation decreases. Periodic 1.5-ka provenance changes did not occur under an overall southward displacement of the SHW during MIS 3.

However, the episodic 3-ka (Ca) and the persistent 6-ka (MS) periodicities (multiples of the 1.5-ka periodicity; Fig. 4.4) suggest that provenance changes respond to a 1.5-ka pacing even during MIS 3. But inconsistencies between Ca and MS spectral plots, less recurrences and increased dating errors at the limit of the radiocarbon dating method (Fig. 4.2) complicate the interpretation of these frequencies.

Conclusions

The Ca and MS records reflect strong wind-triggered dust input of basaltic shore sediments to the lake. Strong winds likely result from intensified catabatic winds caused by an expansion of the SPI into the eastern Andean Foreland. The SPI glaciers advanced due to an increased influence of the Easterlies (= Ca and MS increase in LPA sediments), while glacier retreats suggest intensified SHW (= Ca and MS decrease in LPA sediments).

Based on spectral analysis of Ca and MS records, a strong 1.5 ka periodicity during MIS 2 (31-17 cal ka BP) has been identified for the first time in the Southern Hemisphere. Our data support a link between the latitudinal position of the SHW band, greenhouse gas emission from the Antarctic bottom waters and thus global climate variations. Because of a major northward displacement of the SHW during MIS 2, the zone of CO_2-rich deep water was not sufficiently affected by the SHW. Therefore, an increased greenhouse effect caused by intensified upwelling did not occur at this time which resulted in the constantly cold climate of MIS 2.

During MIS 3, however, an overall southward displacement of the SHW increased the probability of upwelling driven by minor latitudinal shifts of the SHW. A 1.5-ka periodicity paces these small scale shifts and thus the prominent climate signal. This southward displacement caused a general change of the geodynamic framework in the catchment and the dominance of

SHW probably also reduced the influence of Polar Easterlies. This finally stopped provenance variations with 1.5-ka periodicity at LPA.

Acknowledgements

This research is supported by the International Continental Scientific Drilling Program (ICDP) in the framework of the "Potrok Aike Maar Lake Sediment Archive Drilling Project" (PASADO). Funding for drilling was provided by the ICDP, the German Science Foundation (DFG ZO 102/11-1,2), the Swiss National Funds (SNF), the Natural Sciences and Engineering Research Council of Canada (NSERC), the Swedish Vetenskapsradet (VR) and the University of Bremen.

References

Alley, R.B., Anandakrishnan, S. and Jung, P., 2001. Stochastic resonance in the North Atlantic. Paleoceanography 16, 57-68.

Anderson, R.F., Ali, S., Bradtmiller, L.I., Nielsen, S.H.H., Fleisher, M.Q., Anderson, B.E. and Burckle, L.H., 2009. Wind-Driven Upwelling in the Southern Ocean and the Deglacial Rise in Atmospheric CO2. Science 323, 1443-1448.

Anselmetti, F.S., Ariztegui, D., De Batist, M., Gebhardt, A.C., Haberzettl, T., Niessen, F., Ohlendorf, C. and Zolitschka, B., 2009. Environmental history of southern Patagonia unravelled by the seismic stratigraphy of Laguna Potrok Aike. Sedimentology 56, 873-892.

Baruth, B., Endlicher, W. and Hoppe, P., 1998. Climate and desertification processes in Patagonia. Bamberger Geographische Schriften 15, 307-320.

Basile, I., Grousset, F.E., Revel, M., Petit, J.R., Biscaye, P.E. and Barkov, N.I., 1997. Patagonian origin of glacial dust deposited in East Antarctica (Vostok and Dome C) during glacial stages 2, 4 and 6. Earth and Planetary Science Letters 146, 573.

Baumgarten, H. and Wonik, T., 2014. Cyclostratigraphic studies of sediments from Lake Van (Turkey) based on their uranium contents obtained from downhole logging and paleoclimatic implications. Geologische Rundschau = International Journal of Earth Sciences [1999].

Bond, G.C., Showers, W., Elliot, M., Evans, M., Lotti, R., Hajdas, I., Bonani, G. and Johnson, S., 1999. The Noth Atlantic's 1-2 kyr Climate Rhythm: Relation to Heinrich Events, Dansgaard/Oeschger Cycles and the Little Ice Age. In: Clark, P.U., Webb, R.S., Keigwin, L.d. (Eds.), Mechanisms of Global Climate Change at Millennial Time Scales. Geophysical Monograph. 112, 35-58.

Braun, H., Christl, M., Rahmstorf, S., Ganopolski, A., Mangini, A., Kubatzki, C., Roth, K. and Kromer, B., 2005. Possible solar origin of the 1470-year glacial climate cycle demonstrated in a coupled model. Nature 438, 208-211.

Buylaert, J.P., Murray, A.S., Gebhardt, C., Sohbati, R., Ohlendorf, C., Thiel, C., Zolitschka, B. and The PASADO science team, 2013. Luminescence dating of the PASADO core 5022-1D from Laguna Potrok Aike (Argentina) using IRSL signals from feldspar. Quaternary Science Reviews 71, 70-80.

Caldenius, C., 1932. Las glaciaciones cuarternarias en la Patagonia y Tierra del Fuego. Geografisker Annaler 22, 1-164.

Caniupán, M., Lamy, F., Lange, B., Kaiser, J., Arz, H., Kilian, R., Urrea, O.B., Aracena, C., Hebbeln, D., Kissel, C., Laj, C., Mollenhauer, G. and Tiedemann, R., 2011. Millennial-scale sea surface temperature and Patagonian Ice Sheet changes off southernmost Chile (53°S) over the past ~60 kyr. Paleoceanography 26.

Clemens, S.C., 2005. Millennial-band climate spectrum resolved and linked to centennial-scale solar cycles. Quaternary Science Reviews 24 (5-6).

Coronato, A., Ercolano, B., Corbella, H. and Tiberi, P., 2013. Glacial, fluvial and volcanic landscape evolution in the Laguna Potrok Aike maar area, southernmost Patagonia, Argentina. Quaternary Science Reviews 71, 13-26.

Dansgaard, W., Johnsen, S.J., Clausen, H.B., Dahl-Jensen, D., Gundestrup, N.S., Hammer, C.U., Hvidberg, C.S., Steffensen, J.P., Sveinbjornsdottir, A.E., Jouzel, J. and Bond, G., 1993. Evidence for general instability of past climate from a 250-kyr ice-core record. Nature 364, 218-220.

Delmonte, B., Andersson, P.S., Schöberg, H., Hansson, M., Petit, J.R., Delmas, R., Gaiero, D.M., Maggi, V. and Frezzotti, M., 2010. Geographic provenance of aeolian dust in East Antarctica during Pleistocene glaciations: preliminary results from Talos Dome and comparison with East Antarctic and new Andean ice core data. Quaternary Science Reviews 29, 256-264.

EPICA community members, 2004. Eight glacial cycles from an Antarctic ice core. Nature 429, 623.

EPICA Community Members, 2006. One-to-one coupling of glacial climate variability in Greenland and Antarctica. Nature 444, 195-198.

EPICA Community Members, 2010. Stable oxygen isotopes of ice core EDML. doi:10.1594/PANGAEA.754444.

Favier-Dubois, C.M., 2007. Soil genesis related to medieval climatic fluctuations in southern Patagonia and Tierra del Fuego (Argentina): Chronological and paleoclimatic considerations. Quaternary International 162-163, 158-165.

Fischer, H., 2008. EPICA EDML chemical concentrations and fluxes. doi:10.1594/PANGAEA.683642.

Funk, J.A., von Dobeneck, T. and Reitz, A., 2004. Integrated rock magnetic and geochemical quantification of redoxomorphic iron mineral diagenesis in Late Quaternary sediments from the equatorial Atlantic. In: Wefer, G., Mulitza, S., Ratmeyer, V. (Eds.), The South Atlantic in the Late Quaternary: Reconstruction of Material Budgets and Current Systems., 237-260.

Gaiero, D.M., 2007. Dust provenance in Antarctic ice during glacial periods: From where in southern South America? Geophysical research letters 34, 107-120.

Garreaud, R., Lopez, P., Minvielle, M. and Rojas, M., 2013. Large-Scale Control on the Patagonian Climate. Journal of Climate 26, 215-230.

Gebhardt, A.C., Ohlendorf, C., Buylaert, J.-P. and PASADO Science Team, 2012. Inter- and intrasite comparison between Sites 1 and 2, PASADO deep drilling project - lake evolution, local paleoclimate history, OSL age information. 4th International PASADO Workshop, 27–29 August 2012, Bremen, Germany. Terra Nostra 2012/2.

Grootes, P.M. and Stuiver, M., 1997. Oxygen 18/16 variability in Greenland snow and ice with 10^{-3}- to 10^{5}-year time resolution. Journal of Geophysical Research 102, 26455-26470.

Grousset, F.E., Biscaye, P.E., Revel, M., Petit, J.-R., Pye, K., Joussaume, S. and Jouzel, J., 1992. Antarctic (Dome C) ice-core dust at 18 k.y. B.P.: Isotopic constraints on origins. Earth and Planetary Science Letters 111, 175-182.

Haberzettl, T., Fey, M., Lücke, A., Maidana, N., Mayr, C., Ohlendorf, C., Schäbitz, F., Schleser, G.H., Wille, M. and Zolitschka, B., 2005. Climatically induced lake level changes during the last two millennia as reflected in sediments of Laguna Potrok Aike, southern Patagonia (Santa Cruz, Argentina). Journal of Paleolimnology 33, 283-302.

Haberzettl, T., Corbella, H., Fey, M., Janssen, S., Lücke, A., Mayr, C., Ohlendorf, C., Schäbitz, F., Schleser, G.H., Wille, M., Wulf, S. and Zolitschka, B., 2007. Lateglacial and Holocene wet-dry cycles in southern Patagonia: chronology, sedimentology and geochemistry of a lacustrine record from Laguna Potrok Aike, Argentina. The Holocene 17, 297-310.

Haberzettl, T., Anselmetti, F.S., Bowen, S.W., Fey, M., Mayr, C., Zolitschka, B., Ariztegui, D., Mauz, B., Ohlendorf, C., Kastner, S., Lücke, A., Schäbitz, F. and Wille, M., 2009. Late Pleistocene dust deposition in the Patagonian steppe - extending and refining the paleoenvironmental and tephrochronological record from Laguna Potrok Aike back to 55 ka. Quaternary Science Reviews 28, 2927-2939.

Hahn, A., Kliem, P., Ohlendorf, C., Zolitschka, B., Rosen, P. and the PASADO science team, 2013. Climate induced changes as registered in inorganic and organic sediment components from Laguna Potrok Aike (Argentina) during the past 51 ka. Quaternary Science Reviews 71, 154-166.

Hahn, A., Kliem, P., Ohlendorf, C., Zolitschka, B., Rosén, P. and the PASADO science team, 2014. Elemental composition of the Laguna Potrok Aike sediment sequence reveals paleoclimatic changes over the past 51 ka in southern Patagonia, Argentina. Journal of Paleolimnology 52.

Heegaard, E., Birks, H.J.B. and Telford, R.J., 2005. Relationships between calibrated ages and depth in stratigraphical sequences: an estimation procedure by mixed-effect regression. The Holocene 15, 612-618.

Hein, A.S., Hulton, N.R.J., Dunai, T.J., Sugden, D.E., Kaplan, M.R. and Xu, S., 2010. The chronology of the Lasr Glacial Maximum and deglacial events in central Argentine Patagonia. Quaternary Science Reviews 29, 1212-1227.

Hofmann, A., 1997. Kurzfristige Klimaschwankungen im Scotiameer und Ergebnisse zur Kalbungsgeschichte der Antarktis während der letzten 200.000 Jahre. Universität Bremen.

Iriondo, M., 2000. Patagonian dust in Antarctica. Quaternary International 68-71, 83.

Jenkins, G.M. and Watts, D.G., 1969. Spectral analysis and its applications. San Francisco: Holden Day.

Kaiser, J. and Lamy, F., 2010. Links between Patagonian Ice Sheet fluctuations and Antarctic dust variabilty during the last glacial period (MIS 4-2). Quaternary Science Reviews 29, 1464-1471.

Kilian, R. and Lamy, F., 2012. A review of Glacial and Holocene paleoclimate records from southernmost Patagonia (49-55°S). Quaternary Science Reviews 53, 1-23.

Kliem, P., Buylaert, J.P., Hahn, A., Mayr, C., Murray, A.S., Ohlendorf, C., Veres, D., Wastegård, S., Zolitschka, B. and the PASADO science team, 2013a. Magnitude, geomorphologic response and climate links of lake level oscillations at Laguna Potrok Aike, Patagonian steppe (Argentina). Quaternary Science Reviews 71, 131-146.

Kliem, P., Enters, D., Hahn, A., Ohlendorf, C., Lisé-Pronovost, A., St-Onge, G., Wastegård, S., Zolitschka, B. and the PASADO science team, 2013b. Lithology, radiocarbon chronology and sedimentological interpretation of the lacustrine record from Laguna Potrok Aike, southern Patagonia. Quaternary Science Reviews 71, 54-69.

Lambert, F., Delmonte, B., Petit, J.R., Bigler, M., Kaufmann, P.R., Hutterli, M.A., Stocker, T.F., Ruth, U., Steffensen, J.P. and Maggi, V., 2008. Dust-climate couplings over the past 800,000 years from the EPICA Dome C ice core. Nature 452, 616-619.

Lambert, F., Bigler, M., Steffensen, J.P., Hutterli, M. and Fischer, H., 2011. The calciumdust relationship in high-resolution data from Dome C, Antarctica. Climate of the Past Discussions 7, 1113-1137.

Lenz, O.K., Wilde, V. and Riegel, W., 2011. Short-term fluctuations in vegetation and phytoplankton during the middle Eocene greenhouse climate; a 640-kyr record from the Messel oil shale (Germany). International Journal of Earth Sciences = Geologische Rundschau 100, 1851-1874.

Li, F., Ginoux, P. and Ramaswamy, V., 2010. Transport of Patagonian dust to Antarctica. Journal of Geophysical Research 115.

Lisé-Pronovost, A., St-Onge, G., Gogorza, C., Haberzettl, T., Jouve, G., Francus, P., Ohlendorff, C., Gebhardt, C., Zolitschka, B. and the PASADO Science Team, 2015. Rock-magnetic proxies of wind intensity and dust since 51,200 cal BP from lacustrine sediments of Laguna Potrok Aike, southeastern Patagonia. Earth and Planetary Science Letters 411, 72-86.

Mayr, C., Lücke, A., Stichler, W., Trimborn, P., Ercolano, B., Oliva, G., Ohlendorf, C., Soto, J., Fey, M., Haberzettl, T., Janssen, S., Schäbitz, F., Schleser, G.H., Wille, M. and Zolitschka, B., 2007a. Precipitation origin and evaporation of lakes in semi-arid Patagonia (Argentina) inferred from stable isotopes ($\delta^{18}O$, $\delta^{2}H$). Journal of Hydrology 334, 53-63.

Mayr, C., Wille, M., Haberzettl, T., Fey, M., Janssen, S., Lücke, A., Ohlendorf, C., Oliva, G., Schäbitz, F., Schleser, G.H. and Zolitschka, B., 2007b. Holocene variability of the Southern Hemisphere westerlies in Argentinean Patagonia (52°S). Quaternary Science Reviews 26, 579-584.

Mayr, C., Lücke, A., Wagner, S., Wissel, H., Ohlendorf, C., Haberzettl, T., Oehlerich, M., Schäbitz, F., Wille, M., Zhu, J. and Zolitschka, B., 2013. Westerlies regulated atmospheric CO_2 during the last deglaciation. Geology 41, 831-834.

Mazzarini, F. and D`Orazio, M., 2003. Spatial distribution of cones and satellite-detected lineaments in the Pali Aike Volcanic Field (southernmost Patagonia): insights into the tectonic setting of a Neogene rift system. Journal of Volcanology & Geothermal Research 125, 291-305.

Meglioli, A., 1992. Glacial geology and geochronology of southernmost Patagonia and Tierra del Fuego, Argentina and Chile. Ph.D. Dissertation, Leigh University, Bethlehem PA U.S.A., 216.

Mercer, J.H., 1976. Glacial history of southernmost South America. Quaternary Research 6, 125-166.

Molinie, A.J. and Ogg, J.G., 1990. Sedimentation-rate curves and discontinuities from sliding-window spectral analysis of logs. Log Analyst 31.

North Greenland Ice Core Project members, 2004. High-resolution record of Northern Hemisphere climate extending into the last interglacial period. Nature 431, 147-151.

Obrochta, S.P., Miyahara, H., Yokoyama, Y. and Crowley, T.J., 2012. A re-examination of evidence for the North Atlantic "1500-year cycle" at Site 609. Quaternary Science Reviews 55, 23-33.

Petit, J.R., Jouzel, J., Raynaud, D., Barkov, N.I., Barnola, J.M., Basile, I., Bender, M., Chappellaz, J., Davis, M., Delaygue, G., Delmotte, M., Kotlyakov, V.M., Legrand, M., Lipenkov, V.Y., Lorius, C., Pepin, L., Ritz, C., Saltzman, E. and Stievenard, M., 1999. Climate and atmospheric history of the past 420,000 years from the Vostok ice core, Antarctica. Nature 399, 429.

Priestley, M.B., 1981. Spectral analysis and time series. New York: Academic Press.

Prokopenko, A.A., Williams, D.F., Karabanov, E.B. and Khursevich, G.K., 2001. Continental response to Heinrich events and Bond cycles in sedimentary record of Lake Baikal, Siberia. Global and Planetary Change 18, 217-226.

Rabassa, J. and Clapperton, C.M., 1990. Quaternary glaciations of the southern Andes. Quaternary Science Reviews 9, 153-174.

Recasens, C., Ariztegui, D., Maidana, N.I., Zolitschka, B. and and the PASADO Science Team, 2014. Diatoms as indicators of hydrological and climatic changes in Laguna Potrok Aike (Patagonia) since the Late Pleistocene. Palaeogeography, Palaeoclimatology, Palaeoecology.

Recasens, C., Ariztegui, D., Maidana, N.I., Zolitschka, B. and and the PASADO Science Team, 2015. Diatoms as indicators of hydrological and climatic changes in Laguna Potrok Aike (Patagonia) since the Late Pleistocene. Palaeogeography, Palaeoclimatology, Palaeoecology 417, 309-319.

Reijmer, C.H., Broeke, M.R.V.D. and Scheele, M.P., 2002. Air Parcel Trajectories and Snowfall Related to Five Deep Drilling Locations in Antarctica Based on the ERA-15 Dataset. Journal of Climate 15, 1957-1963.

Ross, P.S., Delpit, S., Haller, M.J., Nemeth, K. and Corbella, H., 2011. Influence of the substrate on maar-diatreme volcanoes - An example of a mixed setting from Pali Aike volcanic field, Argentina. Journal of Volcanology and Geothermal Research 201, 253-271.

Schneider, C., Glaser, M., Kilian, R., Santana, A., Butorovic, N. and Casassa, G., 2003. Weather observations across the southern Andes at 53°S. Physical Geography 24, 97-119.

Schulz, M., 2002. On the 1470-year pacing of Dansgaard-Oeschger warm events. Paleoceanography 17.

Snowball, I. and Muscheler, R., 2007. Palaeomagnetic intensity data: an Achilles heel of solar activity reconstructions. The Holocene 17 (6).

Sprenk, D., Weber, M.E., Kuhn, G., Rosén, P., Frank, M., Molina-Kescher, M., Liebetrau, V. and Röhling, H.-G., 2013. Southern Ocean bioproductivity during the last glacial cycle – new detection method and decadal-scale insight from the Scotia Sea. Antarctic Palaeoenvironments and Earth-Surface Processes 381, 245-261.

St-Onge, G., Stoner, J.S. and Hillaire-Marcel, C., 2003. Holocene paleomagnetic records from the St. Lawrence Estuary, eastern Canada: centennial- to millennial-scale geomagnetic modulation of cosmogenic isotopes. Earth and Planetary Science Letters 209 (1-2).

Sugden, D.E., McCulloch, R.D., Aloys, J.-M., Bory and Hein, A.S., 2009. Influence of Patagonian glaciers on Antarctic dust deposition during the last glacial period. Nature Geoscience 2, 281-285.

Toggweiler, J.R., 2009. Shifting Westerlies. Science 323, 1434-1435.

Weber, M.E., Kuhn, G., Sprenk, D., Rolf, C., Ohlwein, C. and Ricken, W., 2012. Dust transport from Patagonia to Antarctica - A new stratigraphic approach from the Scotia Sea and its implications for the last glacial cycle. Quaternary Science Reviews 36, 177-188.

Weedon, G., 2003. Time-series analysis and cyclostratigraphy; examining stratigraphic records of environmental cycles. Cambridge University Press: Cambridge, United Kingdom, United Kingdom.

Weischet, W., 1996. Regionale Klimatologie. Teil 1: Die Neue Welt: Amerika, Neuseeland, Australien. Teubner, Stuttgart.

Weninger, B. and Jöris, O., 2008. A 14C age calibration curve for the last 60 ka: the Greenland-Hulu U/Th timescale and its impact on understanding the Middle to Upper Paleolithic transition in Western Eurasia. Journal of Human Evolution 55, 772-781.

Wonik, T., 2001. Gamma-ray measurements in the Kirchrode I and II boreholes. Palaeogeography, Palaeoclimatology, Palaeoecology 174, 97-105.

Zolitschka, B., Schäbitz, F., Lücke, A., Corbella, H., Ercolano, B., Fey, M., Haberzettl, T., Janssen, S., Maidana, N., Mayr, C., Ohlendorf, C., Oliva, G., Paez, M.M., Schleser, G.H., Soto, J., Tiberi, P. and Wille, M., 2006. Crater lakes of the Pali Aike Volcanic Field as key sites for paleoclimatic and paleoecological reconstructions in southern Patagonia, Argentina. Journal of South American Earth Sciences 21, 294-309.

Zolitschka, B., Anselmetti, F.S., Aristegui, D., Corbella, H., Francus, P., Ohlendorf, C., Schäbitz, F. and the PASADO Scientific Drilling Team, 2009. The Laguna Potrok Aike Scientific Drilling Project PASADO (ICDP Expedition 5022). Scientific Drilling 8.

Chapter 5:

Conclusions and outlook

Conclusions

The studies presented in Chapters 2-4 demonstrate the outstanding value of research on lake and catchment sediments of LPA to extent our knowledge about the paleo climate and paleo environment of southern Patagonia and the role of the SHW for the global climate system.

Based on lacustrine sediment cores from the profundal zone of LPA a continuous, radiocarbon-dated and high resolute composite profile (5022-2CP) of the past 51.200 years was established for subsequent multi-proxy-analyses. For the first time, climatically important intervals of the last glacial period (MIS 2 and MIS 3) can be studied in high resolution on continental sediments in the belt of the SHW. Frequency analytics revealed recurring climate signals with a periodicity of ~ 1.500 years during MIS 2. Their predominant minor climatic dimensions likely resulted from the very northern latitude of the SHW during MIS 2 as it inhibited the amplification of minor climate signals by green house gas ventilation from the southerly located ACC. The results emphasize the importance of the SHW in the quaternary global climate system.

The examination of geomorphological, seismic and sedimentary evidences in the lake basin and the proximity of the lake extended the knowledge about the geomorphological evolution of the lake basin, the geomorphological processes in the catchment and the lake level history. The sensitivity of the lake water balance to climatic and environmental variations of the past ~ 50.000 years is documented by lake level oscillations between 136 and 85 m a.s.l.; active overflow conditions and the local ground water table inhibited even higher and lower lake levels. The lowest lake level characterizes the warm/dry climate of the mid-Holocene. High lake levels specify the cold/wet climate of the last glacial period and the Little Ice Age. However, the interpretation of lake levels during the glacial period is complicated due to the formation of permafrost in the catchment. The abrasion due to lake level oscillations caused distinct lake internal and external responses, e. g., the lake basin expansion from originally ca. 2.2 km to ca. 3.8 km and lake internal mass movement deposits due to subaquatic collapses of lake level terraces.

Outlook

The results of the presented studies indicate the high scientific potential of future studies on datasets and samples retrieved on composite profile 5022-2CP.

The radiocarbon based age-depth-model of 5022-2CP could be updated by transferring available OSL ages from composite profile of site 1 (5022-1CP). This might especially improve the time range 40.000-51.200 years as the precession of radiocarbon dating reduces at limit of the method (> 40.000 years) and as some radiocarbon age determination on 5022-2CP suggest distortion by very short living fluctuations of the atmospheric ^{14}C concentration. Furthermore, this offers the opportunity to study the nature of the short living variations of atmospheric ^{14}C concentration itself.

The predominance of clastic compound as well as revealing results gained by the investigation of parameters indicating clastic compound in 5022-2CP point to the high potential of grain size determinations on LPA sediments. The examination of available data sets about the grain size composition of 5022-2CP is a promising task of future studies.

Chapter 6:

Appendices

A-1: Detailed lithological description, photographs and dry density of composite profile 5022-2CP (Legend).

Legend

Sedimentary Structures

- Laminated (cm-dm)
- Finely laminated (mm-cm)
- Laminated (cm-dm) with fine sand/ coarse silt layers (<=1cm)
- Normal graded
- Homogeneous
- Bended/Dipping layer
- Nodular
- Lenses
- Fault
- Layer with high content of macro remains of aquatic mosses (>=1cm)
- Gastropod
- Shell
- Fish bone
- Bone (Ctenomys)
- Gravel piece
- T Thin Tephra Layer

Facies

- Pelagic sedimentation
- Pelagic sedimentation interrupted by frequent sedimentation events (<=1cm)
- Gravites (undifferentiated)
- Tephra

Lithostratigraphic Unit

- A: Laminated silts prevail. Relatively high amount of authochton calcites.
- B: Dominance of laminated silts intercalated with thin fine sand and coarse silt layers; normal graded units and ball and pillow structures occur; high content of plant macro remains and gastropods; a few carbonate crystals occur.
- C-1: Dominance of laminated silts intercalated with thin fine sand and coarse silt layers; normal graded units and ball and pillow structures occur.
- C-2: Dominance of normal graded units and ball and pillow structures among laminated silts intercalated with thin fine sand and coarse silt layers.
- C-3: Dominance of normal graded units, ball and pillow structures, sand and gravel layers; a few laminated silts intercalated with thin fine sand and coarse silt layers occur.

A-1: Detailed lithological description, photographs and dry density of composite profile 5022-2CP (composite depth: 0-20 m).

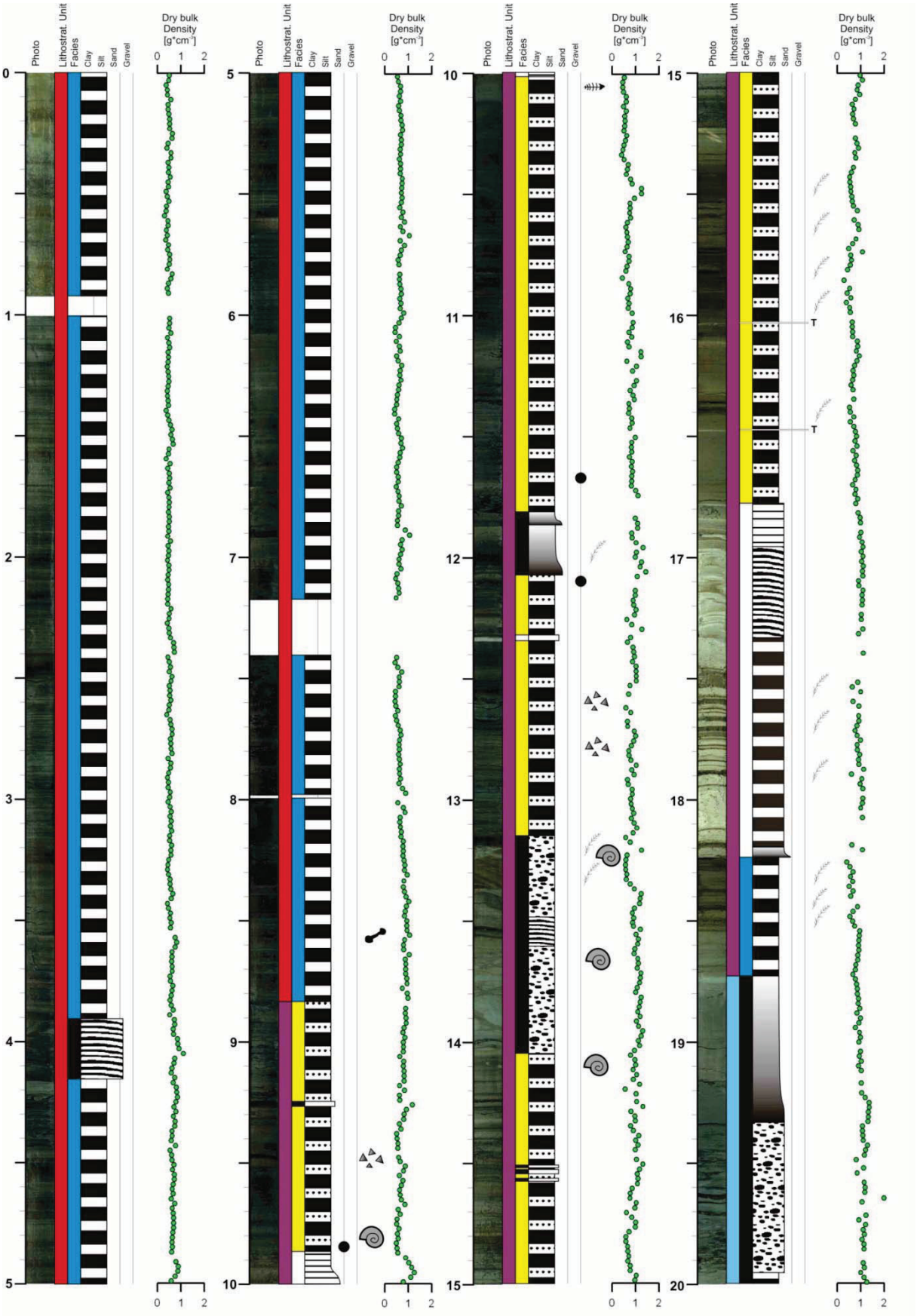

A-1: Detailed lithological description, photographs and dry density of composite profile 5022-2CP (composite depth: 20-40 m).

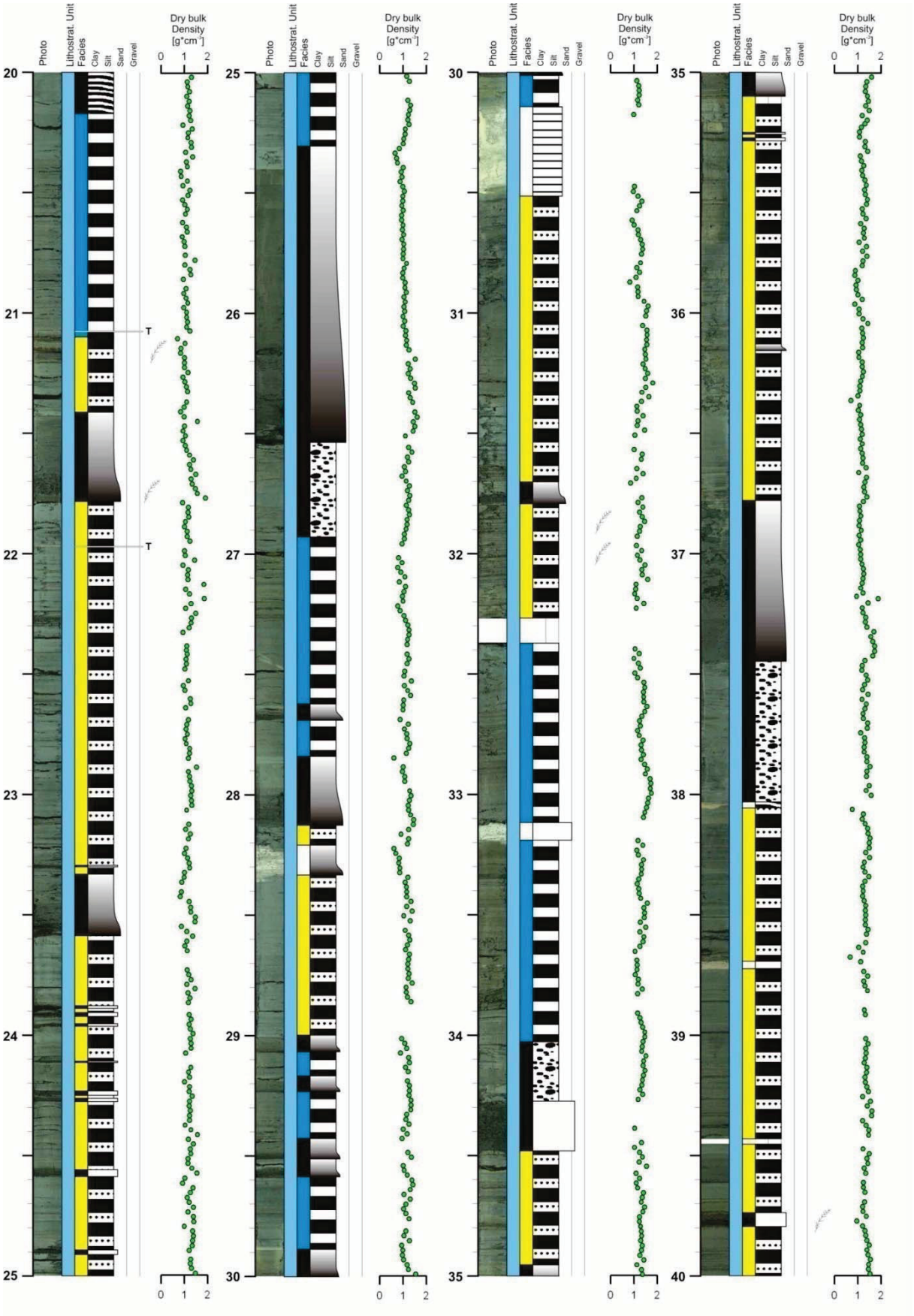

A-1: Detailed lithological description, photographs and dry density of composite profile 5022-2CP (composite depth: 40-60 m).

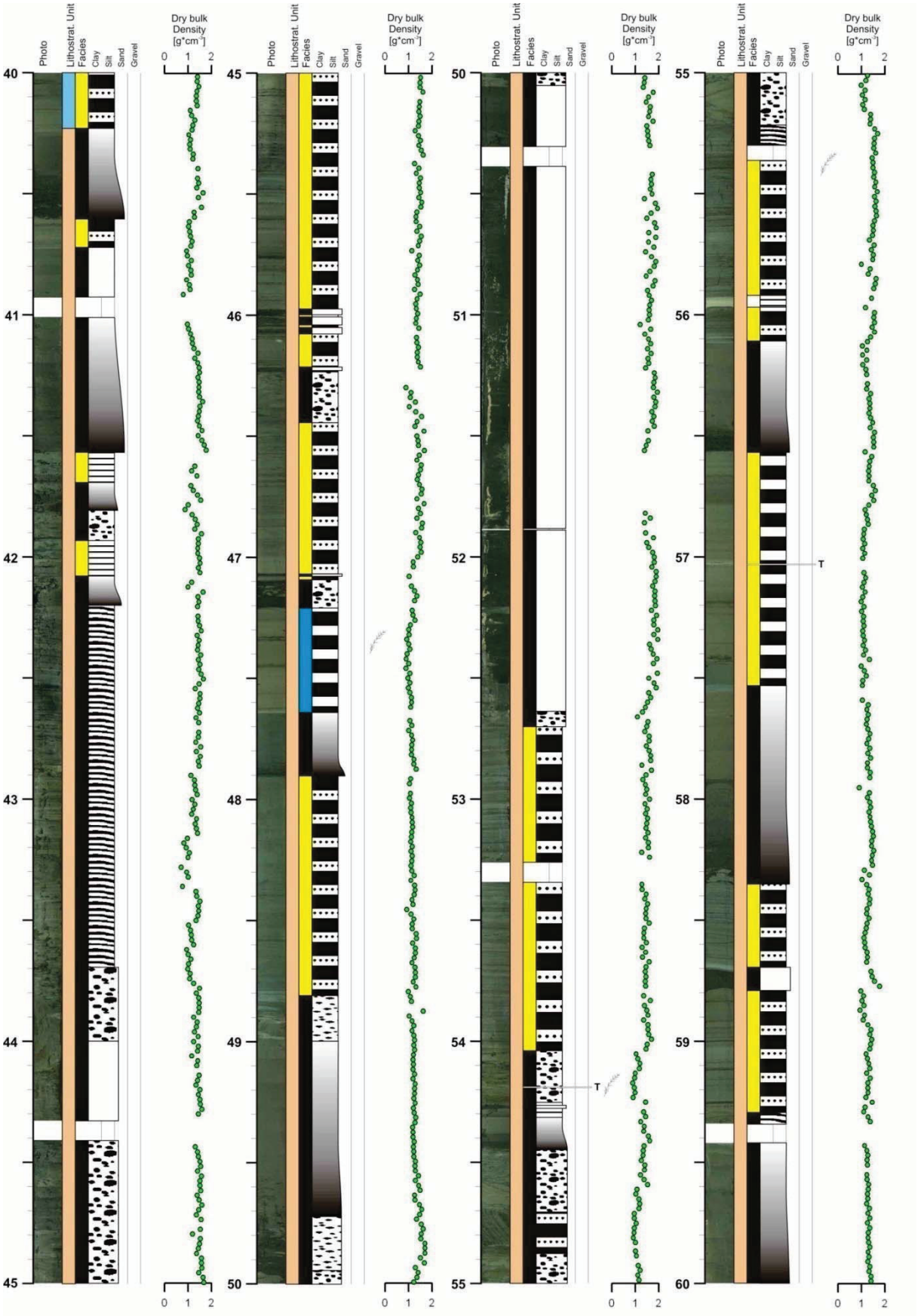

A-1: Detailed lithological description, photographs and dry density of composite profile 5022-2CP (composite depth: 60-80 m).

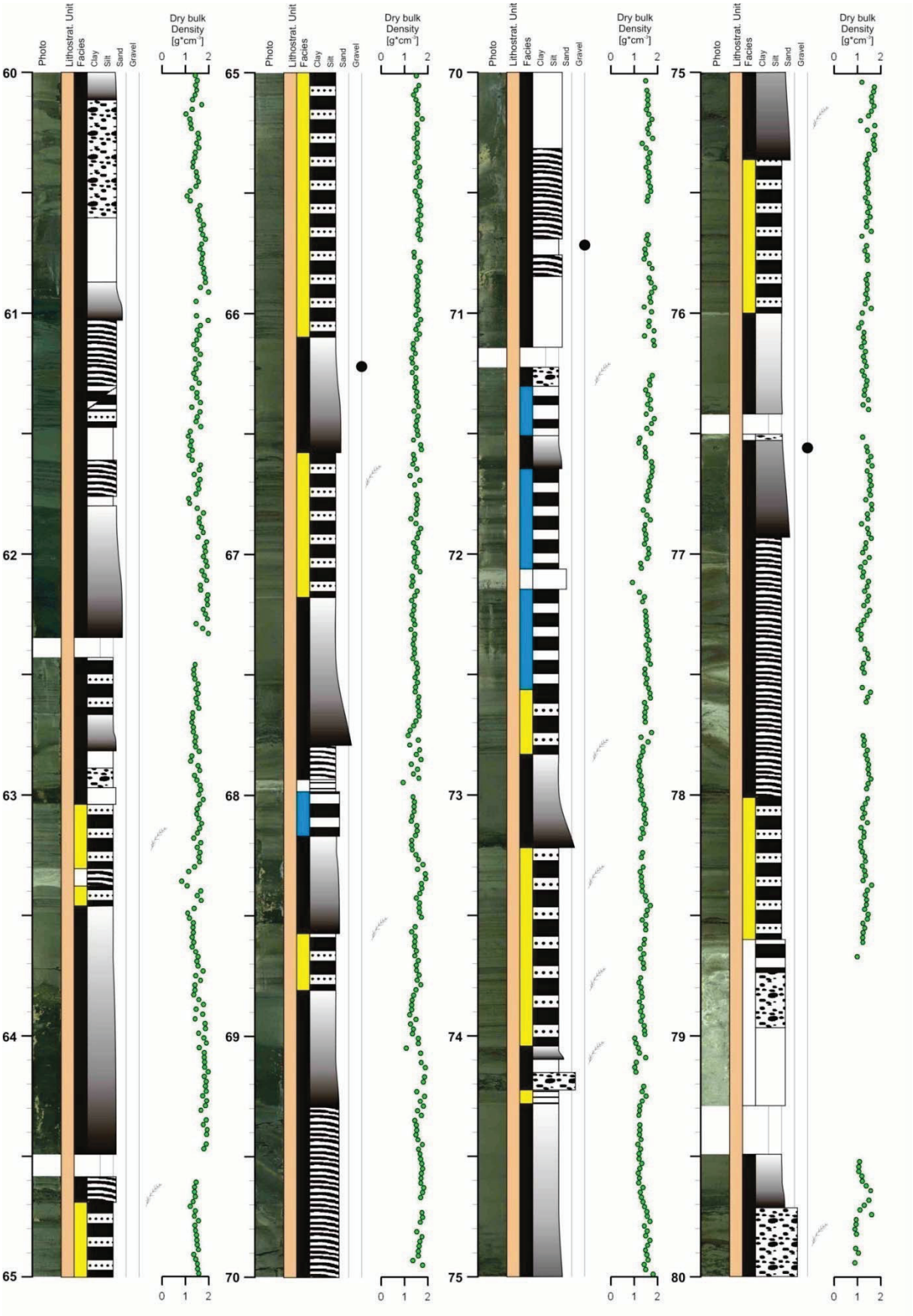

A-1: Detailed lithological description, photographs and dry density of composite profile 5022-2CP (composite depth: 80-100 m).

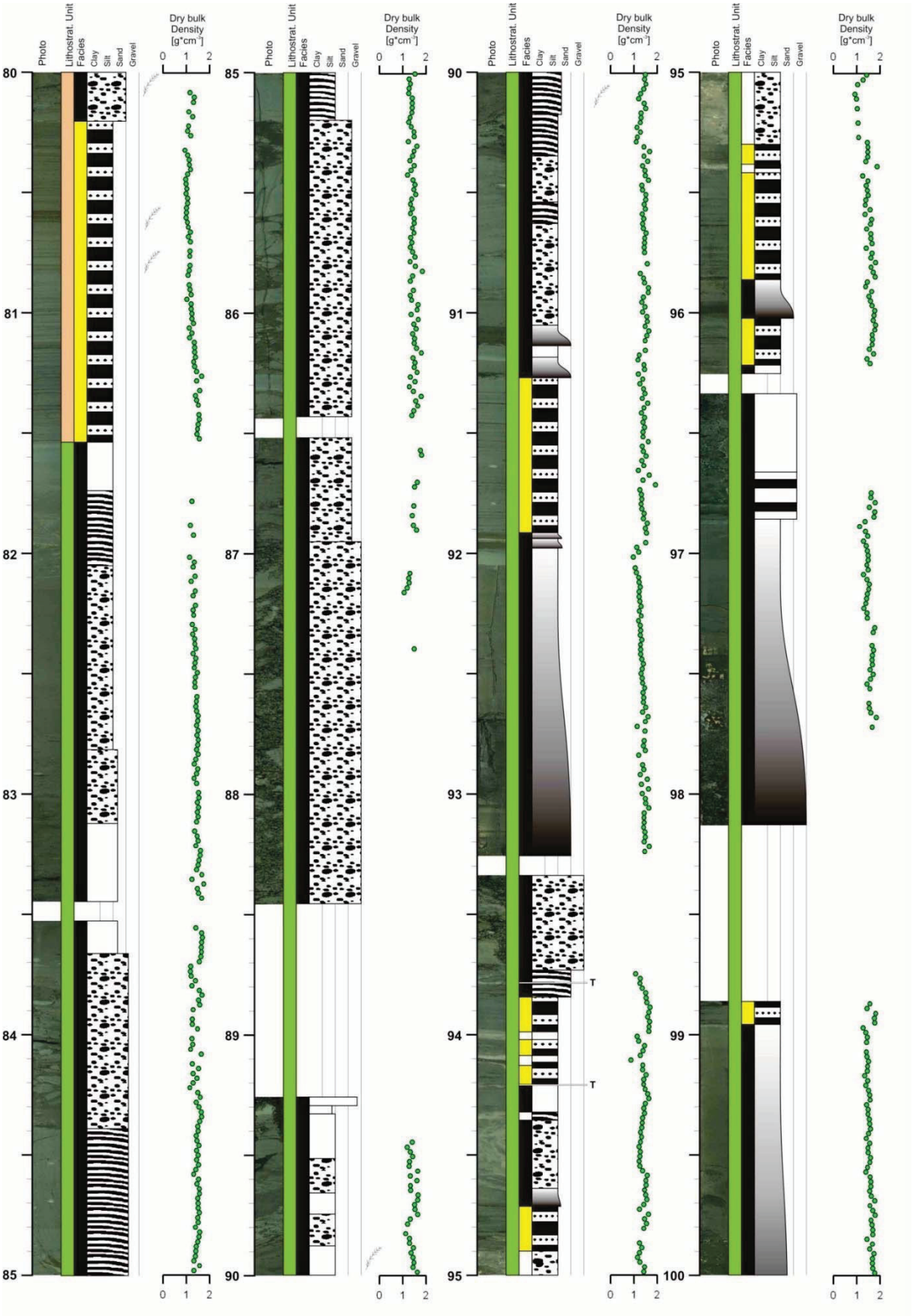

A-1: Detailed lithological description, photographs and dry density of composite profile 5022-2CP (composite depth: 100-106.09 m).

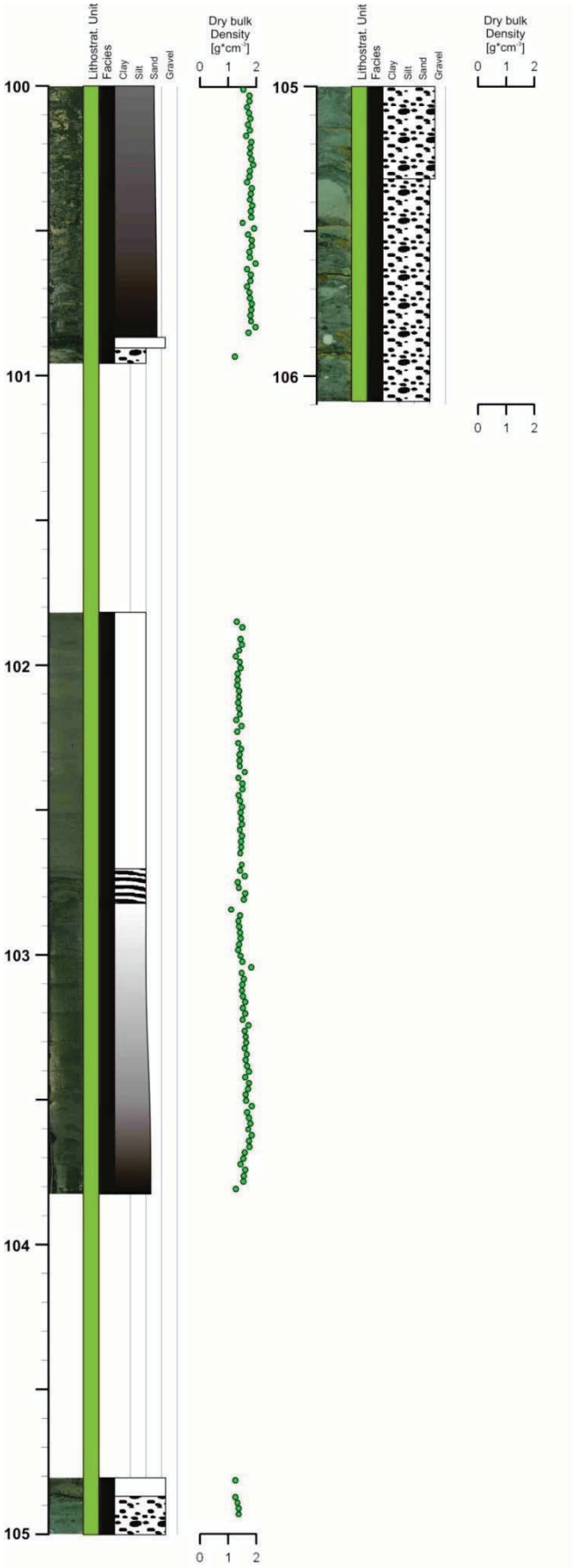

A-2: Data presented in this thesis can be obtained from the author on request.

Declaration

I declare that:

- this dissertation was not prepared by unfair means
- only the stated references and resources were used
- contents and literal statements of all used sources were cited.

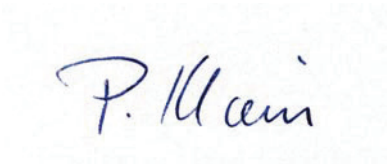

Göttingen, January 2019